Master's thesis

Hydrogeology and environmental geology

Hydraulic properties of peat and hydrogeochemical characteristics of groundwater and porewater in Viiankiaapa mire

Harri Turtiainen

2020

Supervisor:

Kirsti Korkka-Niemi

Master's Programme in Geology and Geophysics

Faculty of Science

HELSINGIN YLIOPISTO
HELSINGFORS UNIVERSITET
UNIVERSITY OF HELSINKI
MATEMAATTIS-LUONNONTIETEELLINEN TIEDEKUNTA
MATEMATISK-NATURVETENSKAPLIGA FAKULTETEN
FACULTY OF SCIENCE

Faculty	Degree programme
Faculty of science	Master's programme in Geology and geophysics

Study track

Hydrogeology and environmental geology

Author

Harri Artturi Turtiainen

Title

Hydraulic properties of peat and hydrogeochemical characteristics of groundwater and porewater in Viiankiaapa mire

Level	Month and year	Number of pages
Master's Thesis	12/2020	79 + 6

Abstract

A promising Cu-Ni-PGE containing sulphide ore deposit was discovered in 2009 by Anglo American and since the company has continued studies aiming towards utilisation of the deposit. The discovered deposit lies underneath a Natura 2000 protected mire complex, Viiankiaapa, in Sodankylä municipality in Finnish Lapland. The research and exploration activities in the area are performed with mitigation and preventing actions in order to minimize the deterioration impact to the delicate ecosystem. The more detailed understanding of the hydrogeochemistry of the mire environment in its current state can assist: in monitoring, mitigating and preventing of potential environmental effects due to future mining operations as well as planning the monitoring program.

Hydrogeochemical studies, consisting of water and peat sampling at eight sampling points, were carried out along a 1.6 km long study line. Water samples were collected from the surface of the mire as well as within the peat layer and the bottom of the peat layer. Water samples were collected using a mini-piezometer. The analyses for the water samples involved: major components, trace elements and $\delta^{18}O$ & $\delta^{2}H$. Groundwater influence in the different sampling points as well as different sections of the peat was investigated using the mentioned chemical and isotopic properties. Peat sampling focused on finding samples which would have different hydraulic properties in order to find the influence of peat in the hydrology in the mire. Hydraulic conductivity of peat samples was determined using rigid wall permeameter test setup. The chemical and physical methods were supplemented by a ground penetrating radar survey completed with 30 and 100 MHz antennas.

Studies of peat showed that the hydraulic conductivity varies substantially even inside the rather small study area. Widely recognized correlation between hydraulic conductivity and depth was not observed statistically, but the sampling sites individually show a clear connection with depth and hydraulic conductivity. The influence of the hydraulic properties of peat on to the flow of water in the mire was observed to be significant. In cases where the hydraulic conductivity of peat was very low, water flow may be prevented altogether. This was confirmed with the use of chemical analyses. With higher hydraulic conductivity, groundwater influence was seen more or less throughout the peat profile.

Keywords

Hydrogeochemistry, Hydraulic conductivity, Peat, Mini-piezometer, Ground penetrating radar

Where deposited

HELDA

Additional information

HELSINGIN YLIOPISTO
HELSINGFORS UNIVERSITET
UNIVERSITY OF HELSINKI
MATEMAATTIS-LUONNONTIETEELLINEN TIEDEKUNTA
MATEMATISK-NATURVETENSKAPLIGA FAKULTETEN
FACULTY OF SCIENCE

Tiedekunta	Koulutusohjelma
Matemaattis-luonnontieteellinen	Geologian ja geofysiikan maisteriohjelma

Opintosuunta

Hydrogeologia ja ympäristögeologia

Tekijä

Harri Artturi Turtiainen

Työn nimi

Hydraulic properties of peat and hydrogeochemical characteristics of groundwater and porewater in Viiankiaapa mire

Työn laji	Aika	Sivumäärä
Maisterintutkielma	12/2020	79 + 6

Tiivistelmä

Anglo American löysi lupaavan Cu-Ni-PGE sulfidimalmiesiintymän vuonna 2009 ja on sen jälkeen jatkanut tutkimuksia, jotka tähtäävät esiintymän hyödyntämiseen. Esiintymä sijaitsee Natura 2000 suojellun suokompleksin alla, Sodankylän kunnan alueella, Suomen Lapissa. Tutkimus- ja malminetsintätyö alueella toteutetaan käyttäen lieventäviä ja ehkäiseviä toimenpiteitä, jotta herkkään suoekosysteemiin ei kohdistuisi haitallisia vaikutuksia. Nykytilassaan olevan suokompleksin hydrogeokemian yksityiskohtaisempi ymmärrys auttaa tulevaisuudessa koittavan kaivostoiminnan ympäristövaikutusten seurannassa ja lieventämisessä sekä ympäristövaikutusten seurannan suunnittelussa.

Hydrogeokemiallisia tutkimuksia, jotka koostuivat vesi- ja turvenäytteenotosta, tehtiin kahdeksassa tutkimuspisteessä pitkin linjaa, jonka pituus oli n. 1,6 km. Vesinäytteitä otettiin mini-pietsometrillä suon pinnalta, turpeen sisäosasta sekä suon pohjalta. Vesinäytteistä analysoitiin: pääionikoostumus, hivenainekoostumus sekä $\delta^{18}O$ & $\delta^{2}H$. Analysoitujen tulosten perusteella pyrittiin tutkimaan vesinäytteissä ilmenevää pohjaveden vaikutusta eri osissa tutkimuslinjaa sekä eri syvyyksissä turveprofiilia. Turpeen vaikutusta suon hydrologiaan arvioitaessa turvenäytteenotossa pyrittiin löytämään näytteitä, jotka eroaisivat hydraulisilta ominaisuuksiltaan toisistaan. Turpeen vedenjohtavuus tutkittiin käyttäen kiinteäseinämäistä permeametrikoetta. Kemialliset ja fysikaaliset analyysit saivat täydennystä suoritetusta maatutkaluotauksesta, joka tehtiin käyttäen 100:n ja 30:n MHz antenneja.

Turvetutkimuksista selvisi vedenjohtavuuden suuri vaihtelu pienehkön tutkimusalueen sisällä. Laajasti tunnistettu korrelaatio turpeen näytesyvyyden sekä vedenjohtavuuden välillä ei näkynyt koko aineistossa tilastollisesti, mutta yksittäisiä tutkimuspisteitä tarkasteltaessa yhteys turpeen syvyyden ja vedenjohtavuuden välillä näytti olleen selvä. Turpeen vedenjohtavuusarvon vaikutus veden virtaukseen suossa vaikutti olevan merkittävä. Turpeen vedenjohtavuuden ollessa riittävän matala veden virtaus turpeessa saattaa jopa estyä. Tämä varmennettiin käyttäen apuna kemiallisia analyyseja. Korkeampi vedenjohtavuus turpeessa näkyi yleensä suurempana pohjavesivaikutuksena läpi koko turveprofiilin.

Avainsanat

Hydrogeokemia, Vedenjohtavuus, Turve, Mini-pietsometri, Maatutka

Säilytyspaikka

HELDA

Muita tietoja

TABLE OF CONTENTS

1. INTRODUCTION

The Sakatti Cu-Ni-PGE mineralization is regarded as one of the most remarkable Cu-Ni sulphide discoveries in recent history (Brownscombe *et al*. 2015). However, the location of the finding has brought concerns about the possible environmental impacts in case of a mine is to be established. The high-graded sulphidic deposit is located some 15 kilometers north from the municipal center of Sodankylä and lies hundreds of meters underneath the Viiankiaapa mire that is protected under the European Union's habitats directive (Council Directive 92/43/EEC on the Conservation of natural habitats and of wild fauna and flora). Viiankiaapa is the natural habitat of many vulnerable, endangered and protected species of both flora and fauna (Pääkkö 2004). The environmental impact assessment (EIA) process for a mining project has been almost completed and AA Sakatti Mining Oy has submitted the EIA report to authorities in November 2020.

An important part of assessing how mining the ore could affect the very delicate mire environment is to establish a detailed understanding of the ecological, hydrogeochemical and sedimentological conditions in the area in its present state. This has been the focus of previous studies by Kääriäinen (2016), Lahtinen (2017), Åberg *et al*. (2017a and b), Korkka-Niemi *et al*. (2017), Bigler (2018) and Åberg *et al*. (2019). These studies described the prevailing geochemical characteristics of surface water, groundwater and peat pore water in the area as well as geochemistry and sedimentology more generally. Many efforts were made in order to find evidence and the locations of groundwater discharge onto the mire (Korkka-Niemi *et al*. 2017, Lahtinen 2017 and Åberg *et al*. 2019). The previous studies used hydrogeochemical and isotopic analyses of water samples, thermal infrared imaging and ground penetrating radar (GPR) survey to locate and model the areas where groundwater is discharging. Flowing and mixing of groundwater and surface water happens within and through the peat of the mire. Suonperä (2016) studied the peat stratigraphy, chronology and geochemistry in a mire north of Viiankiaapa mire. However, the hydraulic properties of the peat in Viiankiaapa have been studied only limitedly (Golder associates 2012). Viiankiaapa was one of the target mires in the very thorough peat studies that were carried out in 1962–1975 by The Geological Survey of

Finland (GTK) (Lappalainen & Pajunen 1980). These studies focused on peat volumes for the estimation of the energy potential in the mires. However, they still provide valuable data that can be used to study the area as shown in Åberg *et al*. (2017a), where more than 300 peat bore profiles were gathered from Lappalainen (1970).

Mires are ecosystems where the biomass production of vegetation exceeds the biomass production of decomposing organisms (Maunu & Virtanen 2005). This is usually coincided with precipitation exceeding evapotranspiration. These two circumstances produce the organic sediment that is peat. The physical, biological and chemical properties of peat have been studied for decades: Kaila (1956), Boelter (1965), Dai & Sparling (1973), Shotyk (1988), Hill & Siegel (1991), Reeve *et al*. (2000), Ronkanen & Kløve (2005), Quinton *et al*. (2008) and Mustamo *et al*. (2016) as few examples. Peat is composed of decomposed plant material in varying humification stages. The humification stage of plant material as well as the decaying plant species themselves have proven to have clear effect on the hydraulic conductivity of peat (Päivänen 1973, Quinton *et al*. 2008, Mustamo *et al*. 2016 and Wong *et al*. 2009). Many different methods can be applied for measuring the hydraulic conductivity of peat. Peat is a soft material usually fully saturated with water, in the natural state, and it can be difficult to determine the hydraulic conductivity via laboratory methods.

Many have used *in situ* piezometer/infiltration methods for measuring the hydraulic conductivity of peat (Boelter 1965, Dai & Sparling 1973, Päivänen 1973, Clymo 2004, Wong *et al*. 2009 and Mustamo *et al*. 2016) but laboratory techniques using different types of permeameters have been used as well (Päivänen 1973, Beckwith *et al*. 2003, Ronkanen & Kløve 2005 and Quinton *et al*. 2008). A chemical tracer compound (potassium chloride) was used to determine the hydraulic conductivity in Canada by Quinton *et al*. (2008). The pitfall of these in situ measurements is that they result in a generalized hydraulic conductivity of the peat material. The laboratory tests provide more specified results for particular sections of peat from a continuous profile. Another aspect for the conductivity measurements to be taken into consideration is that the hydraulic conductivity of peat can vary considerably with respect to the orientation of the flow. The horizontal hydraulic conductivity has been observed in some cases to be larger than the

vertical conductivity (Sarasto 1963. Beckwith *et al*. 2003) but also vice versa in some cases (Ronkanen & Kløve 2005). It is the anisotrophy of hydraulic conductivity as well as variations in the peat composition that creates a local variation of water flow in peat material. On a larger scale, the water flow in a mire is controlled by bedrock and sediment topography as well as the sediment material itself.

Sodankylä region lies within the central Lapland greenstone belt (CLGB), which consists of Paleoproterozoic (2.9–1.9 Ga) supracrustal volcanic and sediment rocks (Brownscombe *et al*. 2015). These have been intruded by mafic and ultramafic intrusions, some of which have proven to possess ore potential. The surficial geology is largely the result of supra-aquatic conditions and close proximity of the ice divide during last glaciations. This translated to low basal erosion rates that prevailed under the sluggish ice sheet, as well as multiple till units that have preserved in the region (Sarala *et al*. 2015). Along with till deposits, the area hosts various ice-marginal outwash and fluvial deposits and some fluvial erosional landforms as well. The newly generated glacial deposit 3D-model from the Viiankiaapa area implies that the mire is mostly peat covered underlain by sorted deposits similar to a braided river system (Åberg *et al*. 2017a). Under the sorted deposits two different till units are found with additional sandy and gravelly deposits.

There are well established methods for studying natural waters and determining their part in the hydrological cycle. Usually, ground and surface waters are analyzed for their chemical composition, stable isotope ratios of oxygen and hydrogen, electrical conductivity, pH and temperature, for example. These properties are used to determine and distinct water samples with groundwater and surface water characteristics. GTK has performed extensive studies of Finnish groundwater and surface water geochemistry (Lahermo *et al*.1990. 1996. 2002) as has the Finnish Environment Institute (Soveri *et al*. 2001). As the groundwater geochemistry varies with the bedrock and quaternary sediment composition these publications provide exceptional background data for studies conducted in different parts of Finland. The stable isotope methods have also been well-established and documented internationally and in Finnish studies by for example: Kortelainen & Karhu (2004), Kortelainen (2007a), Rautio & Korkka-Niemi (2011 and 2015).

This study aims to develop an understanding of the hydraulic conductivity in different peat layers in the study site as well as investigate the possible water flow patterns through and within the peat. An additional goal is to detect and classify the type of clastic sediments that underlie the peat. The primary results will focus on whether or not distinct geochemical groups of water are found and the distribution of them. In order to interpret the interactions of groundwater and surface waters, the hydrogeochemistry will be combined with the results of peat studies and ground penetrating radar surveys that were conducted along the sampling profile. Lastly, the results and interpretations are compared to previous studies from Viiankiaapa and Finland in general.

Sampling of the surface-, pore- and groundwaters as well as the peat sampling were carried out in eight sampling points, which create an east–west cross section of the mire. Peat and water sampling points were targeted in locations to cover different peat thicknesses (from shallow to deep) based on peat thickness model by Åberg. *et al.* (2017a), and to gain a representative cross-section of the western part of Viiankiaapa mire.

2. STUDY AREA

Viiankiaapa mire complex is located in Sodankylä municipality in Finnish central Lapland (Figure 1). As the name suggests, the mire is an aapa type mire. Aapa mires are found in the northern boreal zone of Finland, Sweden, Norway and Northwestern Russia (Pakarinen 1995). Aapa mires are mostly minerotrophic with occasional ombrotrophic areas. Minerotrophic aapa mires acquire the majority of nutrients and water from surface runoff from surrounding forested areas and precipitation, but also via groundwater discharge. The abundance of nutrients from the surrounding forested areas and from groundwaters creates an environment where the plant biodiversity is high (Metsähallitus 2006). The central parts of aapa mires are usually lower in elevation than the margins, this leads to increased water content towards the center and a flark and string pattern where wet fen type vegetation (flark) alternates with drier bog type vegetation (string)

(Pakarinen 1995). A sloping topography is also very common for aapa mires (Lappalainen 2004), which is seen in Viiankiaapa as well.

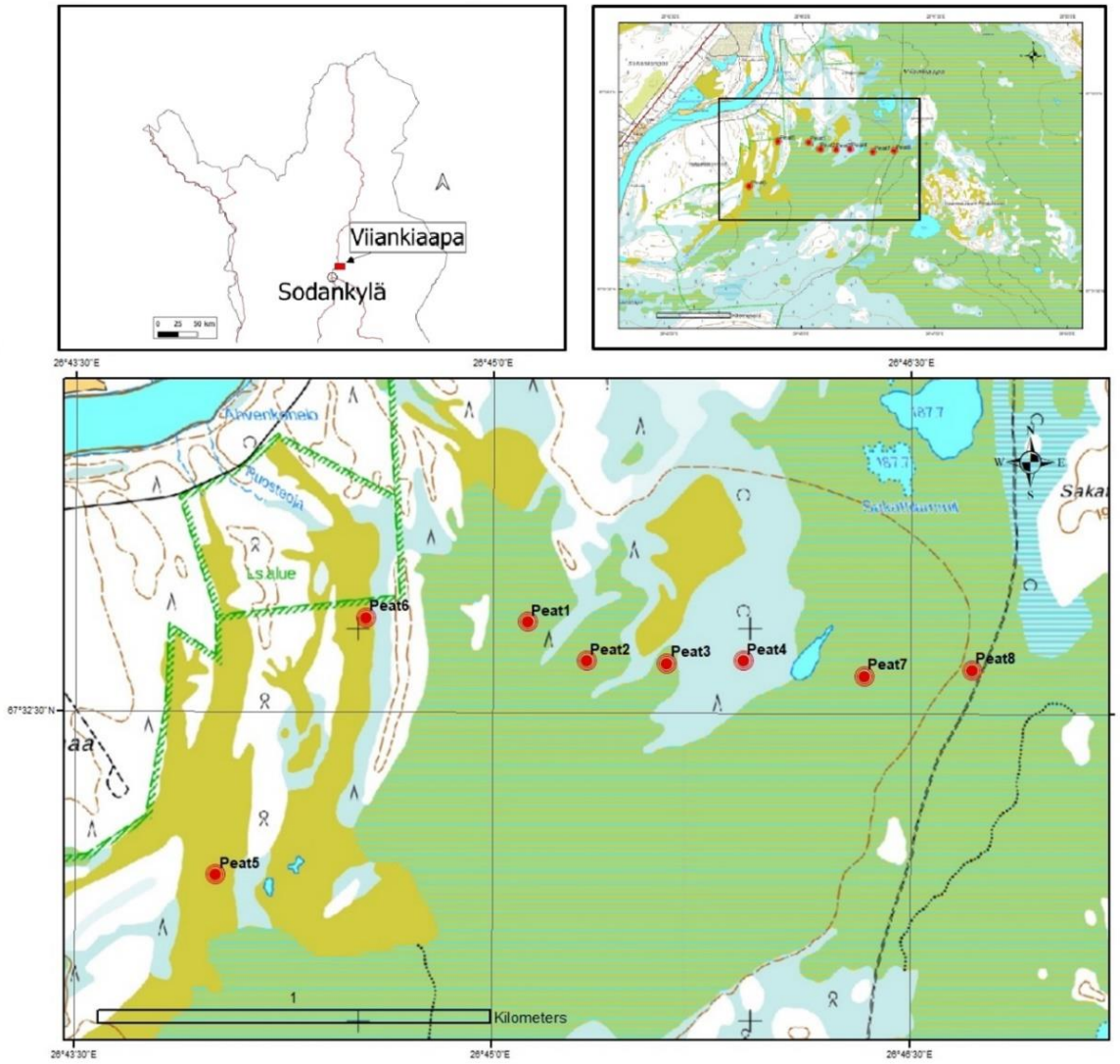

Figure 1: The location of Viiankiaapa in Northern Finland. The sampling points run roughly W–E across the mire.

Viiankiaapa spans over an area more than 65 square kilometres with approximately 35 square kilometres of open fen (Lappalainen 2004). Parts of it have been protected under the mire conservation programme of the nature conservation act since 1988. The vast mire complex consists of meso– eutrophic fen dominated areas, raised bog type areas and some wooded islets formed on paleodunes. Viiankiaapa Natura 2000-area also includes a few ponds and the rather small lake Viiankijärvi (Metsähallitus 2006). The diverseness of the mire complex is reflected on the fauna as well, particularly bird species. There have been 90 species of birds identified in Viiankiaapa, 21 of which are classified as near threatened

or vulnerable (Räinä & Hjelt 2004). In addition, seven vascular plant species and three moss species either near threatened or vulnerable inhabit the area (Metsähallitus 2006). Many of the mentioned species are included in the Birds Directive (2009/147/EC) or the Habitats Directive (92/43/EEC) of the European Union.

Viiankiaapa is located very close to river Kitinen, which has been regulated by Kemijoki Oy from the 1960s. Flooding was a very common feature of river Kitinen in the past, and it may have affected the hydrology of the mire historically (Åberg *et al*. 2017a). It was found in another recent study that the main groundwater flow direction in Viiankiaapa is found to be towards river Kitinen (Åberg *et al*. 2019).

2.1 Geological setting

2.1.1 Bedrock features

The southern parts of Sodankylä municipality are located in the Central Lapland greenstone belt (CLGB). The CLGB is a paleoproterozoic greenstone belt that runs for 200 kilometers roughly east–west from Salla to Kolari (Figure 2a). It is surrounded by archaean granite-gneiss in the east and southwest, Lapland granulite belt in the north and granitic intrusions in the south–southeast (Hanski & Huhma 2005). The CLGB represents rocks that formed during a period of over 500 Ma. The major constituent rocks of the belt are metavolcanic and -sedimentary rocks hosted by an archean granite-gneisses. Multiple layered mafic–ultramafic intrusions have been documented from the CLGB; some have proven interesting sites for ore exploration (Silvennoinen 1997).

The study area and the sampling points are hosted by Sodankylä and Savukoski lithostratigraphic group members (Hanski & Huhma 2005). The sampling points lie on a small Paleoproterozoic picritic volcanic bedrock unit overlying the metasedimentary rocks, aged between 2060–2100 Ma (Figure 2b). Silicate siltstone paraschist lies immidietly to the north, dated 2300–2100 Ma. Further north, a 2300–2100 Ma gabbro belt and a 2100–2060 Ma graphite paraschist are found. The lithological units to the south from the sample points include a 2300–2100 Ma Quartzite body and a mafic vulcanite of similar age (Geological survey of Finland 2017).

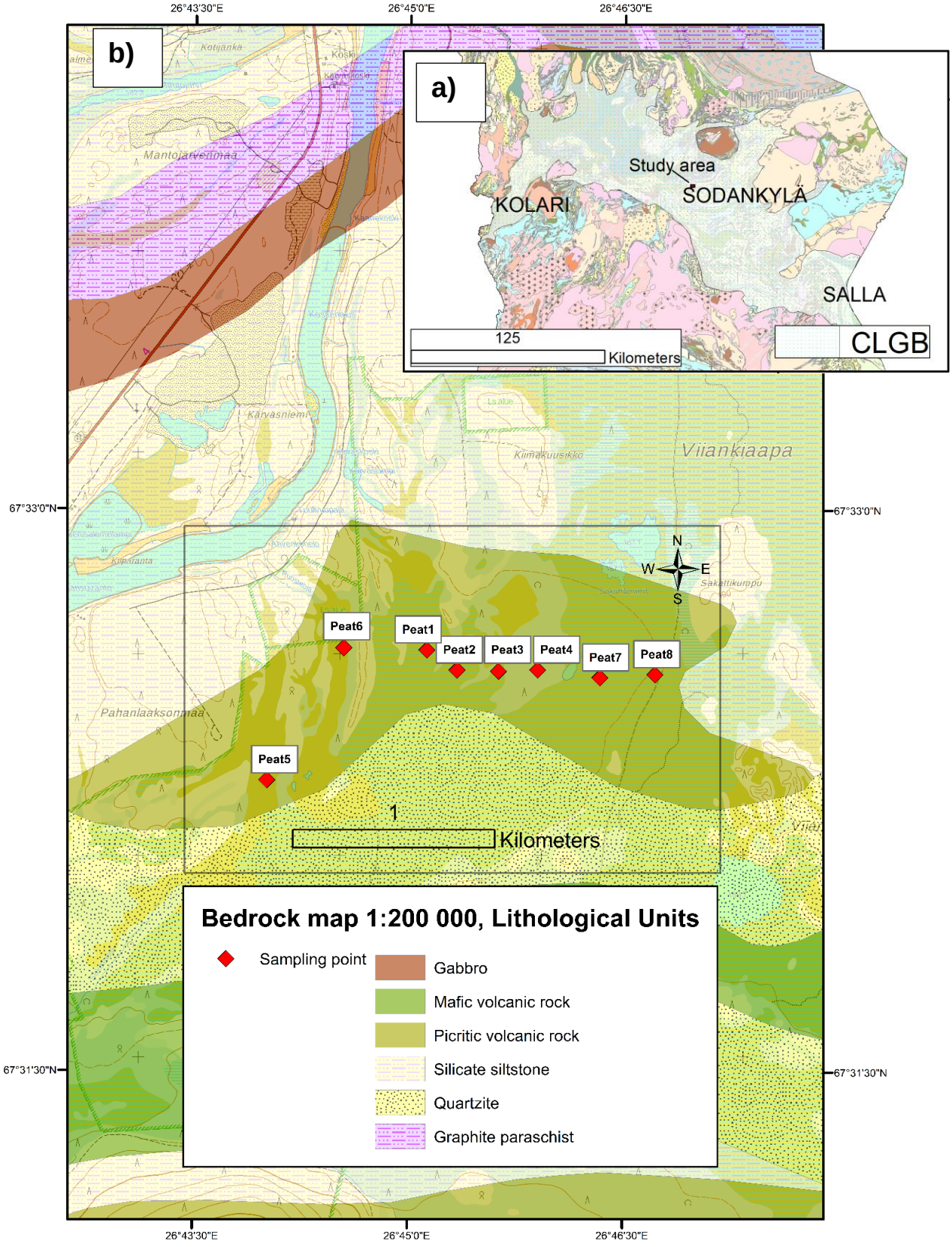

Figure 2: The location of the Viiankiaapa study area withing the Central Lapland Greenstone Belt (a) and the lithological units in the study location (b). The CLGB defined approximately from the description by Hanski & Huhma (2005).

2.1.2 Quaternary deposits

Sodankylä is located in northern Finland; in an area which is called the ice divide zone. The Ice divide zone is where the movement of the ice sheet during the Quaternary glaciations has been very sluggish resulting in low erosion and deposit rates. In many other parts of Finland glacial erosion has shaped the landscape in areas where the ice has flown in stream like fashion. Glacial deposition occurs in the ice margin area as well. Consequent glaciations are not preserved in the ice stream areas. Putkinen *et al*. (2017) presented eight different ice stream lobes in Finland that have been discovered from studying glacial erosional landforms. However, there are areas that get caught in between these flowing ice streams where the ice remains passive. The ice divide zone of Lapland is a similar area, serving as the divide for the flowing ice streams. In places the ice divide zone has preserved five different till units (Hirvas 1991), whereas typically only the most recent till unit is preserved in the rest of Finland. It is also not atypical that glaciofluvial landforms or weathered bedrock are overlain by till units in the ice divide zone (Johansson 1995). Central Lapland had no connection to the Baltic basin and was largely a supra-aquatic environment, where the ice sheet terminated on land (Johansson & Kujansuu 2005). Meltwaters from the ice sheet formed numerous ice-lakes in the area. Glaciofluvial processes have been active and well preserved in the area during the deglaciations.

GTK has published Quaternary maps of the study area; the coverage of the more detailed 1:20 000 map is limited on the western side of the area (Figure 3). This map defines different landforms based on their morphology and material. The more general map is in 1:200 000 scale and it covers the eastern part of the area.

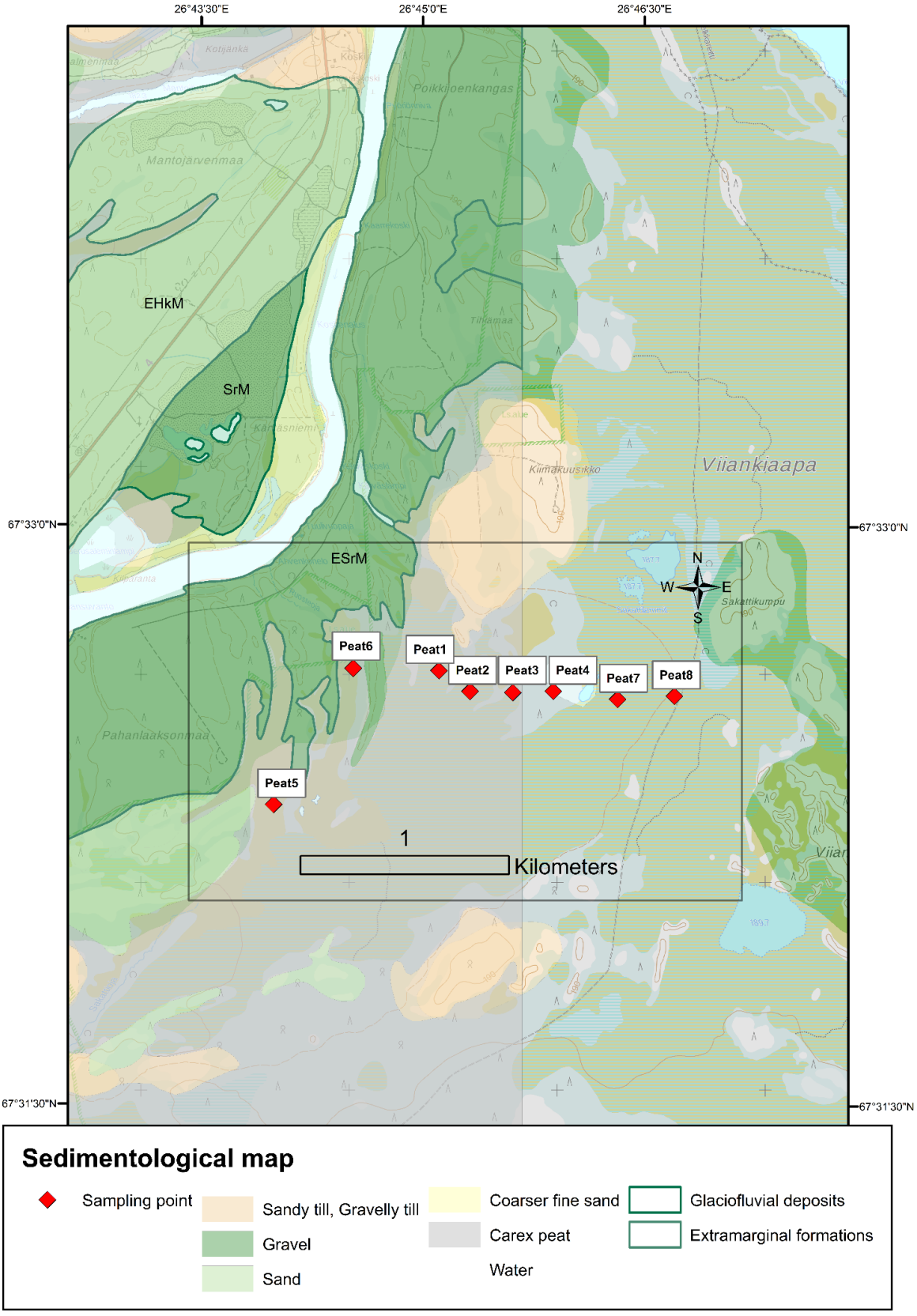

Figure 3: Quaternary deposit map of the study area showing extramarginal sand and gravel formations on the banks of river Kitinen as well as peat and sandy till on the mire area. Created using ArcMap 10.3. Superficial deposit data 1:20 000 and 1: 200 000 from Geological Survey of Finland. Background map, basic map raster, from the National Land Survey of Finland.

The banks of river Kitinen are covered with extramarginal sand and gravel deposits. There is a gravel dominated formation on the western bank of river Kitinen, that is classified a glacial river deposit *e.g.* esker or delta. The mire itself is largely covered by carex/sedge peat with occasional sandy till outcrops as forested areas. The till deposits show no distinct signs of glacial flow but rather seem quite randomly shaped. They stand out from the peat cover by being over 1.5 meters above the peat layer. The mire itself is a relatively flat area, excluding the string and flark patterns and the till outcrops. In the study area, the elevation from the easternmost point (Peat 8) to the westernmost point (Peat 1) declines by only two meters. The mire surface is dipping towards river Kitinen slightly as seen in the topographic profile in Figure 4. Viiankiaapa was covered by Moskujärvi ice-lake after the last deglaciation. Moskujärvi ice-lake was one of many ice-lakes that formed at different parts of Lapland and at different stages of the deglaciation. The level of Moskujärvi ice-lake was 195 m (Johansson & Kujansuu 2005). After the ice sheet had retreated from the area, the water level of the Ancylus-lake was at 186 meters in the area and reached all the way to the southern parts of Viiankiaapa (Johansson & Kujansuu 2005).

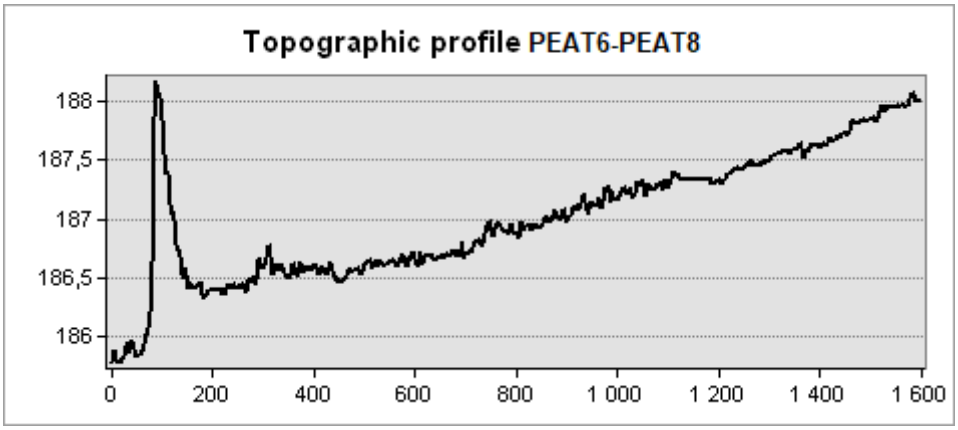

Figure 4: Topographic profile of the mire surface along the sampling points from PEAT6 to PEAT8. The sudden ascend in the profile in the 120m mark results from the sand deposit between sample points peat 6 and peat 1. The level of river Kitinen in the Digital elevation model is 181 meters.

Till covered glaciofluvial deposits have been identified as eskers, deltas/sandurs and drainage channels by Sarala *et al*. (2015) just 15 kilometers south of Viiankiaapa. The OSL dating suggested that the glaciofluvial deposits at some locations were formed during the early Weichselian, whereas the majority of the superficial deposits are of Late-Weichselian age.

The peat studies that were performed in the 1960's and 1970's by Lappalainen & Pajunen (1980) recorded that Viiankiaapa had an average peat depth of 2.29 m with the majority being 1–2m deep. According to their studies, the mire is underlain by a variety of glacial till to fine sediments. The most recent studies from Viiankiaapa used all the previously gathered peat and other data in addition to collecting new data as well in order to create a 3D sedimentological model of the area (Åberg *et al*. 2017a). The model suggested that under the peat there could be three layers of tills and three very discontinuous layers of sorted sediments. Overall, the sediment thickness varied between 0–15 m.

3. MATERIALS AND METHODS

Sampling of groundwater, pore water, and surface water as well as peat took place in the eight pre-determined sampling points. Ground penetrating radar surveys were done by skiing with GPR equipment along the sampling points. All the field work was conducted during two weeks in the winter of 2019. The first field period was between 11.3.2019 and 15.3.2019 and the work involved sampling of PEAT8, PEAT7 and PEAT4. The second field work period was during 1.4–5.4.2019. and this included the sampling of the remaining five sites as well as all the GPR field work.

3.1 Peat samples

Peat samples were collected from each sampling point, a total of 17 samples. The samples typically weighed between 1–2 kg, sampling depth being between 20–300 cm. In attempt to find differences in the hydraulic properties of the peat, the samples were chosen by visually estimating a change in the composition of peat in the core. This was thought to represent a change in the humification degree of the peat or other significant change. The humification degree of peat is one of the main factors affecting the hydraulic conductivity (*e.g.* Päivänen 1973, Quinton *et al*. 2008, Kesäniemi 2009). The humification degree was determined for the whole peat cores *in-situ* using the qualitative Von-Post scale (1–10), where 1 represents least humified peat and 10 most humified. The K-value samples were

not tested separately for their humification degree. Corresponding humification stage for the K-value samples were determined from the entire peat core humification values that were given in the field.

The peat samples for hydraulic conductivity analyses were collected using a Russian peat corer (Figure 5). The instrument is made up of three different parts: The sampler head that encapsulates the sample when rotated, extension rods and a handlebar that allows the sampler head to be rotated and withdrawn. The instrument is hand-operated and manual force is applied to push the sampler into the sediment, this can include the use of hammers or mallets.

Figure 5: A Russian peat corer at sample site PEAT7 with the peat core exposed.

The sampling depths were selected by apparent changes in peat composition, which includes changes in vegetation type, humification, water content and other differences, which are reported separately in the master's thesis of Mimmi Takalo.

3.1.1. Measuring the hydraulic conductivity of the peat

Hydraulic conductivity (K-value [m/s]) was measured at Tampere University during 15.5.2019–12.8.2019 using a rigid wall constant head permeameter test in accordance to ISO 17892-11:2019 standard.

The hydraulic conductivity (K) describes the flow velocity of water through a medium in the direction of the hydraulic gradient (Päivänen 1982). The unit for hydraulic conductivity in this study is m/s. The magnitude of K is controlled by the properties of the fluid and the medium (Eq. 1). The equation for K consists of the volume of water per unit of time (Q), the surface area (s) of the measured flow and the change in hydraulic head, or the hydraulic gradient ($\Delta h/\Delta l$) (Päivänen 1982).

$$K = \frac{Q}{s\frac{\Delta h}{\Delta l}} \quad (1)$$

The amount of water that will flow through a medium (Q) is dependent of the temperature and viscosity of water, the permeability of the medium as well as the hydraulic gradient.

Constant head permeameter test was selected as the method for measuring the hydraulic conductivity of peat. This is a widely used method for soil samples of different varieties. This method is very similar to the one used by Kesäniemi (2009) in her studies of the hydraulic properties of Finnish peats. The equipment consists of a proctor mold that contains the water saturated peat sample, and water is conducted through the mold typically two times with different pressure gradients (Figure 6). As a result, two different hydraulic conductivity values are obtained. The standard for the method (ISO 17892-11:2019) includes a recommendation for the maximum hydraulic gradient that can be used in the test for a given sample. This recommendation varies according to the presumed hydraulic conductivity of the material. The hydraulic gradient was adjusted in

the second test if the first test indicated an unsuitable conductivity for the initially used gradient. Since the viscosity of water is dependent on its temperature, the test results were reported for water temperatures of +20 and +10 °C. The difference between the two different temperature related K-values was noticeable and +10 °C was chosen for use in this work as it is a better representative of groundwater and winter surface water temperatures.

1 Pressure from tap
2 Pressure container
3 Water from tap
4 Float valve
5 Water inflow to sample
6 Digital pressure display
7 Water elevation head tube
8 Screened aggregate
9 Test sample
10 Water outflow from sample
11 Porous stone
H Pressure difference
$\mathbf{t_1}$ Temperature of outflowing water
- - - Filter paper

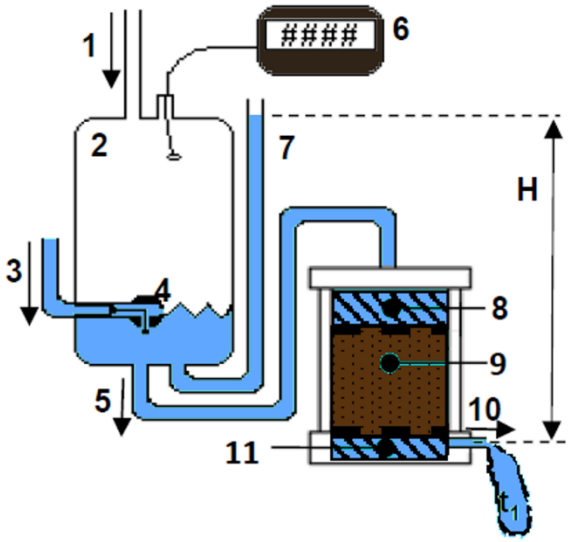

Figure 6: Hydraulic conductivity of peat was measured using a standardised method for soil samples. Water is flown through a peat sample which is placed inside a proctor cell. When the hydraulic gradient is known, water flow is measured against time. Modified from unpublished report, Tampereen teknillinen Yliopisto.

Päivänen investigated hydraulic conductivity of peat using both *in-situ* (1973) and laboratory methods (Päivänen 1968 as referred to in Päivänen 1973). There was a clear conflict between the results from the methods at the time. Laboratory hydraulic conductivities appeared 3–25 times higher than what was attained from the *in-situ* methods. The laboratory methods used in his investigations are different from the one used in the study at hand as well as Kesäniemi's (2009). The method that was used in the study at hand is very close to what was used by Kesäniemi (2009). The variety of peat samples in different humification stages and from different depths was quite large in her study in comparison to this study. The hydraulic conductivities of Sphagnum peat range from $1.39 \cdot 10^{-9}$ to $3.34 \cdot 10^{-5}$ ms^{-1} (Kesäniemi 2009), while sedge and other peat types typically possess higher conductivities (Päivänen 1973).

In addition to the hydraulic conductivity, humification degree, dry and wet densities were also determined for the samples in this study. Päivänen (1973) and others have noted the relationship between the bulk density and the hydraulic conductivity of peat.

3.2 Water Samples

Water samples were collected from peat pores in the surface of the peat layer, in the middle of the peat and from the bottom of the peat layer, with the deepest sample collected from a depth of 404 centimeters. In addition, four snow samples were collected from the snow cover. Before the sample bottles were sealed and contained with the sample, they were rinsed twice with the water that was collected.

Three subsamples were prepared from each depth at each sampling point; these included a trace element analysis sample, a stable isotope analysis sample and a major ion analysis sample total amount of water samples being 28. For the major ionic composition analyses, the volumes of the samples were typically 2 x 60 ml. The trace element samples were pre-filtered with a 0.45 μm membrane filter and collected to a 10 ml vial containing 0.1 ml of HNO_3 in order to preserve the samples. For stable isotopic analyses the sample volumes were 50 ml, with the bottles filled completely in order to inhibit evaporation. Water samples were stored in cool boxes after collection and during transportation and storing.

Before any samples could be taken, the sampling points were first prepared by removing the snow layer with a shovel and exposing the mire surface. Hand operated ice augers were then used to penetrate the frosty top layer of the mire. The exposed surface water immediately under the frost layer was collected with a mini-piezometer connected to a 60 ml syringe. After the surface water was collected, the mini-piezometer was hand driven to the bottom of the peat wherever this was possible, and a water sample from the bottom of the mire was collected; representing either pore water or groundwater. Lastly, the mini-

piezometer was set to a depth between the top and bottom and a pore water sample was taken.

The mini-piezometer is made up of a perforated mesh covered small vessel at the end of a flexible plastic tube (Figure 7). It can be used to measure hydraulic head in different materials saturated under positive pressure (Lee and Cherry 1978 as cited by Rautio and Korkka-Niemi 2011).

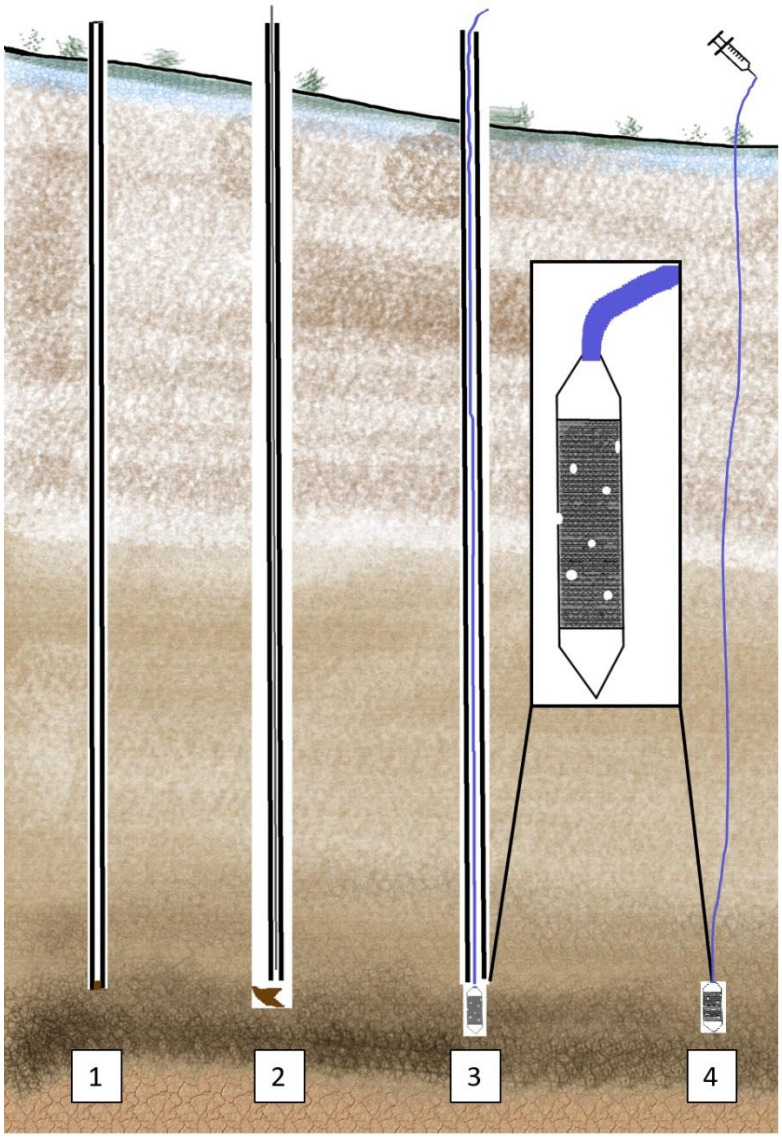

Figure 7: The mini-piezometer water collecting principle. In the first phase (1) a cover tube with a removable plug at the bottom tip is forced into the ground. During the next step (2) the plug is removed from the cover tube and the mini-piezometer is inserted into the cover tube (3). The final stage (4) involves removing the cover tube and forcing water through the tubing using the suction created by a syringe. The mini-piezometer tip is a mesh covered perforated plastic vessel that allows water to flow through it.

Another advantageous property of the device is the ability to collect water samples with very cost-efficient materials from any desired depth. It is very easy to operate; first a stainless-steel cover tube is manually pushed into the material, to which the plastic tube with the perforated vessel is then inserted, and the cover tube removed. When a vacuum is introduced into the open end of the plastic tubing via a syringe for example, water will be collected at a very precise depth in the material (Figure 8).

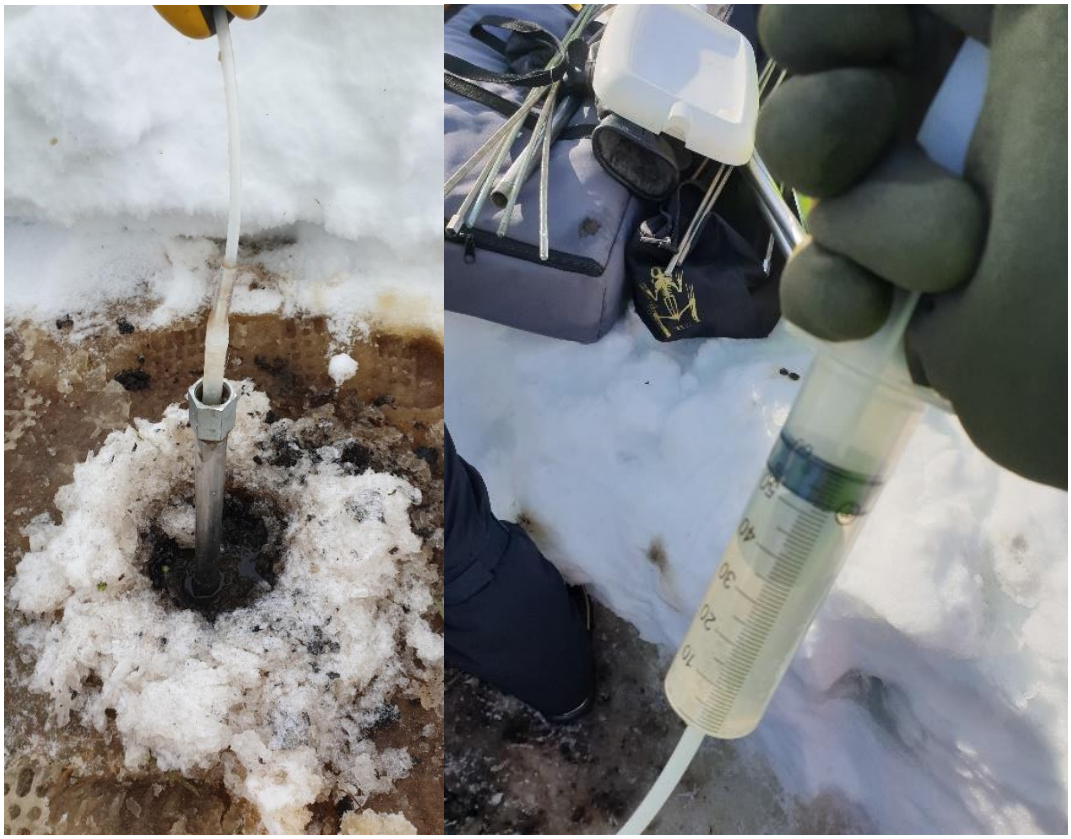

Figure 8: Mini-piezometer is inserted into the cover tube, stage 3 of the procedure. Afterwards, the sample is drawn using a syringe.

The snow cover thickness varied between approximately 80 cm to 30 cm depending on the sampling site. Snow samples from depths of 40–50. 20–30 and 10 cm were collected on March 13th from sampling point PEAT7 using a PVC tube with a 10 cm diameter. In addition, a fresh surface snow sample from PEAT5 was collected on April 4th using a snow shovel. The snow was collected into clean sealable plastic bags. Afterwards, the snow was melted in room temperature and the liquid was bottled, treated and analysed similarly to all other water samples.

During the collection of the water samples, field measurements were carried out using a YSI 600XL multiparameter device. The measured parameters were pH electric conductivity and temperature. This procedure required a relatively large volume of water for the YSI analyser probe. The water was collected to a 400–500 ml plastic container where the analyser head was dipped. The analysed field sample was discarded after the measurement, due to risk of contamination and unstable environment in the plastic container. These measurements were heavily dependent on the hydraulic conductivity of the material from which the water was being collected. In many sampling depths, the field measurements were not completed due to very low hydraulic conductivity of the material, increasing the effort and time required to extract sample, which sometimes resulted in freezing of the mini-piezometer tube.

3.2.1 Chemical analyses of water

The chemical analyses were completed in the environmental laboratory of the department of geoscience and geography of Helsinki University using standardised methods and following the procedures of the laboratory's manual (Virkanen *et al*. 2017). The used analysis methods included the use of standard solutions and blank samples (ICP-MS and IC). Quality control was performed by completing double analyses for random samples and calculating the ionic balance.

One way to classify natural water types is to analyse their major ion composition and classify water types based on the chemical components and their relations. A widely used classification and visualisation technique for water types is the piper diagram, first introduced by Piper (1944) and later developed by e.g Dalton (1978). The major ion components of the samples were analysed using an ion chromatograph (IC) (Metrohm™ MIC-12) with an autosampler to determine Na^+, K^+, Mg^{2+}, Ca^{2+}, Cl^-, NO_3^-, SO_4^{2-} and F^- (SFS-EN ISO 14911, SFS-EN ISO 10304-1). An automatic titrimeter (Titroline 5000) was used to determine the alkalinity (HCO_3^-) of the samples in accordance to the standard SFS EN-ISO 9963 1-2.

There are different amounts of trace elements present in the water samples, which can provide additional information on the hydrological processes undergone by the sampled waters. Trace element analyses included 17 different elements (Al, Si, P, V, Cr, Mn, Fe, Co, Ni, Cu, Zn, As, Se, Mo, Cd, Pb and U) and they were analysed with inductively coupled plasma–mass spectrometer (ICP-MS) (Agilent 7800) according to the standard ISO 17294-2:2003.

Electric conductivity of natural waters is a function of all the dissolved ions present in the water (Lahermo *et al*. 2002), and thus provides a useful first glance in the characteristics of the different waters. Groundwater typically contains more dissolved ions than surface water and has a greater electric conductivity (Lahermo 1970). Anomalous electric conductivity values can be the result of increased groundwater component present in the samples. The hydrogeochemistry of groundwater reflects the chemical composition of the local bedrock in an area. Depending on the type of material in the aquifer, the bedrock signal can vary in strength. Finer material has more water-rock contact area and longer residence times and results in more dissolved solids (Lahermo *et al*. 1990). The residence time effect can be seen in deeper samples from the same aquifer as well.

The electric conductivities for all the samples were measured in Septemper 2020 according to SFS-EN-27888 using a Eutech EcoScan CON 6 hand-held instrument in the environmental laboratory of the department of geoscience and geography of Helsinki University. The measurements required a stable +25°C temperature for the samples. The method in question was also verified with a standard solution and completion of double analyses on random samples.

3.2.2 Stable isotope analyses of water

A water molecule (H_2O) consists of two atoms of hydrogen and one oxygen atom. Both elements are found naturally with varying masses called isotopes. Two stable isotopes exist for hydrogen (^{1}H and ^{2}H) and three for oxygen (^{16}O, ^{17}O and ^{18}O). The heavier isotope of hydrogen is called deuterium (D), and it contains a neutron and a proton in its nucleus. The most abundant isotope of oxygen is ^{16}O and ^{1}H for hydrogen. A water molecule can consist of any combination of these isotopes, the most abundant isotopes

being the main constituents naturally. Molecules with different isotopic compositions are called isotopologues. Water isotopologues differ only in mass, and therefore are prone to fractionation when processes are controlled by the weight of a molecule such as evaporation and condensation. Evaporation favours lighter isotopologues of water for evaporation and this alters the isotopic composition of a water body with time. The isotopic composition of precipitation varies depending on the latitude, altitude, amount of precipitation, season and continental effect (Dansgaard 1964).

The oceans have been studied to show a relatively uniform isotopic composition (Epstein & Mayeda 1953). As ocean water evaporates near the equator, it gets transported as vapor towards the poles where it precipitates depleted in the heavier isotopes according to the climate (Clark & Fritz 1997). Oxygen and hydrogen isotope data are typically presented as ratios of the heavy isotope concentration against the light isotope. The sample ratio is then compared to a known standard, commonly the Vienna standard mean ocean water (VSMOW). The result is a delta value, which is a per mille difference of the isotopic composition of a sample from that of the standard (Clark & Fritz 1997). (Eq. 2)

$$\delta^{18}O_{sample} = \left[\frac{\left(\frac{18_O}{16_O}\right)_{sample}}{\left(\frac{18_O}{16_O}\right)_{reference}} - 1 \right] * 1000 \quad VSMOW \qquad (2)$$

In Finland the isotopic composition of meteoric water follows the local meteoric water line (LMWL), as noted by Kortelainen & Karhu (2004) and Kortelainen (2007a). This trend differs only slightly from the global meteoric water line (GMWL) which was described by Craig (1961). Isotope sample data is often compared to either the local precipitation data or the global. Groundwater forms from precipitation that infiltrates into the ground. Most of the groundwater recharge in Finland happens after the snow melts in spring and in the autumn when evapotranspiration stops. The seasonal differences in isotopic composition of precipitation and surface waters gets mixed up and equalised as groundwater recharges. It follows that the isotopic composition of shallow groundwater resembles the average annual precipitation quite well in Finland (Kortelainen & Karhu 2004). Surface water is always exposed to air and thus prone to evaporation, whereas groundwater cannot evaporate nearly as much. This leads to a remarkable difference in

the isotopic composition of surface water and groundwater and allows the comparison of the isotope data from the samples to that of the local precipitation.

This is done by comparing the obtained analysis results with the global meteoric water line (Craig 1961) and the local meteoric line for Finland (Kortelainen 2007a). If a sample falls directly on the meteoric line it represents shallow groundwater or rainwater. Clear deviations from the meteoric line imply surface water influence. The stable isotope method was used by Rautio & Korkka-Niemi (2011) to detect groundwater-surface water interactions at lake Pyhäjärvi in southwestern Finland, and later in the river Vantaa catchment (Korkka-Niemi *et al*. 2012). These studies showed the scale of groundwater–surface water interactions in Finnish water bodies as well as established many methods for the investigations. The stable isotope analyses were carried out at the GTK research laboratory in Espoo using cavity ring down spectroscopy method (Picarro).

3.3 Ground penetrating radar

Ground penetrating radar (GPR) is a widespread non-destructive geophysical method that utilizes radio waves transmitted to the ground via a transmitting radio antenna. The radio waves propagate with different velocities depending on the electrical properties, mainly electrical conductivity and dielectric permittivity, of the material in question (Reynolds 2011). As the transmitted wave encounters a change in the electrical properties of two different ‘layers’, the wave can be refracted, reflected or scattered. One of the most distinct layers that is usually observed in GPR surveys is the water table, which could be challenging to distinct in a mire setting. Ultimately, all the transmitted waves are received with a receiver antenna and processed for interpretation. The radio waves are attenuated as they propagate further into the ground. Depending on the frequency of the transmitted radio waves, the resolution of the GPR survey can be optimized for desired accuracy. Lower frequency waves propagate further and deeper but result in poor resolution and vice versa (Reynolds 2011). Typical depth range for a GPR survey varies from centimeters to few tens of meters. In the recent 3D-geological model by Åberg *et al*.

(2017a), ground penetrating radar was among other methods that were used to build a very large three-dimensional geological model from the same study area.

GTK started experimenting with GPR on peatlands in 1984, when they started to examine the applicability of the method in Finnish peatlands (Lappalainen *et al*. 1984). Initially, much of the work focused on finding the optimal surveying antenna frequencies for different peatland environments. Early investigations then focused on determining the depth of peat layer. GTK approved GPR as a method to study peatlands, which was then a minor contribution in helping to build the peat inventory of Finland (Hänninen & Lappalainen 1987. Hänninen 1992. Hänninen & Leino 1998). Since then, GPR has been used in Finland for peatland studies involving structural studies of peatlands. Suomi & Mäkilä (2000) achieved very detailed interpretations of their study sites using up to 300 MHz antennas. They even identified the peat stratigraphy with changes in fossil plant matter and fire events. Because the equipment was very bulky and clumsy to operate in the early years, being suitable mostly for vast treeless areas, GPR didn't achieve a widespread use. However, as technological progress has pushed the equipment and software forward, GTK reassessed the methods usefulness for peat inventory investigation again in 2011 (Laatikainen *et al*. 2011).

The GPR survey extends the depth dimension of the sampling cross-section beneath the peat layer of the mire and possibly provides additional information on the influence of the bottom sediments on the hydrology of the mire. The GPR data requires rather extensive processing, and interpretation can be difficult in areas with complex geology or sediment strata inapplicable for GPR method. Reflexw version 9.1.3 was used in this study in processing the GPR raw data. However, the contrast between peat and the sediment below should be clear and the electrical properties of the possible materials are unequal (Table 1). If possible, interpretations of the geomorphology of the sediments are to be made as well as the bedrock level and topography.

Table 1: Electrical properties for the expected geological materials according to (Neal 2004).

Medium	Relative dielectric permittivity (ε_r)	Em-wave velocity (m/ns)	Conductivity (mS/m)
Air	1	0.3	0
Freshwater peat	57–80	0.03–0.06	<40
Saturated sand	20–31.6	0.05–0.08	0.1–1
Saturated sand /gravel	15.5–17.5	0.06	0.7–9
Saturated till	24–34	0.1–0.12	2–5

With given properties, freshwater peat and saturated sand yield a reflection coefficient of -0.2 (Neal 2004). The electrical properties are affected greatly by porosity and water content in clastic and organic sediments.

The equipment that was used in the survey for this study consisted of MALÅ ProEx control unit with two optical modules, MALÅ XV monitor and the 30 and 100 MHz unshielded rough-terrain antennas. Because the surveying was done on skis, acquisition mode for the data was set to time triggered. Simultaneously with the 100 MHz antenna, a 50 MHz antenna was used, but the connection between the antenna and the control unit was faulty and no actual data was collected.

GPR raw data signal contains static and undesired air and ground waves in addition to flaws or unrepresentative data caused by the equipment. There are many different possibilities to enhance desired qualities of the GPR data by processing the signal. For the GPR lines used in this study, the processing of the raw data usually took eight steps (Figure 9).

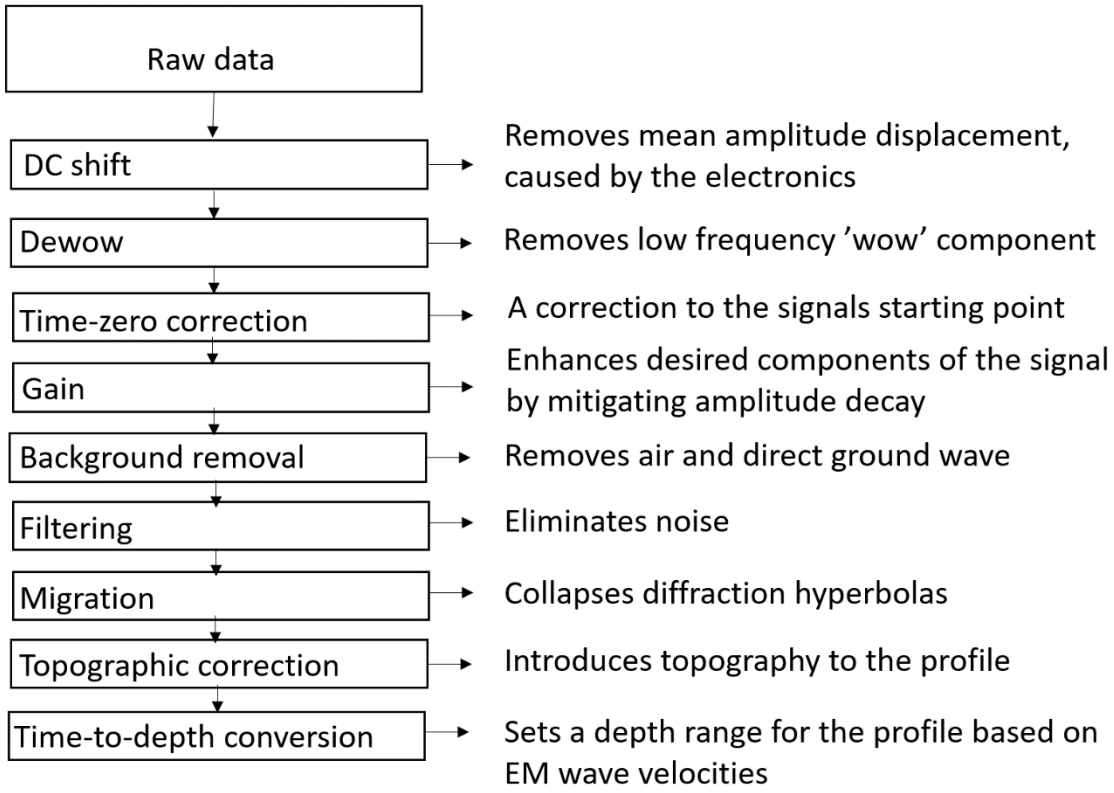

Figure 9: Typical processing flow that is used to process GPR data. the parameters for each step can be individually adjusted for different GPR lines.

For this study, GPR surveys were performed with 30 and 100 MHz antennae. The 100 MHz antenna was used to survey the sampling points excluding peat 5. The total length of the survey line was 1.6 kilometers (Figure 10). The 100 MHz line was surveyed on skis starting from PEAT8 in the east and ending in PEAT6 in the west. The line from PEAT6 to PEAT8 running W–E, was surveyed with a 30 MHz antenna. The lines were almost overlapping.

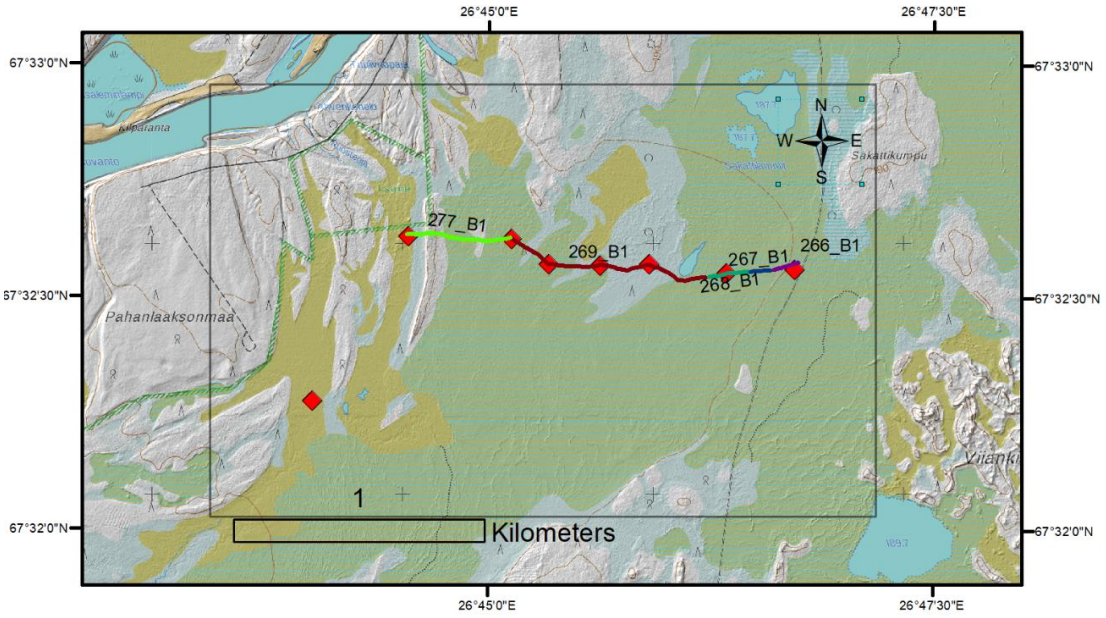

Figure 10: GPR survey line that was done using a 100MHz antenna. The 30MHz line was almost identical.

3.4 Statistical methods

The acquired data involved mainly numeric values with same variables measured for different samples. Large datasets can be made easier to understand when statistical analyses are performed upon it. Some of the analysed samples measured concentrations of elements below the analysing methods detection limit and reported as below detection limit. Statistic calculations require a fixed value for a parameter. In these cases, the censored values were set to be equal to half of the detection limit in question as suggested by Reimann & Filzmoser (2000).

Geochemical/Hydrogeological data are suitable for use in conventional methods of statistical analyses such as hierarchical cluster analysis (HCA), bivariate correlation and principal component analysis (PCA). Often these methods require that the data points are normally distributed. Geochemical data rarely is normally distributed, because it is usually spatially and temporally varied (Reimann & Filzmoser 2000). To test whether a variable was normally distributed, a Shapiro-Wilk test of normality was computed on all the variables (Shapiro & Wilk 1965). The test compares the observed distribution to a normal distribution and yields a percentage of resemblance. This is translated into probability (p) for a random sample to represent a normally distributed group. A null

hypothesis for the test states that a variable is normally distributed. Generally, if $p < 0.05$ the null hypothesis is rejected, and the data is not normally distributed. Whenever the null hypothesis was rejected, a log10 transformation was calculated for the variables in order to achieve normal distribution. Two important variables didn't still display normal distribution (NO_3 and SO_4).

4 RESULTS

The water chemistry analyses were carried out at the University of Helsinki. The major ions, pH and electric conductivity were analysed by the Author and the trace elements were analysed by the department of geoscience and geography environmental laboratory staff. Water isotopes were analysed in GTK, Espoo. Hydraulic conductivities of peat were analysed in the geolaboratory of the University of Tampere.

Data visualisations have been done using Microsoft® excel® for Office MSO (version: 16.0.12527.21230) and IBM® SPSS® statistics version 25. SPSS was used in statistical analyses and in the making of different graphs. Excel was used to create tables as well as graphs and as the data storage. Bivariate correlations represent two-tailed linear correlations (pearson correlation), and the significant correlations are expressed as either * or ** in the text, where single asterix symbolises significance at the 0.05 level and double asterix at the 0.01 level.

4.1 Properties of peat

The K-values ranged between $5.00 \cdot 10^{-7} – 9.80 \cdot 10^{-6}$ ms^{-1} (Table 2). The lowest K-values were observed at PEAT6 and the highest k-value at PEAT7 PEAT6 and PEAT8, which are the western and eastern ends for the survey line, represent the least conductive sampling points. The separate sampling point PEAT 5 also shows low K-value as well as the lower part of PEAT4. The sampling points (PEAT1, PEAT2, PEAT3, PEAT4 and PEAT7) in the middle or the survey line have higher hydraulic conductivities generally.

Humification degree of the peat samples was determined using the qualitative Von-Post scale, apart from samples taken from PEAT5 and PEAT6. The range of humification in the samples used for hydraulic conductivity measurements varied from 3 to 5 (Table 3). Lappalainen & Pajunen (1980) determined the average humification stage in Viiankiaapa to be 4.5, with a clear difference between the surface peat and the bottom.

Table 2: Results from the hydraulic conductivity measurements of the peat samples. K-values are expressed in m/s.

	PEAT1	**PEAT 2**	**PEAT3**	**PEAT4**	**PEAT5**	**PEAT6**	**PEAT7**	**PEAT8**
Depth (cm)	**30–130**	**100–200**	**20–160**	**30–100**	**196–270**	**40–115**	**60–160**	**105–170**
K-value	5.90E-06	6.30E-06	4.90E-06	3.30E-06	8.00E-07	5.60E-07	3.30E-06	1.90E-06
Depth (cm)	**130–230**	**200–300**	**165–235**	**100–130**		**60–115**	**150–250**	**170–205**
K-value	4.00E-06	5.40E-06	1.90E-06	5.60E-07		5.00E-07	9.80E-06	5.70E-07
Depth (cm)							**200–250**	
K-value							5.80E-06	
Depth (cm)							**200–300**	
K-value							6.40E-06	

The humification was determined *in-situ*, separately from the K-value sampling. This resulted in an inconvenience with combining the humification data to the K-value samples. In many cases, it was difficult to give a single humification value for a small sample representing a large peat section. The K-value sample that was ultimately used for PEAT2 (100–200) for example, was approximately 10 cm long and it represents 100 cm of peat in the profile. This profile section showed some variance in humification from 3 to 4. Therefore, it was assigned a humification value of 3.5 in a depth of 150 cm for use in correlations. All the rest of the samples were treated similarly, which unquestionably affects the quality of the humification data. Von Post classification uses only whole numbers and decimals are introduced only to increase the variance of the data and to account for the slight differences in humification that were present in the peat.

The dry density represents the density of the sample being dried after its hydraulic conductivity was measured. There is a moderate statistically significant negative correlation between the dry density and the K-value of the samples (r = -.575*).

Table 3: Humification and dry density of the peat samples.

Sample site	Depth (cm)	Avg. depth	Humification	dry density (kg/m³)
PEAT1	30–130	80	3.0	99.00
PEAT1	130–230	180	3.5	115.00
PEAT2	100–200	150	3.5	94.00
PEAT2	200–300	250	4.2	94.00
PEAT3	20–160	90	3.0	110.00
PEAT3	165–235	200	4.4	99.00
PEAT4	30–100	65	3.0	104.00
PEAT4	100–130	115	3.0	109.00
PEAT5	196–270	232	-	102.00
PEAT6	40–115	77.5	-	134.00
PEAT6	60–115	78.5	-	132.00
PEAT7	150–250	200	3.5	92.00
PEAT7	200–250	225	4.2	90.00
PEAT7	200–300	250	4.2	92.00
PEAT7	60–160	110	5.0	92.00
PEAT8	105–170	137.5	4.0	92.00
PEAT8	170–205	187.5	4.3	104.00

4.2 Composition of water samples

Water samples were analysed from un-preserved samples using ion chromatograph (IC) for Na^+, K^+, Ca^{2+}, Mg^{2+}, Cl^-, NO_3^-, F^- and SO_4^{2-}. In addition, phosphate (PO_4^{2-}) was analysed but it was not present in the samples and therefore, left out of the results. Alkalinity was measured with an automatic titrimeter. Trace elements were analysed from acid preserved and pre-filtered samples with ICP-MS.

4.2.1 Major ions and in-situ analyses

The concentration of fluoride was under the detection limit (0.11 mg/l) in all samples, and the result is omitted from the table. Nitrate concentration was below the detection limit as well in 16 of the 24 samples, and it was decided to be left out of the statistical analyses. Sulphate also had 9 cases where the measured concentration was below the detection limit. In spite of this, sulphate was used in the bivariate correlation, although no interesting correlations were observed.

The *in-situ* analyses involved pH, temperature and electric conductivity measurements. The temperature measurement was declared inaccurate due to the sample collecting process, which involved extracting the water from the peat through a narrow tube with a syringe. Sometimes very small volume of water could be extracted at a time while the collected water was exposed to air temperature for extended periods. After enough water was collected for the YSI multiparameter probe, the temperature didn't reflect the natural state anymore.

The missing values of pH (field) and EC (field) that are presented in Table 4 arise from similar reasons; in some of the sampling locations the amount of water that could be extracted was insufficient for the application of the *in-situ* analyses. To account for this problem, new laboratory measurements of electric conductivity were made in September 2020 (Table 5). One sample (P5_233) contained a very small amount of water and the result for this sample could be unreliable. The two measured electric conductivitites correlate significantly (r = .777**), although their absolute values differ greatly. Field measured electric conductivity is generally significantly higher.

Table 4: Major ion composition and field measurement results of the water samples. Values which are marked with the < symbol represent results that are below the detection level. For the statistical analyses, these were replaced with the value equal to the detection limit.

sample	pH field	pH lab	EC field µS/cm	Na mg/l	K mg/l	Ca mg/l	Mg mg/l	Cl mg/l	NO3 mg/l	SO4 mg/l	Alkalinity mmol/l
p1_pinta	6.22	6.56	120.5	1.65	0.66	8.84	4.96	1.56	<	<	0.89
p1_140	6.42	6.5	168.8	1.64	0.80	9.19	5.08	1.49	<	<	0.94
p1_275	6.55	6.5	179	1.51	0.62	11.18	5.71	1.40	<	0.071	1.07
p2_pinta	-	6.27	-	2.46	2.82	9.53	5.32	1.57	<	3.57	0.91
p2_230	-	6.5	-	0.93	0.27	7.64	2.89	1.16	0.06	<	0.65
p2_404	-	6.14	-	2.13	0.84	15.04	4.44	1.82	0.076	8.36	0.71
p3_pinta	6.2	6.13	147.7	2.29	4.08	7.04	4.07	2.00	<	<	0.93
p3_150	5.96	6.01	183.5	<	<	12.70	5.30	1.15	<	<	1.01
p3_257	5.8	6.3	196.3	1.19	0.45	13.54	5.60	1.15	0.043	0.083	1.11
p4_pinta	6.53	6.52	240	1.78	1.17	10.99	6.74	1.58	<	5.56	1.06
p4_170	6.6	6.4	126.5	1.03	0.29	6.49	3.12	1.21	<	<	0.63
p4_270	6.23	6.45	172.2	1.53	0.56	13.20	6.38	1.10	<	0.065	1.24
p5_pinta	5.3	6.01	177.3	2.07	1.59	9.99	4.17	1.79	<	<	0.86
p5_233	-	6.13	-	1.45	1.10	13.98	4.51	1.36	0.063	<	0.98
p5_307	6.1	5.92	150.6	1.08	0.44	9.80	3.18	1.16	<	0.091	0.74
p6 pinta	5.2	5.34	54.9	0.80	0.54	3.74	1.30	1.38	<	0.081	0.24
p6_110	-	5.49	-	0.72	<	6.38	1.85	0.94	0.09	0.10	<
p6_155	-	5.94	-	1.55	0.29	7.43	2.53	1.03	0.064	0.089	0.6
p7_pinta	5	4.98	50.3	0.73	1.44	2.84	0.90	1.62	<	2.15	<
p7_180	6.25	6.37	233.6	1.58	<	15.79	7.42	0.86	0.11	<	1.42
p7_340	6.22	6.57	212.5	2.76	1.06	13.88	5.62	1.47	<	0.26	1.33
p8_pinta	5.83	5.61	50.8	0.93	0.33	2.72	0.79	1.20	<	0.59	<
p8_159	-	5.88	-	0.92	0.29	2.67	0.75	1.09	0.11	0.12	0.23
p8_263	6.26	6.17	150.2	0.92	<	4.60	1.35	1.27	<	0.078	0.55
detection limit				0.2	0.26	0.2	0.07	0.001	0.04	0.07	0.2

According to Appelo and Postma (2004), the electric conductivity of water can be approximated by Equation 3.

$$E.C. \approx 100 \times meq \sum cations\ or\ anions \quad (3)$$

The newly acquired laboratory electric conductivity values (EC (lab)) correspond with the approximation much more precisely, therefore the field measurements for electric

conductivities were not used in the statistical analyses. The laboratory measured EC-values also displayed normal distribution and no log-transformation was needed.

Table 5: Results of electric conductivity measurements done in September 2020 compared with the field measurements. The table also shows the correspondence of the ionic sum to the different electric conductivity values. The field measurements show a very poor correspondence with the approximation equation.

Sample_ID	EC (field) [µS/cm]	EC (lab) [µS/cm]	$100 \times \text{cat}$	$\frac{100 \times \text{cat}}{\text{EC (lab)}}$	$100 \times \text{an}$	$\frac{100 \times \text{an}}{\text{EC (lab)}}$	$\frac{100 \times \text{cat}}{\text{EC (field)}}$	$\frac{100 \times \text{an}}{\text{EC (field)}}$
p1_pinta	120.5	86.1	93.8	109 %	-94.1	-109 %	78 %	-78 %
p1_140	168.8	89.5	96.8	108 %	-98.9	-111 %	57 %	-59 %
p1_275	179	97.2	110.9	114 %	-111.7	-115 %	62 %	-62 %
p2_pinta	-	111.2	109.2	98 %	-103.5	-93 %		
p2_230	-	57.3	66.6	116 %	-69.0	-120 %		
p2_404	-	112.3	123.0	109 %	-94.2	-84 %		
p3_pinta	147.7	92.1	89.0	97 %	-99.4	-108 %	60 %	-67 %
p3_150	183.5	89.3	108.1	121 %	-105.0	-118 %	59 %	-57 %
p3_257	196.3	100.7	120.0	119 %	-115.1	-114 %	61 %	-59 %
p4_pinta	240	100.7	121.1	120 %	-122.7	-122 %	50 %	-51 %
p4_170	126.5	56.6	63.3	112 %	-67.2	-119 %	50 %	-53 %
p4_270	172.2	114	126.4	111 %	-127.8	-112 %	73 %	-74 %
p5_pinta	177.3	85.1	97.3	114 %	-91.8	-108 %	55 %	-52 %
p5_233	-	60.6	116.0	191 %	-102.6	-169 %		
p5_307	150.6	65	80.8	124 %	-78.1	-120 %	54 %	-52 %
p6_pinta	54.9	39.2	34.2	87 %	-28.7	-73 %	62 %	-52 %
p6_110	-	48.6	50.9	105 %	-61.0	-126 %		
p6_155	-	52.1	65.4	126 %	-63.8	-122 %		
p7_pinta	50.3	38.5	28.4	74 %	-29.7	-77 %	56 %	-59 %
p7_180	233.6	124.9	147.4	118 %	-147.4	-118 %	63 %	-63 %
p7_340	212.5	121.7	130.2	107 %	-138.3	-114 %	61 %	-65 %
p8_pinta	50.8	17.25	24.9	145 %	-25.3	-146 %	49 %	-50 %
p8_159	-	27	24.2	90 %	-27.1	-100 %		
p8_263	150.2	55.1	38.7	70 %	-59.4	-108 %	26 %	-40 %

Another variable that was measured both in the field and in the lab was pH. There is a clear correlation between the two measurements (r = .849**), but in the case of few samples the difference between the two is high. For example, p5_pinta and p3_257 where the difference in pH measurements is 0.71 and 0.5 respectively. In general, pH (lab) yielded higher values in the samples. The arithmetic mean of pH (field) is 6.04 while the arithmetic mean of pH (lab) for the same samples that were measured in the field is 6.14.

The snow samples had concentrations below detection limits for all major ions excluding chloride, sulphate and nitrate (Table 6). Every snow sample contains detectable chloride, but sodium is absent. The method detection limit for sodium using the IC was 0.2 mg/L. Snow samples had a relatively low pH, lower than in all the peat water samples. The pH in precipitation measured at Sodankylä observatory in March of 1998 was 4.7 and 4.36 in April (Vuorenmaa *et al*. 2001).

Table 6: the major ion and selected trace element results from the snow samples. Trace element concentrations are reported in ppb. Numbers have been rounded in order to fit the page.

sample	pH lab	Na	K	Ca	Mg	Cl mg/L	NO3 mg/L	SO4 mg/L	alk.	P	V	Mn	Fe	Ni	Cu	Zn	Cd	Pb
pintalumi	5.01	<	<	<	<	1.04	0.14	0.27	<	19.8	0.05	0.3	1.9	0.04	0.1	1.3	0.001	0.004
lumi10	4.82	<	<	<	<	0.89	0.37	0.29	<	15.2	0.03	0.3	1.5	0.08	0.1	4.2	0.003	0.05
lumi2030	4.87	<	<	<	<	1.00	0.2	0.26	<	14.8	0.03	0.2	0.7	0.07	0.2	0.8	0.001	0.008
lumi4050	4.81	<	<	<	<	0.96	0.25	0.30	<	14.3	0.06	0.4	1.5	0.2	0.2	2.1	0.04	0.02

The measured concentrations for the major ions are very low in almost all samples. This created a situation where the electroneutrality of a few samples was heavily dependent on the accuracy of the alkalinity analysis. The automatic titration method has a reported detection limit of 0.2 mmol. By using the replacement method suggested by Reimann & Filzmoser (2000) for values that were under the detection limit, the samples generally showed some cation excess. In this method, those measured concentrations that are under the method detection limit are replaced with one half of the detection limit. In order to make the samples in this study more electroneutral for more realistic representation of natural waters, the major ion results where the measured concentrations were under the detection limit were replaced with a value equal to the detection limit. This affects mainly sulphate as it contains 9 cases of concentrations below detection limit.

Greatest variance is seen in the concentrations of calcium, which is also the dominant cation in the samples. Least variance is observed in chloride (Table 7). Of all samples, sample p2_404 shows highest concentrations of SO_4 as well as high concentrations of Ca, Cl and Na. This sample represents the deepest of all samples gathered for this study (404 cm deep). Sulphate exhibits neither normal or log-normal distribution, this is evident by the large difference in the mean and median values. There were 9 replacements done for the missing values in sulphate though.

Table 7: Descriptive statistics of the major ion components for mire water.

	pH lab	Na mg/l	K mg/l	Ca mg/l	Mg mg/l	Cl mg/l	SO4 mg/l	Alkalinity mmol/l
Mean	6.11	1.41	0.84	9.13	3.92	1.35	0.90	0.79
Median	6.16	1.48	0.55	9.36	4.31	1.31	0.08	0.88
St.dev	0.42	0.63	0.92	4.06	2.01	0.29	2.08	0.35
Range	1.59	2.66	3.95	13.12	6.67	1.15	8.32	1.22
Min.	4.98	0.10	0.13	2.67	0.75	0.86	0.035	0.20
Max.	6.57	2.76	4.08	15.79	7.42	2.00	8.36	1.42

4.2.2 Trace elements

The highest mean concentration (21.1 ppm) of all trace elements is found in iron (Table 8). Iron also displays the widest range in concentrations. In fact, iron concentration exceeds the background concentrations presented by Lahermo *et al*. (1990 and 1996) in groundwater and flowing surface waters by a very large margin. The arithmetic mean concentration for iron in the study at hand is very different from Lahermo *et al*. (1990), where they report a mean value of 0.53 ppm in groundwaters from dug wells and a typical range for flowing streams as 0.06 – 2.6 ppm (Lahermo *et al*. 1996). Earlier geochemical investigations from Viiankiaapa show similar results that were discovered in this study (Lahtinen 2017, Bigler 2018).

Uranium and Cadmium are present in the lowest concentrations in the samples (Table 9). There are no samples with anomalous Cu or Ni concentrations that could possibly serve as tracers from the sulphide ore beneath the mire, apart from p2_404 which shows slight nickel excess (9.5 ppm) of the groundwater background concentration (mean: 8.6 ppm) by Lahermo *et al*. (1990). The background values for Ni and Cu are not specified for different lithological environments and the distribution of them in Finnish groundwaters seems not to be controlled by geology in any known way (Lahermo *et al*. 1990).

Table 8: Trace element concentrations of the water samples. All values are in ppb, except for Si, Mn and Fe (ppm). The values are rounded to include only one decimal. More precise results are found in Appendix 1.

Sample	Al	Si	P	V	Cr	Mn	Fe	Co	Ni	Cu	Zn	As	Se	Mo	Cd	Pb	U
p1_pinta	16.8	6.4	28.0	0.1	0.7	0.2	11.3	1.0	0.3	0.1	4.8	1.1	0.02	<	0.06	0.06	<
p1_140	2.4	7.5	91.4	0.1	1.2	0.3	25.7	2.5	0.7	0.2	6.1	1.7	0.03	0.03	0.005	0.01	<
p1_275	49.1	7.1	66.5	2.1	2.6	0.4	25.7	3.1	1.6	0.5	35.7	1.8	0.03	0.02	<	0.04	0.008
p2_pinta	<	8.7	141.1	0.2	1.3	0.3	17.7	1.7	0.6	0.2	6.9	0.7	0.02	0.02	0.01	0.03	0.001
p2_230	3.5	4.0	125.2	0.1	0.6	0.3	20.2	2.6	1.3	0.3	9.3	1.6	0.02	0.06	0.01	0.01	0.002
p2_404	57.1	5.9	56.0	4.5	8.8	0.4	30.7	5.3	9.5	1.1	615.1	43.3	0.03	2.1	0.02	0.16	0.03
p3_pinta	19.1	6.7	161.1	0.2	0.8	0.1	20.6	1.5	1.1	0.4	12.5	1.7	0.04	0.07	0.02	0.14	0.001
p3_150	20.2	3.8	232.5	0.2	0.5	0.3	28.8	2.7	0.8	0.1	7.1	3.4	0.03	0.01	0.06	0.01	<
p3_257	68.5	6.4	51.9	3.6	4.1	0.3	29.7	3.1	2.3	0.2	136.7	1.3	0.03	0.05	0.04	0.02	0.02
p4_pinta	46.8	7.8	105.7	1.5	2.9	0.2	17.1	1.4	1.0	0.1	13.8	1.3	0.02	0.04	0.006	0.01	0.006
p4_170	9.1	4.7	153.5	0.2	0.6	0.2	20.3	1.8	0.3	0.1	2.6	1.8	0.02	0.01	<	0.00	0.001
p4_270	46.8	8.0	106.9	1.5	2.9	0.2	17.3	1.4	0.9	0.1	11.6	1.3	0.02	0.03	0.01	0.01	0.005
p5_pinta	<	7.7	165.9	0.1	1.1	0.3	25.3	2.0	1.1	0.5	12.7	2.7	0.02	<	0.009	0.01	0.009
p5_233	11.7	5.3	74.8	1.5	1.8	0.3	35.0	2.8	2.4	0.3	87.5	5.2	0.04	0.1	0.2	0.04	0.02
p5_307	60.2	5.8	109.6	5.2	4.1	0.2	25.3	2.0	1.3	<	14.8	2.1	0.03	0.03	0.003	0.01	0.008
p6_pinta	16.2	6.0	192.9	0.05	0.3	0.1	5.5	1.0	1.5	0.6	5.1	1.0	0.03	0.09	0.03	0.04	<
p6_110	27.7	6.2	144.9	1.3	3.3	0.2	21.1	1.3	2.8	3.1	15.1	1.6	0.03	0.1	0.02	0.1	0.007
p6_155	81.0	7.0	66.7	5.7	6.9	0.2	26.5	1.5	3.2	1.6	63.5	2.2	0.04	0.1	0.04	0.1	0.02
p7_pinta	3.9	3.4	224.3	0.1	0.6	0.04	7.1	0.5	0.5	0.4	7.5	0.8	0.03	<	0.02	0.07	<
p7_180	<	5.0	59.0	0.1	0.8	0.3	32.5	1.3	0.5	0.1	3.7	1.5	0.01	0.01	<	0.01	0.001
p7_340	17.2	13.0	221.7	5.6	10.4	0.2	26.2	0.7	1.3	0.2	34.8	2.3	0.03	0.1	0.01	0.03	0.01
p8_pinta	7.4	4.3	61.5	0.1	0.7	0.04	8.1	1.2	0.4	0.3	6.6	0.4	0.03	0.01	0.02	0.04	0.002
p8_159	19.9	1.9	84.7	0.2	0.8	0.1	6.6	1.8	0.9	0.7	36.1	0.9	0.02	0.03	0.009	0.1	0.005
p8_263	86.3	7.2	43.8	4.9	2.6	0.1	22.1	5.2	1.1	0.3	43.3	1.1	0.04	0.04	0.004	0.02	0.01
detection limit	1.50	0.003	1.0	0.002	0.02	0.00006	0.0003	0.002	0.03	0.06	0.05	0.01	0.01	0.005	0.002	0.003	0.001

Table 9: Descriptive statistics of the trace element analyses. Values are in ppb, except for Si, Fe and Mn (ppm).

	Al	Si	P	V	Cr	Mn	Fe	Co	Ni	Cu	Zn	As	Se	Mo	Cd	Pb	U
Mean	28.1	6.2	115.4	1.6	2.5	0.2	21.1	2.1	1.6	0.5	49.7	3.5	0.03	0.1	0.02	0.05	0.01
Median	18.1	6.3	106.3	0.2	1.2	0.2	21.6	1.7	1.1	0.3	12.6	1.6	0.03	0.03	0.01	0.03	0.005
st.dev	26.9	2.2	60.8	2.1	2.7	0.1	8.4	1.2	1.9	0.7	124.5	8.6	0.01	0.4	0.04	0.05	0.01
range	85.6	11.1	204.5	5.6	10.0	0.4	29.5	4.8	9.3	3.1	612.5	43.0	0.03	2.1	0.2	0.2	0.03
min.	0.8	1.9	28.0	0.0	0.3	0.04	5.5	0.5	0.3	0.0	2.6	0.4	0.01	0.003	0.001	0.005	0.001
max.	86.3	13.0	232.5	5.7	10.4	0.4	35.0	5.3	9.5	3.1	615.1	43.3	0.04	2.1	0.2	0.2	0.03

4.2.3 Stable isotopes of oxygen and hydrogen/ $\delta^{18}O$, $\delta^{2}H$ and d-excess

The sample with the most positive values of $\delta^{18}O$ and $\delta^{2}H$ is p8_159 while p3_pinta has the most negative values (Table 10). The snow samples have values far more negative than the water samples. There is also a wide range in d-excess values, possibly adding to the complexity of interpreting the hydrology of the study site based on these results.

Table 10: The measured delta values of all the water samples and the calculated d-excess values for the samples.

Sample	$\delta^{2}H$, ‰ VSMOW	$\delta^{18}O$, ‰ VSMOW	d-excess
p1_pinta	-102.36	-13.32	4.2
p1_140	-96.41	-12.4	2.79
p1_275	-95.04	-12.19	2.48
p2_pinta	-96.99	-12.50	3.01
p2_230	-85.92	-10.87	1.04
p2_404	-85.55	-10.86	1.33
p3_pinta	-104.88	-13.72	4.88
p3_150	-86.80	-11.20	2.8
p3_257	-88.80	-11.50	3.2
p4_pinta	-95.23	-12.40	3.97
p4_170	-89.35	-11.43	2.09
p4_270	-92.41	-11.99	3.51
p5_pinta	-99.93	-13.28	6.31
p5_233	-99.49	-13.00	4.51
p5_307	-95.98	-12.54	4.34
p6_pinta	-94.33	-12.48	5.51
p6_110	-91.70	-12.56	8.78
p6_155	-90.26	-12.14	6.86
p7_pinta	-93.98	-13.34	12.74
p7_180	-97.75	-12.72	4.01
p7_340	-93.87	-12.07	2.69
p8_pinta	-88.50	-11.34	2.22
p8_159	-83.92	-10.32	-1.36
p8_263	-94.73	-12.12	2.23
pintalumi	-153.09	-20.51	10.99
lumi10	-150.95	-19.79	7.37
lumi2030	-167.79	-21.99	8.13
lumi4050	-143.20	-18.84	7.52

Deuterium excess (d-excess) value is a dimensionless second order quantity that is often used to trace past precipitation and to analyse the moisture source for current

precipitation. First described by Dansgaard (1964) and since then used in countless climatic and hydrological studies (*e.g.* Froehlich *et al*. 2002, Kortelainen & Karhu 2004, Kortelainen 2007a, Rautio 2015). The definition for d-excess is shown in Equation 4.

$$d = \delta^2 H - 8\delta^{18} O \quad (4)$$

For global average precipitation, the d-excess value is 10‰ following the global average relation of deuterium and ^{18}O in precipitation described by the global mean water equation (Eq 5).

$$\delta D = 8 \times \delta^{18} O + 10‰ \quad \text{(Craig 1961)} \quad (5)$$

D-excess-value in precipitation records the humidity and temperature conditions of the source and is frequently used as past temperature proxy in ice core studies for example (*e.g.* Jouzel *et al*. 2005). D-excess variability arises from non-equilibrium fractionation near the moisture source (Pfahl & Sodemann 2014) and evaporation events after precipitation.

Samples with d-excess value close to 10 should represent precipitation in temperate climates while d-excess values above 10 result from mixing of an airmass with a more evaporated water content (Kendall & Coplen 2001). In the case of this study, most of the d-excess values are in fact considerably lower than 10. Values under 10 reflect water that has undergone fractionating evaporation after its initial precipitation.

4.3 Ground penetrating radar

A two-layer EM-wave velocity model was used in the depth conversion for the peat material and sediments below the peat. Neal (2004) listed EM-wave velocities for different geologic materials. The EM-wave velocity for peat (0.04 m/ns) was chosen from the mentioned article. The unknown sediments were assumed to have an EM-wave velocity of 0.1 m/ns, which represents saturated till and is close to saturated sand as well. The velocities that were chosen, result in a decent estimation of real depths. For example, at PEAT8 the bottom sediment was reached with the mini-piezometer at approximately

260 cm and the GPR interface lies at the same depth (Figure 11). The 100 MHz showed much more detail in the structure of the peat as well as some morphology in the clastic sediments compared to the 30 MHz. The 30 MHz antenna was mainly used in an attempt to find bedrock reflections and to enhance the depth penetration at more unclear parts of the profile.

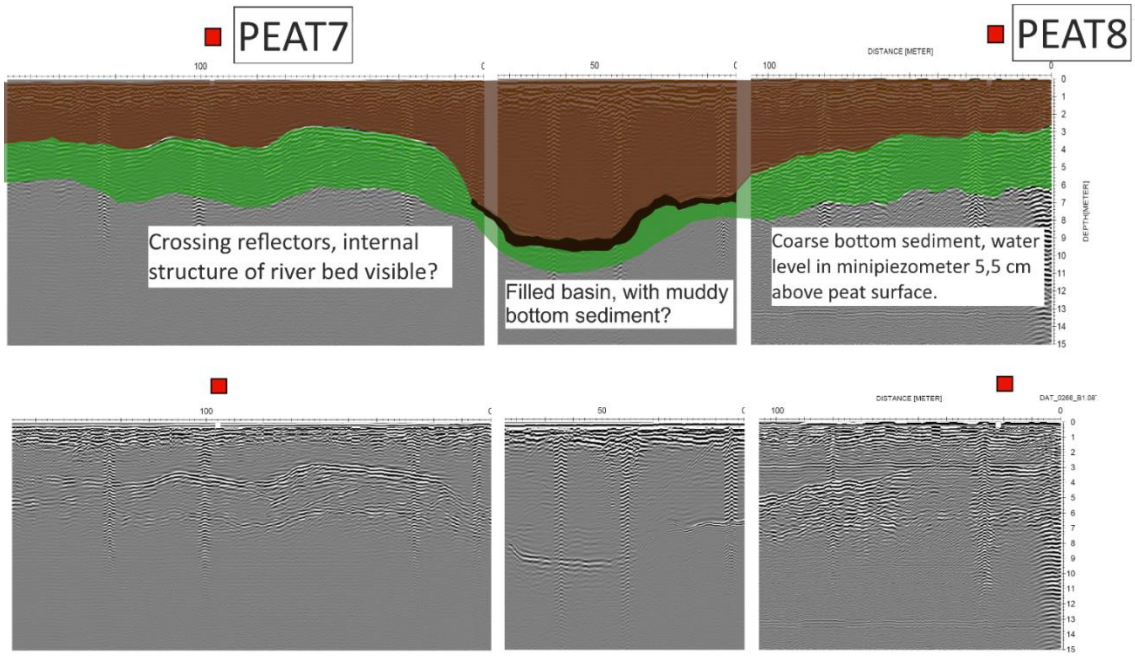

Figure 11: An extract of the interpreted GPR profile showing the two-layer concept with added mud layers. Top layer (brown) illustrates peat, and the bottom layer (green) sorted glaciofluvial sediments (sand/gravel). Lower profile is the processed but not interpreted data.

The surface topography along the GPR profile is straightforward, gently dipping slope towards river Kitinen. The bottom of the mire, on the other hand, showed a lot of variation in its topography. It was possible to distinguish at least three deeper basins as well as some very shallow areas with very little peat. The conceptual stratigraphic cross-section that was created was based on the GPR results combined with field observations regarding the peat and sediment properties. There seemed to be internal layering in peat, which could be identified with the 100 MHz antenna. However, this has not been considered in the larger scale interpretation. The difference in the electric properties of peat, can arise due to change in humification stage, fossil plant material species and changes in pore water chemistry (Suomi & Mäkilä 2000).

Most of the clastic sediments that were detected, were interpreted as sorted (sand/gravel) glaciofluvial sediments. In some parts, most notably underneath PEAT7, a cross bedded

structure could be seen suggesting a flowing medium was present during its formation. This is strongly supported by the previous study by Åberg *et al*. (2017) where they argue for braided river system sediments present beneath Viiankiaapa. At few locales, the continuous reflectors from the peat and sand/gravel were disrupted by a dense collection of discontinuous reflectors, which were interpreted as till deposits (Figure 12). The till deposits had very different vegetation on the surface with growing trees in abundance. This is also visible in aerial photographs from the area (Figure 13).

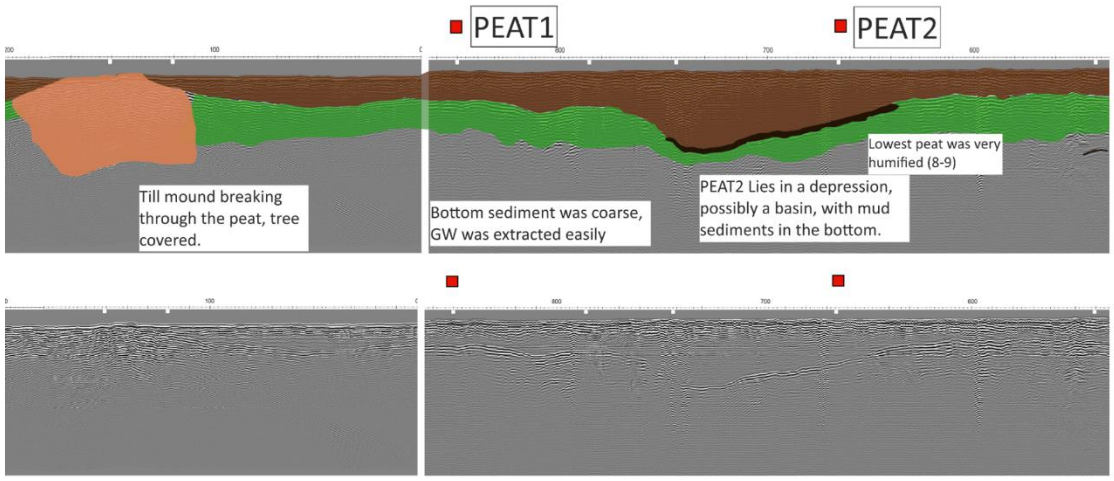

Figure 12: Till deposits on the western and eastern side of PEAT1. The western till deposit is distinguishable from aerial photograph as well.

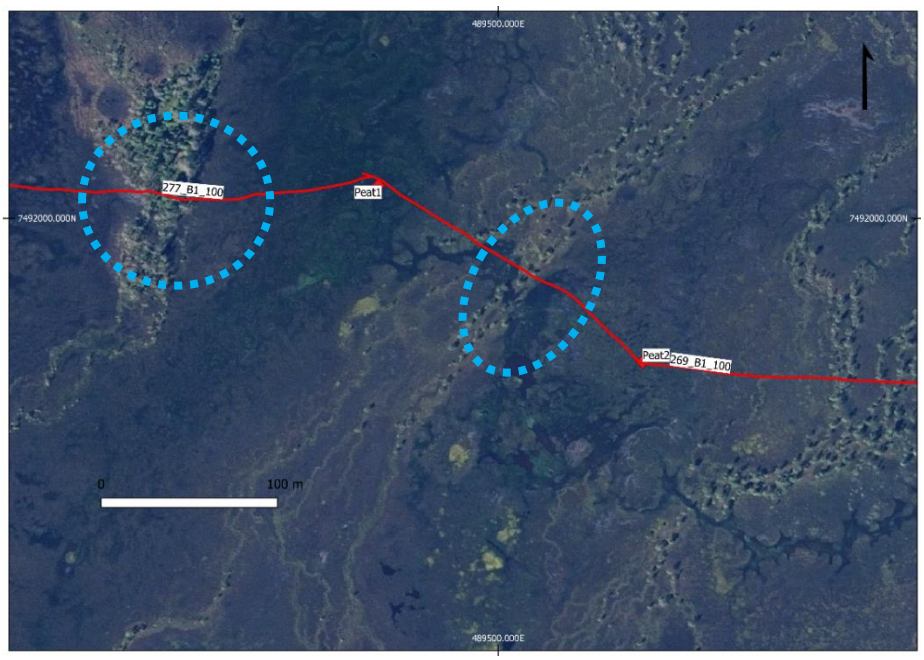

Figure 13: Aerial photograph along the GPR profile. There is a tree covered mound to the west of PEAT1. A long continuous string of trees can be seen between PEAT1 and PEAT2. which is not as clear in the GPR data, but still visible.

5 DISCUSSION

5.1 Properties of peat and the underlying sediments

The general trend for the sampling sites individually seems to indicate that as depth increases, K-value decreases, with an exception at PEAT7 (Figure 14). However, the combined correlation of K-value and depth between all sampling sites was not as clear as the scatterplot shows (Figure 15). Interestingly, the outermost sampling points have lowest K-values (PEAT6 and PEAT8). They both seem to locate on the rim of a depression in the sediments, as the GPR shows. Water sampling results also show very little groundwater tracers, these are locations where peat possibly acts as an aquiclude.

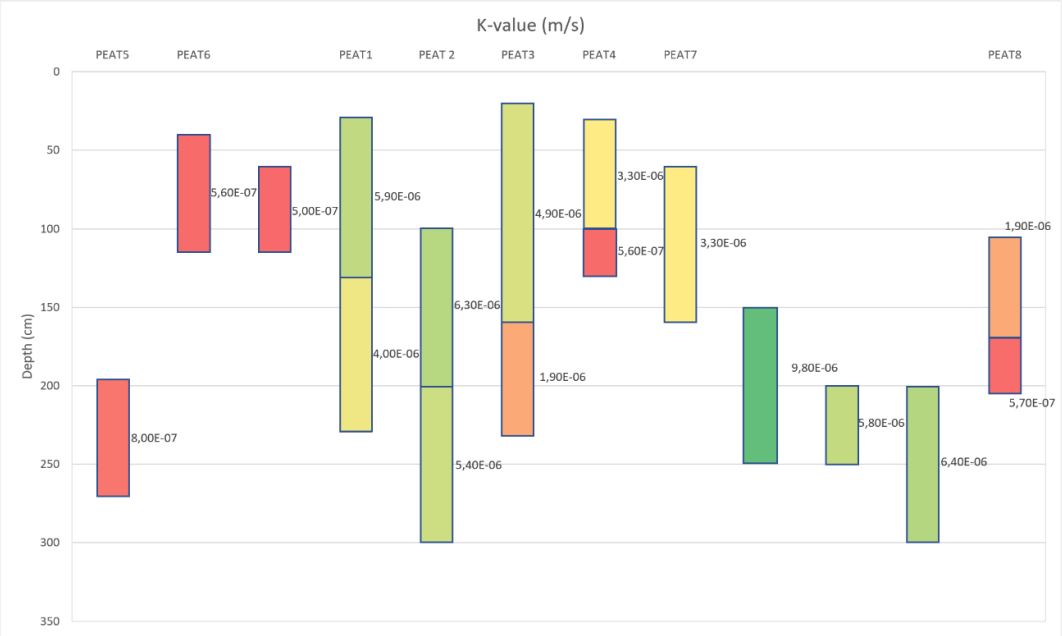

Figure 14: The measured K-values plotted as a bar chart in relation to depth. The colour of the bars indicate the magnitude of the k-values and the bar length corresponds to the sample size. Red colour marks low K-value while green marks high K-value. On individual sites, the K-value gets lower with increasing depth, with an exception at PEAT 7 where the situation is more complex. Sampling points are arranged similarly to their locations in the field.

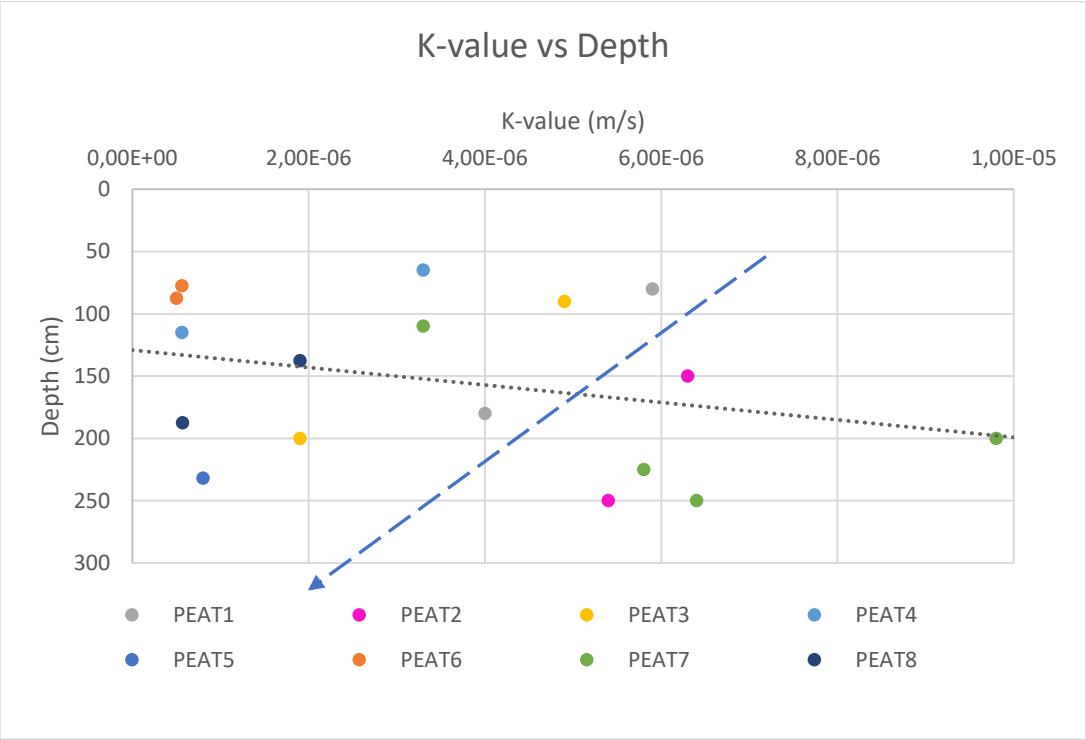

Figure 15: Scatterplot showing the relationship of the measured K-values with depth. The depth values used in the plot were calculated as mean depth values of the samples, since the real samples represented a wide section of the peat profile. The correlation is very poor and shows opposite trend from what is usually expected. The blue dotted arrow describes the trend within individual sampling points, with this inspection, the K-value was observed to decrease as depth increased.

Even though the determination of humification degree was not one of the goals for this study, and the detected changes in humification degree didn't coincide very well with the collected K-value samples, there is a clear correlation between humification and depth (Figure 16). This has been reported in numerous other studies as well, Päivänen (1973) for example.

The same study by Päivänen (1973) and studies by Sarasto (1963), Quinton *et al*. (2008) and Mustamo *et al*. (2016) bring forth a lot of evidence for the relationship between humification degree and hydraulic conductivity of peat. However, in the study at hand, no such correlation was observed (Figure 17). The Pearson correlation coefficient between humification and K-value was regarded insignificant. This could be the result of real hydrological properties in the peat, but potential error sources for these results are plentiful: analytical errors, sample generalisation or the low number of samples and analyses.

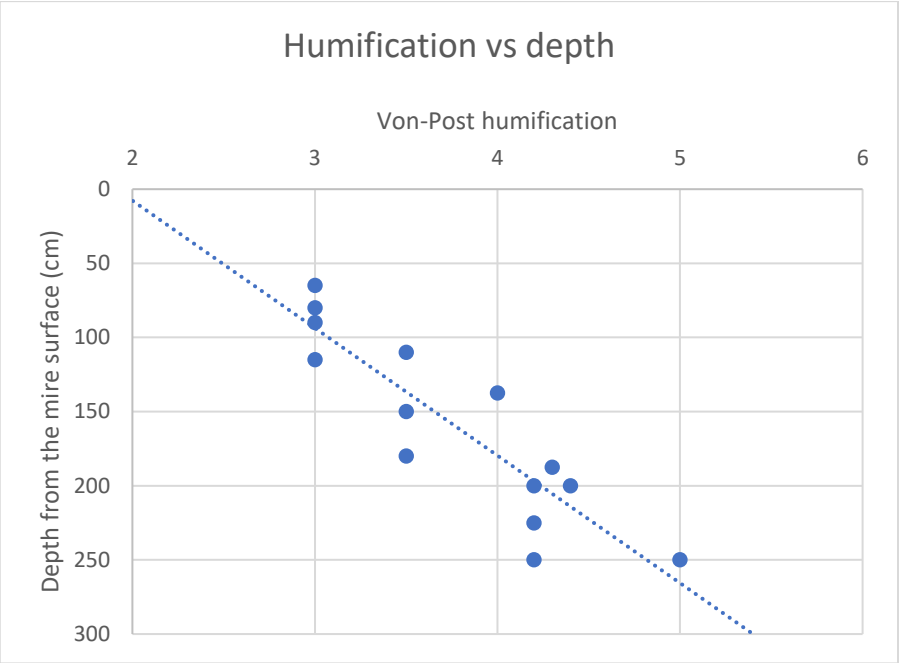

Figure 16: Correlation of Von Post humification and depth. Correlation coefficient (r =,554*) shows significant correlation between the two ($p<0.05$).

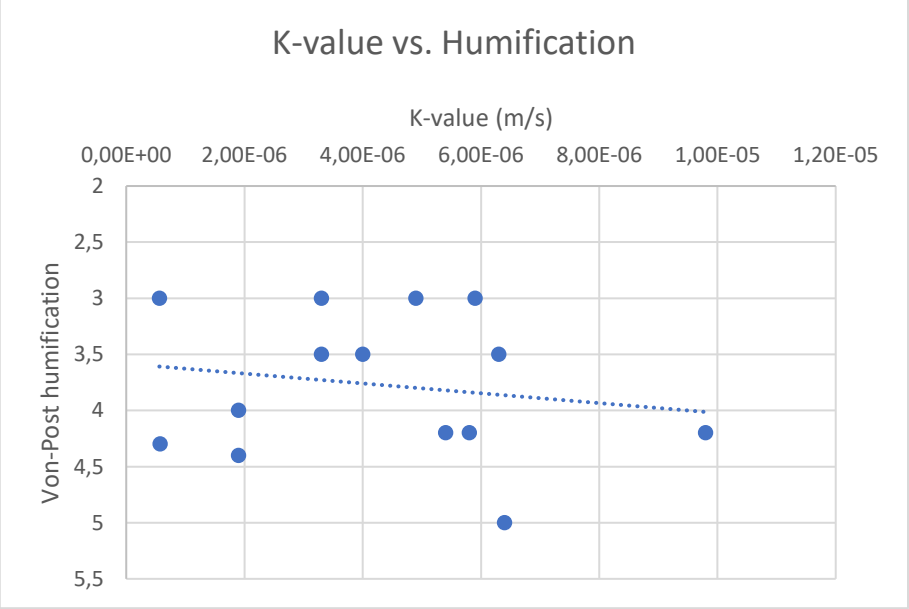

Figure 17: The comparison between humification and K-value. There is no true correlation observed.

When the dry density of the peat samples is compared to the K-value (Figure 18), a statistically significant ($p<0.05$) negative correlation is observed (r = -.575*). This result is consistent with the results recorded by Päivänen (1973). In his paper he reported correlation coefficients of K and bulk density for Sphagnum peat (r = -.714**), sedge

peat (r = -.359), woody peats (r = -.115) and a combined number for all the material as r = -.409**.

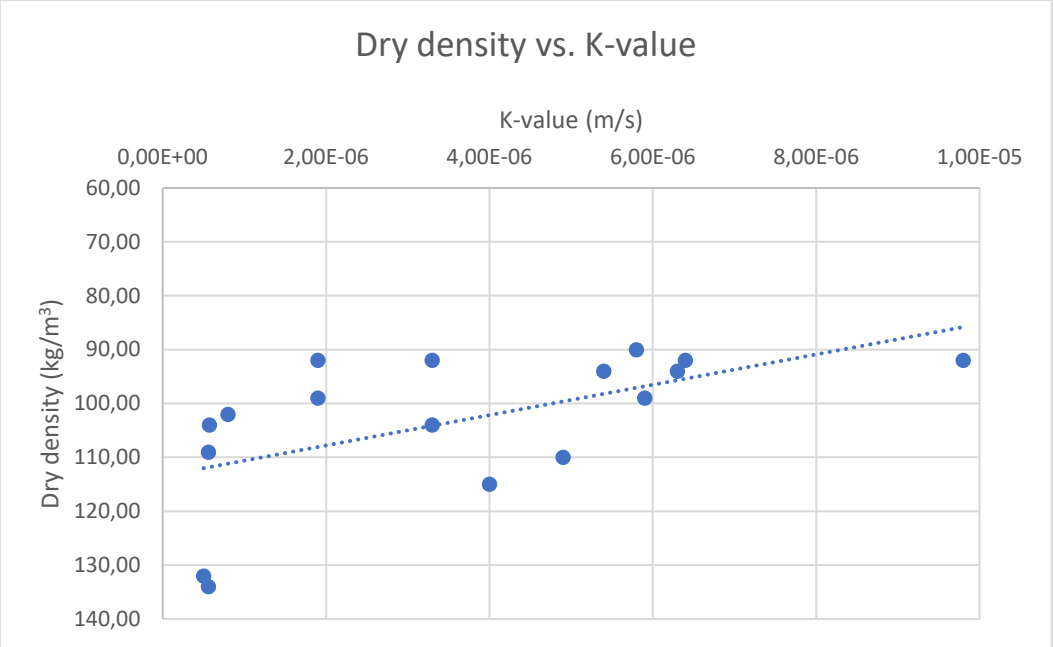

Figure 18: Dry density correlates moderately with the k-value in the samples (r = -.575*, p<0.05).

From these results it appears that the hydraulic properties of peat vary quite a lot spatially, but certain trends do occur in relation to depth. Humification lowers with depth, as does the hydraulic conductivity generally when a single location is observed. The poor correlations of K-value with depth and humification are unexpected as many have showed that humification is one property that correlates strongly with K-value. Possibly with more precise peat samples as well as a larger quantity of samples a different result could have been achieved.

Peat samples that were used, were not ideally suited for the chosen examinations. Firstly, the sample size varied a lot between the samples and not all samples represented similar sections of the vertical peat profile. Secondly, the unsystematic nature for collecting the peat samples resulted in dissatisfactory interpretations of the K-values in the peat. Site specifically the properties of peat seemed to agree with previous observations. Even though the coverage of the study was not very extensive, the results show the complexity of the peat layer in Viiankiaapa.

Peat studies are generally quite difficult to compare between different locations. Peat plant composition, climate and precipitation, as well as hydrology show significant variation in different geographical areas. The very heterogeneous nature of peatlands and peat material prove a challenging matrix for consistent study. Different study methods have been used and are still in use around the globe. Some focusing on field methods and others on laboratory methods. There has been great contradiction between the two, as explained by Kesäniemi (2009). For future hydrological studies of peat in Viiankiaapa or Finnish peatlands, the presented laboratory methods seemed to be suitable and repeatable, but the sampling structure could be further improved and its systematicity increased.

One additional caveat for the laboratory measurement of K is in the handling of the samples. Undisturbed peat samples can be difficult to extract and transport, l*et al*one use in a permeameter test. In almost all cases the samples get disturbed to some extent with the laboratory method (Figure 19).

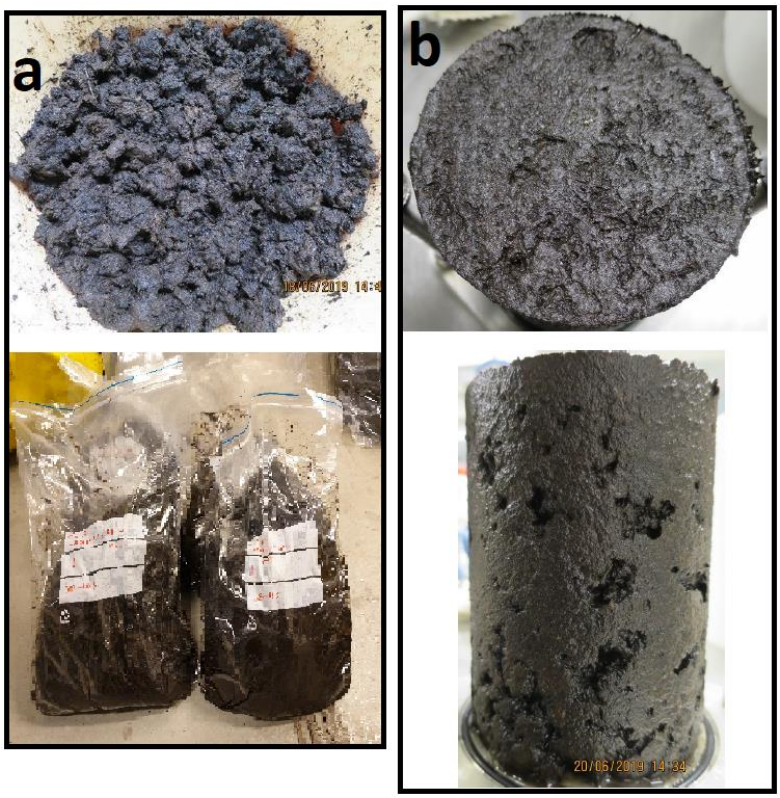

Figure 19: Peat samples disturbed after collection and during the analyses. Peat samples were collected to plastic bags (a lower) where they got disturbed the first time. After the required amount of the original sample was collected for use in the permeameter test, the sample got disturbed again (a upper). And finally, during the constant head test the samples deformed and compressed to some degree, although care was taken to not intentionally compress them (b).

Whereas field tests would provide realistic natural conditions of peat, but they are difficult to pinpoint to a certain depth for example and would require larger scale operations on the field, which would be difficult in the nature conservation area.

General groundwater and surface water flow directions in Viiankiaapa are towards river Kitinen (Åberg *et al*. 2017b). The topography along the studied profile is also sloped towards Kitinen. Groundwater flows in the sediments underneath the peat, and to a degree, through the peat as well. Sorted glaciofluvial sediments were interpreted as the most common type of sediment beneath the study site. This type of material was formed by flowing glacial meltwaters during deglaciation. The mini-piezometer showed pressurised waters at PEAT4 and PEAT8. suggesting confining nature of peat at these locations. Both sampling sites showed a clear decrease in K-value towards the bottom of the peat. Water chemistry results showed a greater groundwater influence in the surface water sample at PEAT4, indicating a possible groundwater discharge location.

There was a distinguishable mixture of peat and sand/gravel that was found at the bottom of PEAT4 at a depth of approximately 210–270 cm. The sudden change in the composition of mainly organic peat into a mixture of peat and sand is clearly visible in Figure 20.

Figure 20: Peat core from sampling point PEAT4. The sudden change in composition from organic dominated to a mixture of clastic/organic is seen in the top side of the figure under the light brown unit, which is decomposed woody material.

Ground penetrating radar possibly revealed the discharging groundwater from the bottom sediments all the way to the surface layer at/near PEAT 4 (Figure 21) in the form of disruptions in the otherwise very continuous reflectors. No bedrock reflections were interpreted with either 30MHz or 100 MHz antennas. The distinction between peat and clastic sediments was very clear and some areas showed internal structure in the gravel/sand deposits.

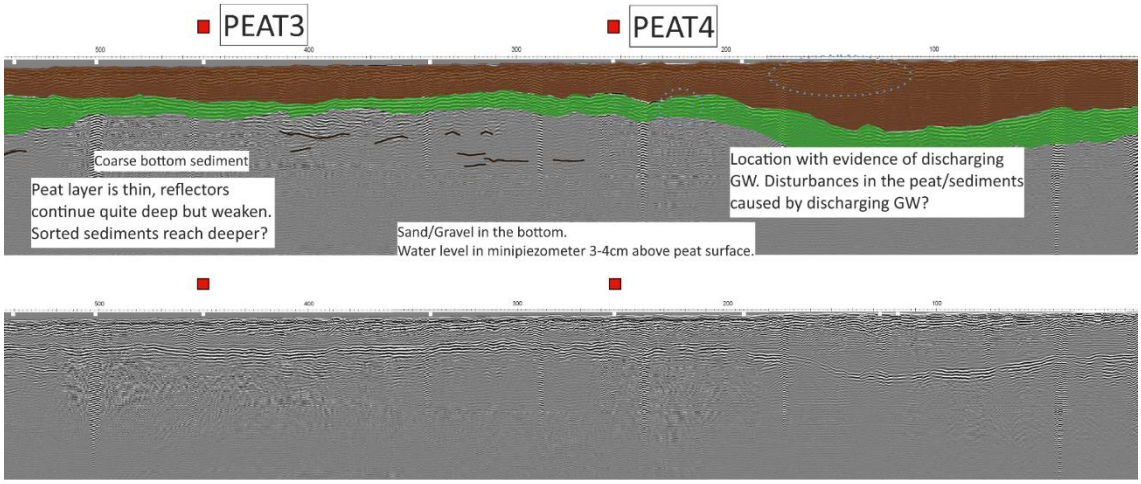

Figure 21: The interpreted GPR profile from sampling sites PEAT3 and PEAT4. Bottom sediment underneath peat at PEAT4 shows interesting breaks in the otherwise continuous reflectors in the sorted sediments. Evidence of discharging groundwater was present on the surface of the mire close to PEAT4.

The final interpretation, made with 100 MHz antenna, did not include any bedrock contacts and ultimately represents only two of the topmost deposits: peat and glaciofluvial/till sediments. The lower frequency antenna (30 MHz) did not show clear bedrock surface either and its resolution was much poorer near the surface. The decision was made to leave it out of the interpretations altogether. According to the hydrostratigraphical 3D-model from the area by Åberg *et al*. (2017b), bedrock could be found at greater depths than those which were achievable with the used GPR surveys. The realistic depth penetration for this GPR survey was approximately 10 meters. The previously mentioned model stated the average bedrock depth as 9.1m, with a very large variation between 0 and 41 meters (Åberg *et al*. 2017b). As no reference borehole data was used to confirm the depth of bedrock, no interpretations could be made about it along the studied line.

5.2 Water samples

5.2.1 Major ions and trace elements

Most of the samples are classified as Ca–HCO type, which is very typical of Finnish natural waters (Lahermo *et al*. 1990 and 1996). The dominant cations are calcium and magnesium, with calcium being more dominant. The anions show a bit more variability because sulphate concentrations changed a lot between samples (<0.07 ppm – 8.36 ppm). Generally, bicarbonate was clearly the most abundant anion in the samples. Chloride concentrations were very similar in all the samples. Chloride also expressed smallest standard deviation (0.29) and range (1.15) in the components. The effects of sodium and potassium to the water type classification were almost negligible in most samples. Figure 22 shows a piper diagram of the water samples.

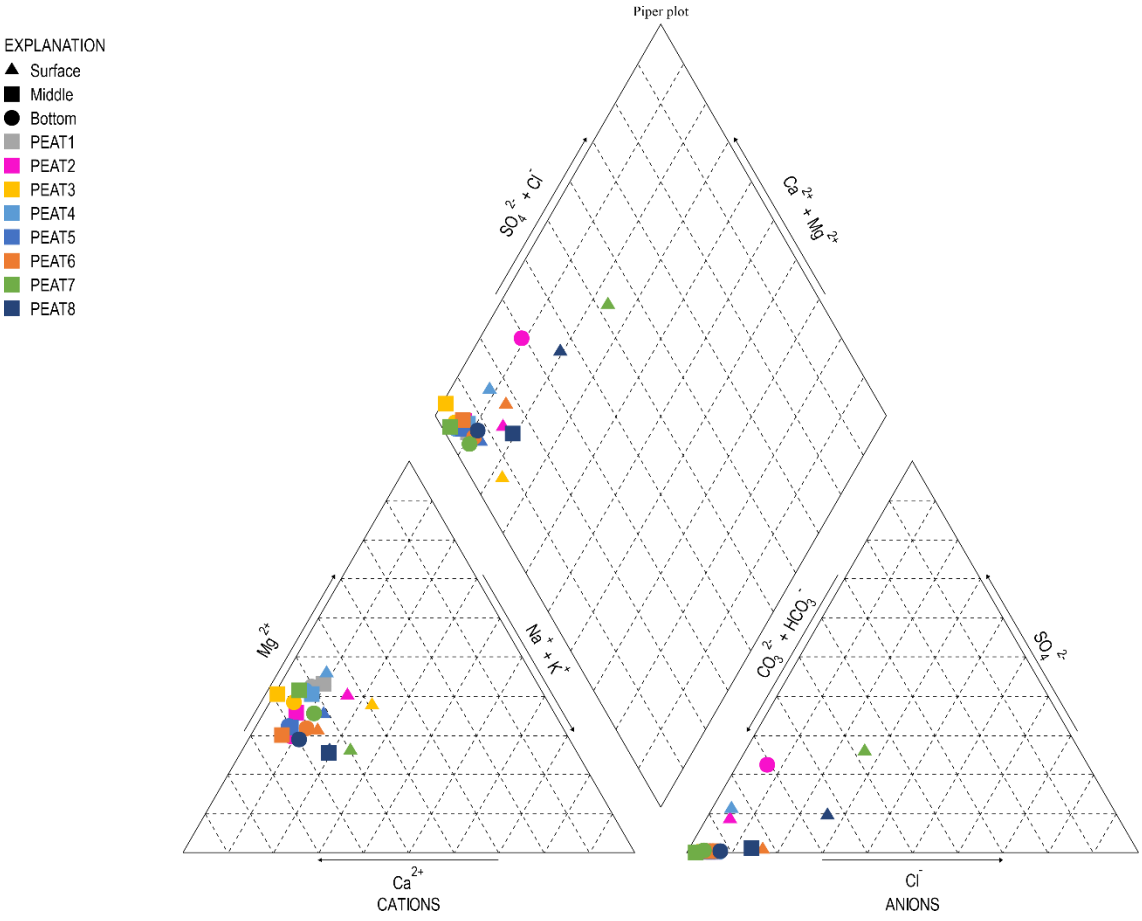

Figure 22: Piper diagram showing the water types of the samples. The dominant water type is Ca– HCO_3^-. Created with: *Winston, R.B., 2020. GW_Chart version 1.30 : U.S. Geological Survey Software Release*, 26 June 2020. https://doi.org/10.5066/P9Y29U1H.

Some samples deviate from the dominant Ca–HCO_3 type waters. Surface samples from PEAT7 and PEAT8 show some characteristics of Ca-SO_4 type, with increased effect of sodium and potassium. The bottom sample from PEAT2 shows similar qualities, but in a more modest manner.

The trace elements highlight once more the deepest sample of the whole dataset (p2_404). The sample in question shows highest concentrations of Mn, Co, Ni, Zn, As, Mo, Pb and U (see Table 8). In the elemental concentrations, no other sample comes even close to the concentrations observed in p2_404. For example, the next highest concentration of arsenic is eight times lower in and the median for arsenic is 26 times lower. The difference to other samples is also striking in the concentrations of zinc and molybdenum. High arsenic concentrations are most often related to bedrock qualities, mainly sulphide minerals. Metasedimentary rocks, mafic volcanics and plutonites are known to cause increased arsenic concentrations in Finnish groundwaters (Kabata Pendias & Pendias 2001, Lahermo *et al*. 2002).

The mini-piezometer water sampling method focused on collecting the samples from three vertical sections of the mire. These included the surface, middle and bottom of the peat layer, sometimes it was possible to penetrate the sediments beneath the peat down to some centimetres. The heterogeneity in the depth of the peat layer was observed to be very high; the deepest peat layer was at PEAT2 (approx. 4m), while the shallowest point was PEAT6 (approx. 1.5 m). Therefore, some water components were examined in case they displayed a distinct distribution based on which section of the peat layer the sample was taken from. In order to battle with the poor correlation between depth and the chemical components, the three samples that were taken from each sampling point were assigned with a property: surface, middle or bottom, based on which section a sample represented. The most distinctive differentiation between the sections of the peat were observed in Al, V, Si and Fe (Figure 23). Aluminium was observed not to correlate with the sampling depth, but it is clear that the distribution of it is different between the sections in the peat profile.

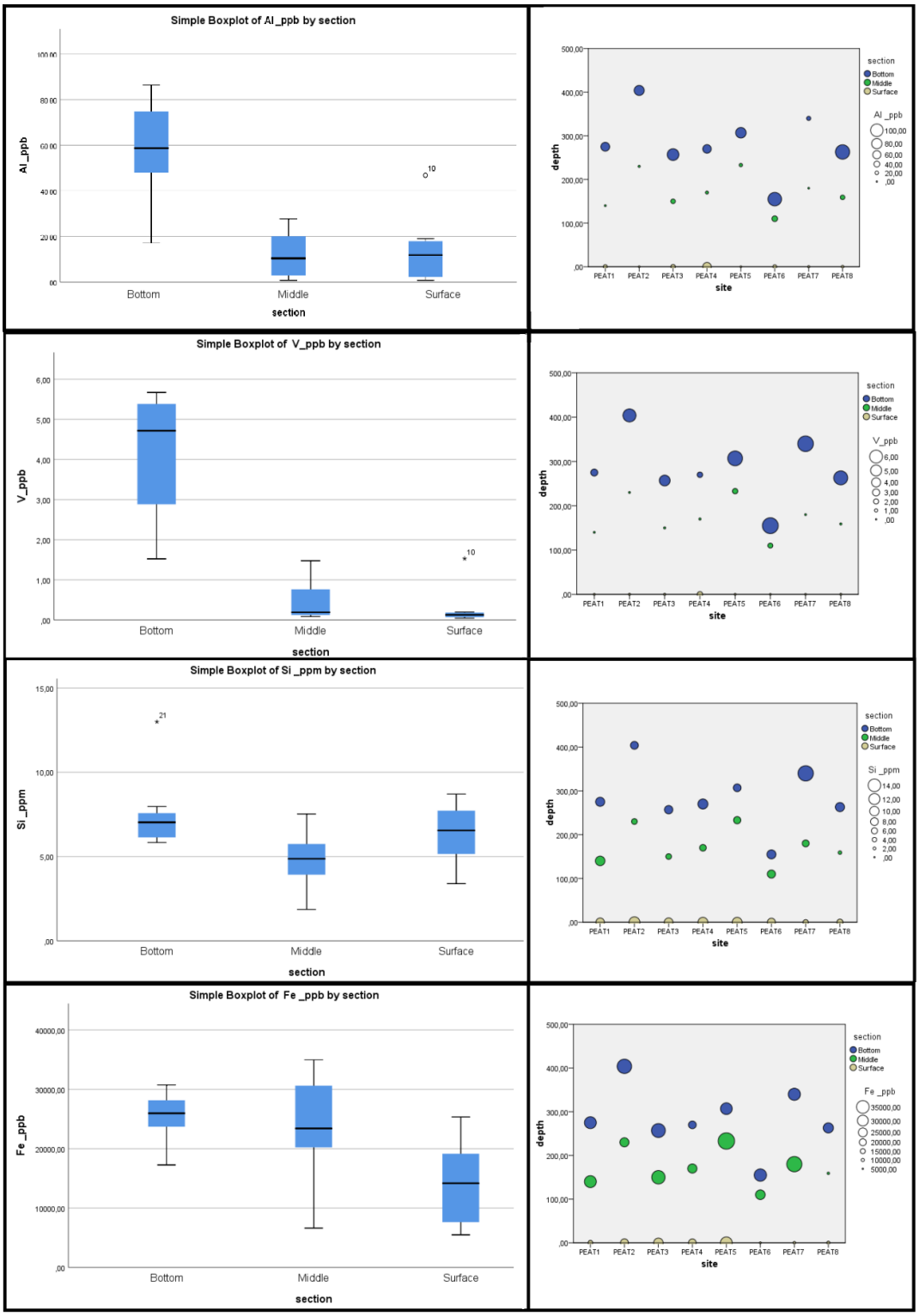

Figure 23: Boxplots of the concentrations of Al, V, Si and Fe based on which vertical section of the mire the sample was taken. The scatterplots show how the concentrations of the selected elements change with depth at each sampling site.

Silicon is a known groundwater indicator in natural waters, vanadium on the other hand is not. It has been noted that vanadium levels in groundwater are higher in areas with mafic bedrock or carbon rich shales and that anthropogenic effects are usually related to

metallurgical plants, foundries, chemical industry and combustion of crude oil (Lahermo *et al*. 2002, Wright & Belitz 2010). The relation is not as simple however, since as pointed out by Wright & Belitz (2010), vanadium is a redox sensitive element, being abundant in oxic and high alkaline groundwaters. In the case of anthropogenic source for the vanadium, one would expect the distribution of V to be maybe more homogenous or surface oriented in regard to the section of the peat profile. Vanadium concentrations are 15 times higher on average in the bottom samples when compared to the surface water samples. Vanadium exists in three oxidation stages (+III, +IV and +V) that are dependent on the pH and redox environment. V(IV) and V(V) are the most important species in natural waters and they are known to form complex ions and adsorb to different matrices (Wright & Belitz 2010). The adsorption of vanadium to peat or other material above the bottom of the mire cannot be further investigated with the materials that were gathered.

A similar but not as clear trend is seen with aluminium, silicon and iron. The case for silicon is not as clear because a few surface samples show increased Si concentrations. Aluminium shows a very distinct concentration distribution in the bottom samples, which are on average higher than the middle or surface samples. This is contrary to the findings by Bigler (2018) and Lahtinen (2017), although their investigations involved many more samples and the variance within their sample types was also noticeable. Iron concentrations display a very wide range in all sections of the mire. Being the most abundant naturally occurring heavy metal, iron is a major component in many mafic minerals, including olivine, pyroxenes, amphiboles and micas (Lahermo *et al*. 2002).

The soluble form of iron is Fe (II), which is stable in anoxic reductive environments. The mobilisation of Fe (III) requires low pH (< 3), which can be promoted by sulphide oxidation reactions (Lahermo *et al*. 2002). Peat contains micro-organisms that decompose organic material by consuming oxygen and organic matter. The decomposing plant matter creates organic acids, carbonic acid and decreases the oxygen level in peat, which in turn increase the solubility of Fe (III) and increases the stability of Fe (II). This change in the redox environment from oxidising to reducing can be seen in the abrupt increase in the concentrations of Fe and Mn beneath the surface. Groundwater in Viiankiaapa area has been observed to contain more iron in comparison with the surface waters (Lahtinen 2017,

Bigler 2018). As Figure 24 shows, iron concentrations increased generally with depth, with exceptions at PEAT5 and PEAT4 and PEAT8 (middle). The difference in iron concentrations between the surface samples and the middle samples were often dramatic.

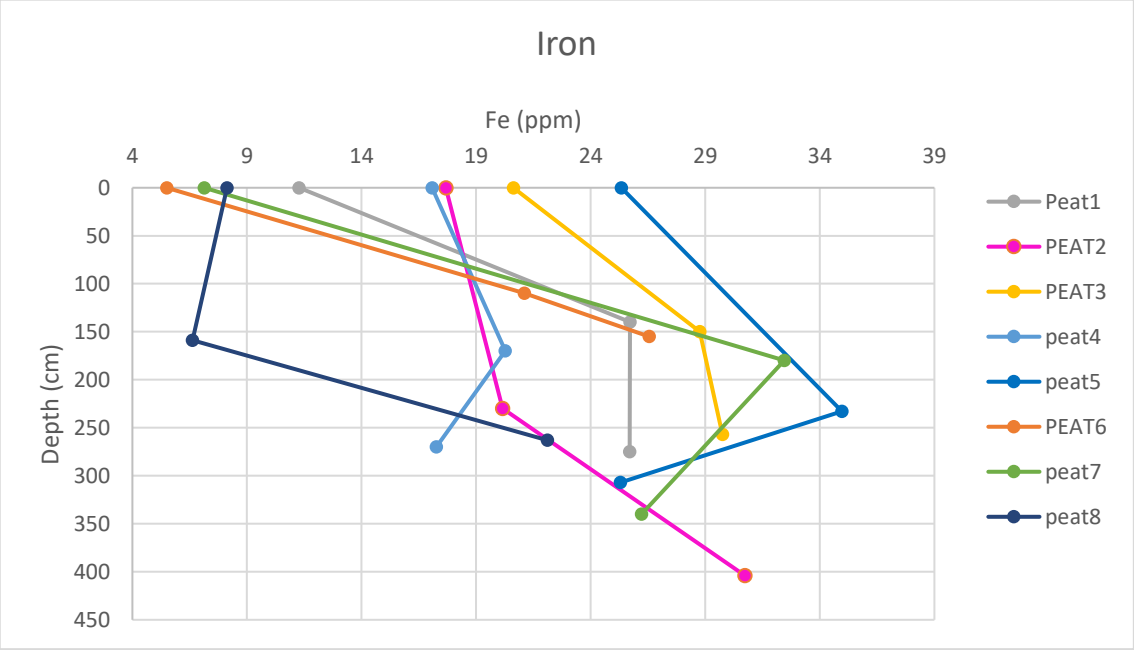

Figure 24: Iron concentrations (ppm) with depth at different sampling points. The iron concentrations are clearly higher in the deeper parts of the peat. Iron concentrations measured from the preserved samples and represent the natural concentrations.

There was a very large difference in the electric conductivities between the field measurement and the laboratory measurement. This could be mainly the result of precipitation, oxidation and complexing of iron compounds. The iron concentration was measured with the ICP-MS from an acid preserved sample that was pre-filtered already on the field, minimising organic matter in the samples. The acidified sample also stabilises iron and prevents iron hydroxide from precipitating. The precipitation of iron depletes bicarbonate, which on the other hand was measured from the un-preserved samples as alkalinity (Eq. 6).

$$2Fe^{2+} + 4HCO_3^- + \frac{1}{2}O_2 + 5H_2O \rightarrow 2Fe(OH)_3 + 4H_2CO_3 \quad (6)$$

High iron concentrations imply that iron was initially a major component in the pore waters of the peat, but when the samples were introduced to air and no preservation was carried out, the plentiful iron depleted bicarbonate by precipitation of iron (III) hydroxide

removing both species form the solution and therefore reducing the electric conductivity. The ion chromatograph analysed samples did show a mismatch with the estimated electric conductivity and the field measured electric conductivity (see table 5). This is most likely due to the described phenomenon. In the calculation of the cation sum, iron was not considered as a major contributor to it and was initially ignored. While in the anion sum, the amount of bicarbonate that had disappeared with the precipitation of iron (III) hydroxides was not taken into account. This resulted in both the cation and anion sums appearing too low for the field measured electric conductivity (Table 11).

Table 11: The cation and anion sums showing the effect of iron on the ion sums and electroneutrality (EN) of the samples. The depletion of iron and bicarbonate from the solution may have caused the cation and anion sums to appear too low when compared to the electric conductivity measured at the field. Values showing a balance error greater than 5 are bolded.

	EC (field)	Σcations with added iron	Σanions with calculated missing HCO3	EN with iron and missing HCO3	Σcations with iron ignored	Σanions with effect of depletion ignored	EN
p1_pinta	120.5	1.34	-1.34	-0.11	0.94	-0.94	-0.15
p1_140	168.8	1.89	-1.91	-0.55	0.97	-0.99	-1.06
p1_275	179	2.03	-2.04	-0.21	1.11	-1.12	-0.38
p2_pinta	-	1.73	-1.67	1.68	1.09	-1.04	2.69
p2_230	-	1.39	-1.41	-0.85	0.67	-0.69	-1.75
p2_404	-	2.33	-2.04	**6.57**	1.23	-0.94	**13.22**
p3_pinta	147.7	1.63	-1.73	-3.12	0.89	-0.99	**-5.56**
p3_150	183.5	2.11	-2.08	0.74	1.08	-1.05	1.46
p3_257	196.3	2.27	-2.22	1.10	1.20	-1.15	2.09
p4_pinta	240	1.82	-1.84	-0.44	1.21	-1.23	-0.66
p4_170	126.5	1.36	-1.40	-1.42	0.63	-0.67	-2.99
p4_270	172.2	1.88	-1.90	-0.38	1.26	-1.28	-0.56
p5_pinta	177.3	1.88	-1.83	1.48	0.97	-0.92	2.90
p5_233	-	2.41	-2.28	2.86	1.16	-1.03	**6.14**
p5_307	150.6	1.71	-1.69	0.81	0.81	-0.78	1.72
p6_pinta	54.9	0.54	-0.48	**5.39**	0.34	-0.29	**8.76**
p6_110	-	1.26	-1.37	-3.85	0.51	-0.61	**-9.05**
p6_155	-	1.60	-1.59	0.51	0.65	-0.64	1.27
p7_pinta	50.3	0.54	-0.55	-1.20	0.28	-0.30	-2.26
p7_180	233.6	2.64	-2.64	-0.01	1.47	-1.47	-0.02
p7_340	212.5	2.24	-2.32	-1.77	1.30	-1.38	-3.01
p8_pinta	50.8	0.54	-0.54	-0.30	0.25	-0.25	-0.64
p8_159	-	0.48	-0.51	-2.91	0.24	-0.27	**-5.61**
p8_263	150.2	1.18	-1.39	**-8.05**	0.39	-0.59	**-21.05**

The electroneutrality equation (Eq 7.) was initially calculated using only the major ion (Na, K, Ca, Mg, Cl, SO4, NO3 and alkalinity) concentrations, this resulted in seven samples expressing a balance error higher than 5%.

$$E.N. = \frac{(\Sigma cations + \Sigma anions)}{(\Sigma cations - \Sigma anions)} * 100\% \quad (7)$$

These calculated anion and cation sums showed a poor correspondence with the estimation of electric conductivity as Table 5 showed and evoked for an explanation. The precipitation of iron hydroxide and depletion of bicarbonate according to Equation 6 offer a likely candidate for the explanation. The result of calculating the Electroneutrality with iron included in addition to stoichiometrically calculated missing bicarbonate result in lower balance errors generally (Table 11) as well as show a lot better correspondence with the electric conductivity estimation.

The other product in Equation 6 is carbonic acid, which in turn exists in equilibrium with carbon dioxide and bicarbonate ion (Eq. 8). Carbon dioxide escapes readily from the solution especially when the temperature is increased, which in turn could accelerate the removal of bicarbonate further by removing available carbon. This could be one possible explanation to the increase in the pH that was observed between pH-field and pH (lab).

$$H_2CO_3 \leftrightarrow CO_2 \uparrow + H_2O$$

$$H_2CO_3 \leftrightarrow HCO_3^- + H^+ \quad (8)$$

According to Lahermo *et al* (2002), the increase in laboratory measured pH may be indeed caused by escaping carbon dioxide from the sample bottles between the collection and the laboratory analyses.

Explanation of the formerly described development, seen with the EC values, can be attempted with the sample p5_pinta, which had an EC (field) value of 177.3 and EC (lab) 85.1 µS/cm. The laboratory measurement for electric conductivity was carried out from a sample that had experienced the precipitation of iron, showing a low EC (lab) value. The analysed iron concentration for this sample was 25.3 ppm or 0.45 mmol, analysed from the preserved sample. If all this iron precipitated after the sample was collected, it would deplete bicarbonate by 0.90 mmol according to Equation 6. Now if this missing

bicarbonate concentration is added to the anion sum and the iron to the cation sum, the estimation for the electric conductivity becomes much better (Table 12).

Table 12: The contribution of calculated missing bicarbonate and iron to the cation and anion sums of sample p5_pinta.

	100*Σcat	**100*Σan**	**EC (field)**	$\frac{100 * \Sigma cat}{EC(field)} * 100\%$	$\frac{100 * \Sigma an}{EC(field)} * 100\%$
p5_pinta	188.0	-182.5	177.3	106 %	-103 %

Similar to iron, the electric conductivity increased with depth in most cases, exceptions being PEAT5 and the middle sections of PEAT4 and PEAT2 (Figure 25). Electric conductivity has been used previously to detect groundwater influence (Rautio & Korkka-Niemi 2015). In the graph, the EC results seem to divide the sampling points into two categories when only inspecting the surface EC values. This could be the result of discharging oxygen-poor groundwater on the surface of the mire at sampling points PEAT1, PEAT2, PEAT3, PEAT4 and PEAT5. while a perched water body could be present at PEAT6, PEAT7 and PEAT8.

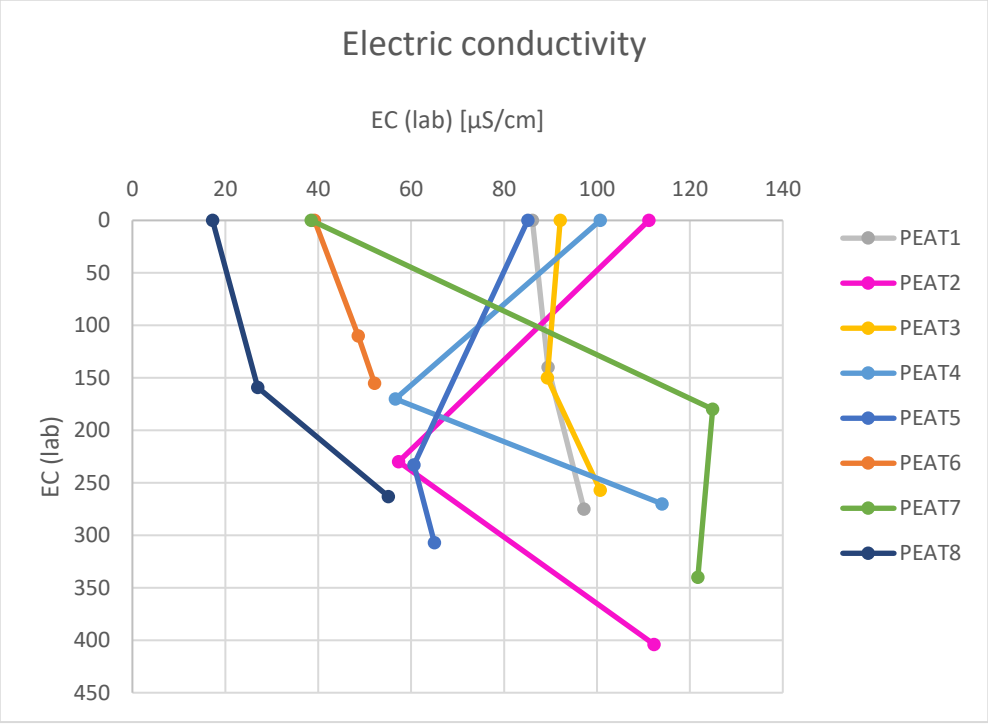

Figure 25: Electric conductivity (EC (lab)) of different sampling sites plotted against depth. General trend is seen with increasing EC values with depth. Laboratory EC were measured from un-preserved samples and are not representative of the natural state.

Dissolved silica showcased a similar trend where the concentrations in the middle section are lowest and surface or bottom section show highest concentrations (Figure 26). Sampling points PEAT8 and PEAT7 stand out containing the lowest dissolved silica in the surface samples. The range in dissolved silica concentrations in the surface samples was a modest 5.3 ppm. PEAT6 surface sample is not strictly in the same group as other analyses put it when dissolved silica is concerned.

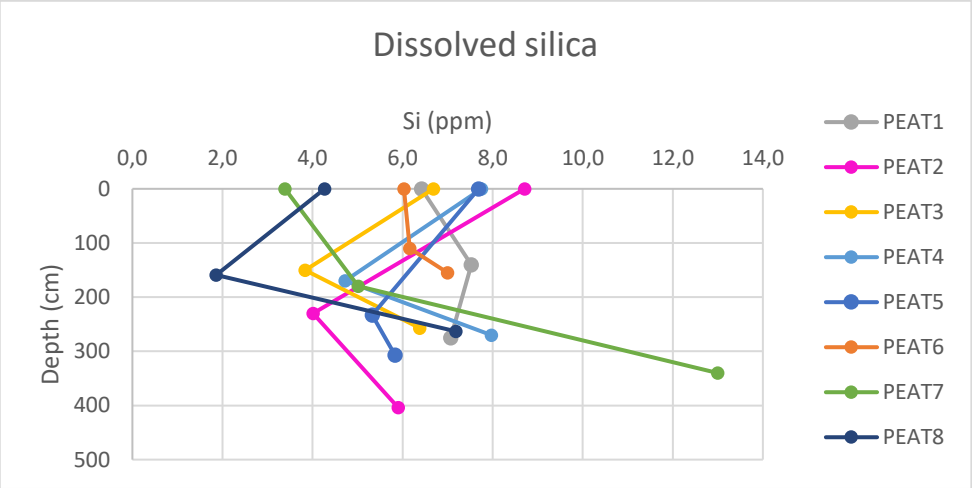

Figure 26: Dissolved silica concentrations plotted against depth.

Alkalinity shows the same systematic that was observed earlier with EC and Si, with PEAT6 being strongly similar to PEAT7 and PEAT8 in the surface at least (Figure 27). Alkalinity generally increases with depth; more data would be required to assess the systematic behind the phenomenon in more detail.

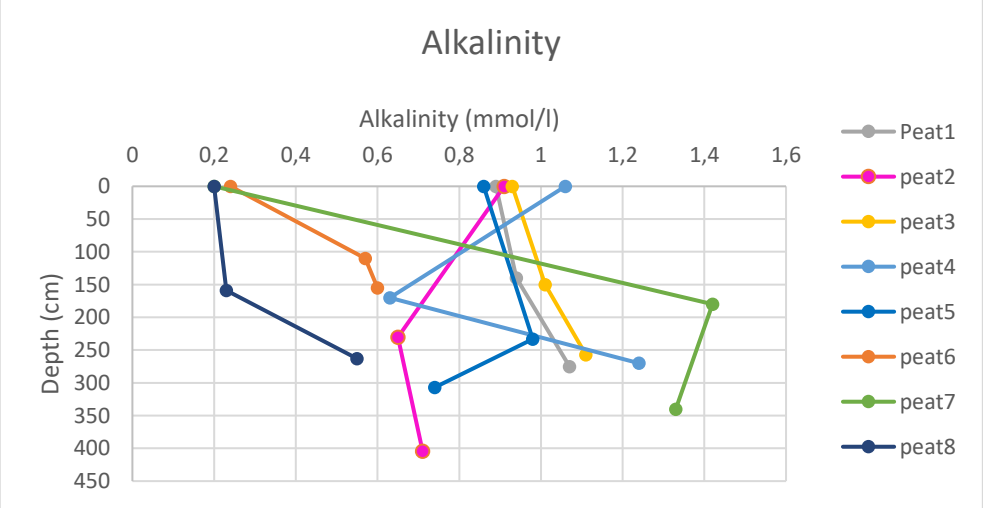

Figure 27: Alkalinity against depth. The separation into two groups in relation to the surface sample composition is clear.

5.2.2 Stable isotopes

The stable isotopes of O and H are measured against the Vienna standard mean ocean water (VSMOW) standard. It is common to plot the delta values of O and H against each other in order to compare the values with the meteoric lines (Figure 28). The closer a sample resembles precipitation, the closer it falls on the GMWL/LMWL line. Samples furthest away to the lower right from the line represent evaporated samples. Evaporated samples result from waters that are made up from infiltrated precipitation that is mixed with surface water, which is evaporated to some degree.

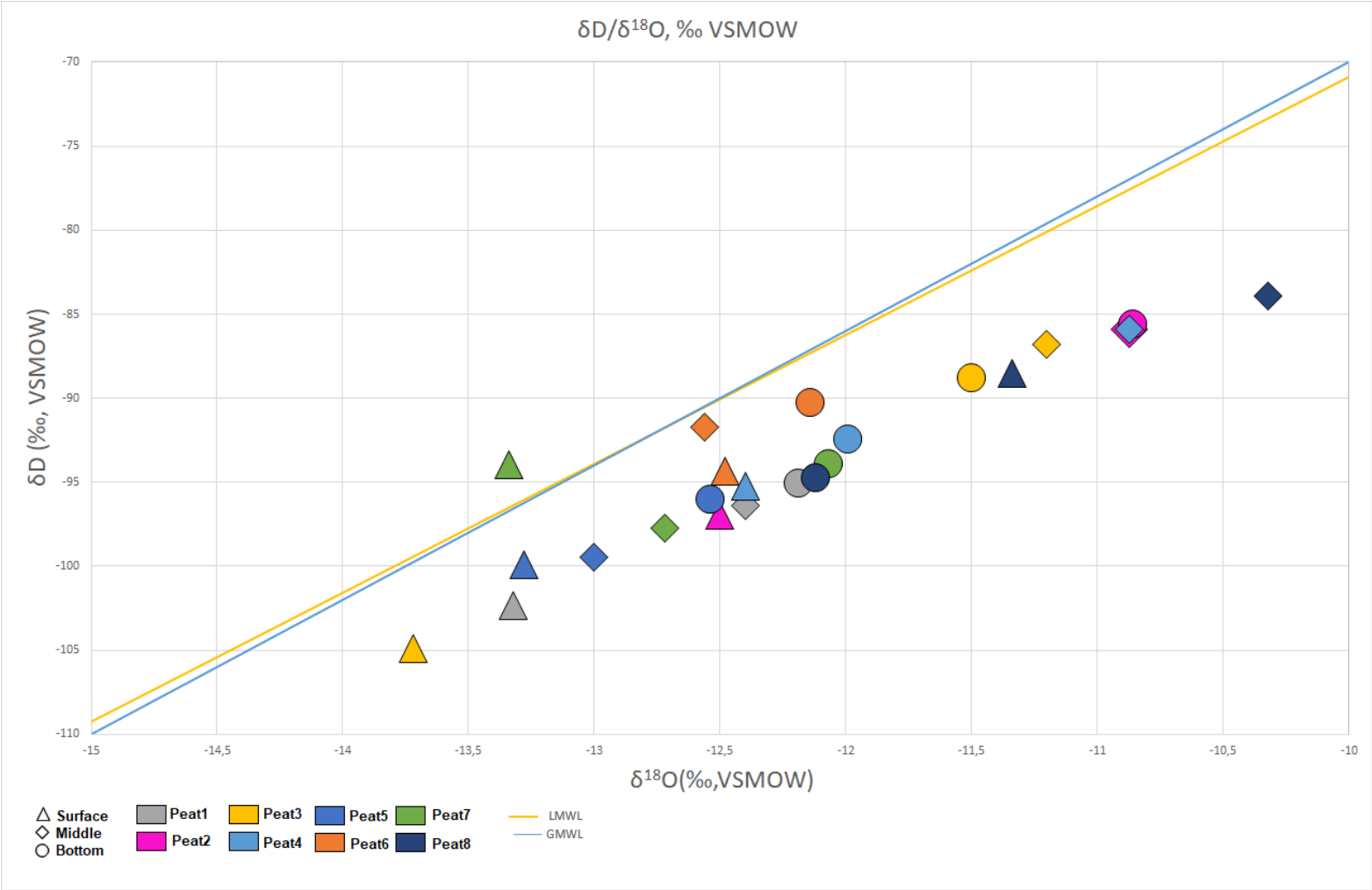

Figure 28: The isotopic delta values from the water samples collected from the mire. Also shown are the global and local meteoric lines according to (Craig 1961, Kortelainen 2007a respectively).

On first glance at Figure 29, it would seem that there could be some dependence on the isotope results with the sampling depth. This is supported with a moderate linear correlation with sampling depth and $\delta^{18}O$ (r = .474*).

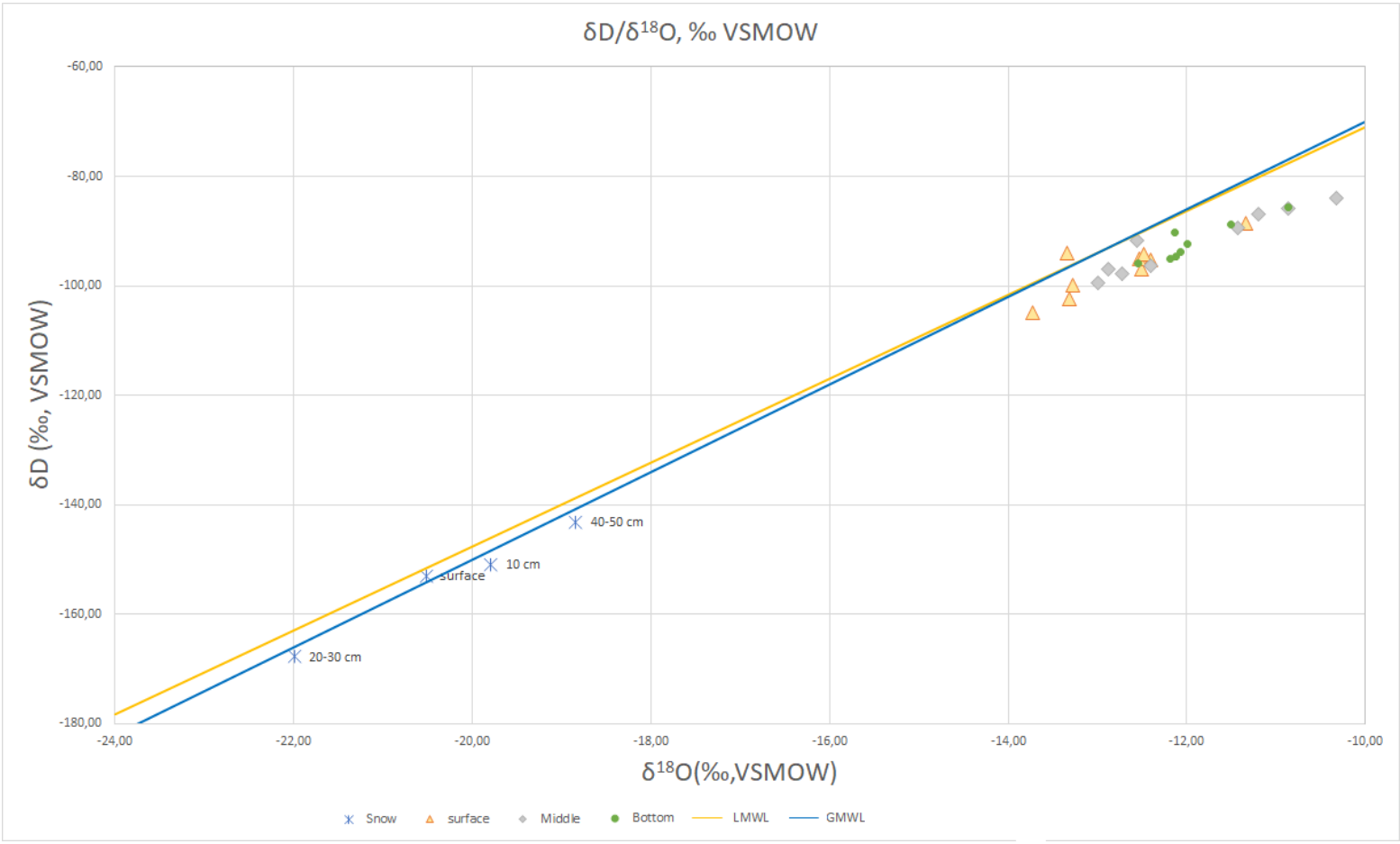

Figure 29: Plotted delta values of the mire water samples as well as the snow samples collected above the surface of the mire.

It is not surprising that the snow samples all fall very close to the GMWL, however only the sample that was collected from freshly fallen snow falls closer to the LMWL, while the other samples show evidence of evaporation. The mire water samples and their relation to the meteoric lines shows a more complex situation. Both $\delta^{18}O$ and $\delta^{2}H$ display quite a wide range of values with a modest standard deviation (Table 13). The delta values for groundwater in Siurunmaa, Sodankylä monitoring station were -106.7 ($\delta^{2}H$, ‰ VSMOW) and -14.55 ($\delta^{18}O$, ‰ VSMOW) in April of 2004 (Kortelainen 2007b). The

measured values in this study differ significantly, for oxygen in particular implying for more evaporated water than groundwater.

Table 13: the descriptive statistics of the stable isotope analysis. The results of the snow samples are not included here because they would affect all the values drastically.

	δ^2H, ‰ VSMOW	$\delta^{18}O$, ‰ VSMOW	d-excess
Mean	-93.51	-12.18	3.92
Median	-94.16	-12.30	3.36
Std. Deviation	5.42	0.87	2.79
Range	20.96	3.4	14.1
Minimum	-104.88	-13.72	-1.36
Maximum	-83.92	-10.32	12.74

All the stable isotope ratios that were measured for mire water, deviate from the LMWL plotting to the lower right side of the line. This is a sign of evaporated water signal that could be the result of evaporation experienced in the mire or the mixing of evaporated waters with precipitation. A clear trend is seen in the $\delta^{18}O$ graph (Figure 30). Surface samples have the most negative delta values, apart from PEAT8, indicating less evaporated water on the surface. Deuterium excess shows a similar trend. Surface samples generally show highest d-excess values, though an exception is seen in PEAT8. The systematic of the isotopic results is not unambiguous. More data from additional sampling points and different depths should be used to properly draw conclusions about the hydrological processes occurring in the mire.

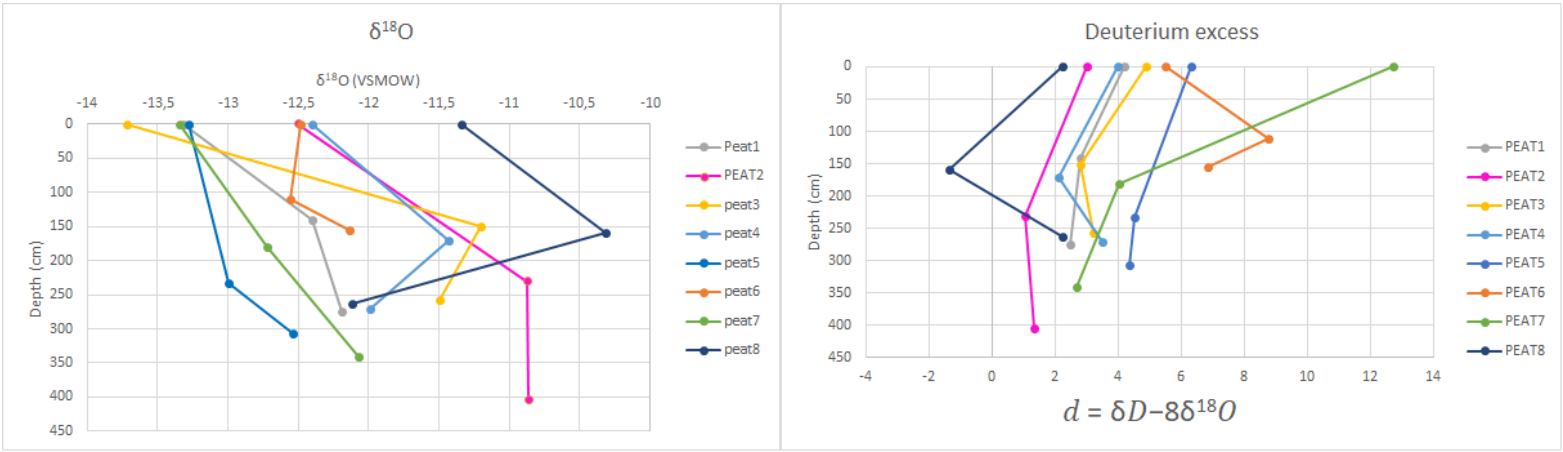

Figure 30: Combined $\delta^{18}O$ and d-excess graphs plotted with depth. Both show a visible trend in relation to depth.

The negative correlation between d-excess and depth is significant (r = -.423*), although not very strong. According to the non-parametric Kruskal-Wallis test, the distribution of d-excess values is not similar in all the sampling sites, so there is distinct spatial variation in the values (Figure 31). Highest values are recorded in PEAT6, while the single maximum value of the dataset is from PEAT7 surface. A single negative value was obtained in p8_159.

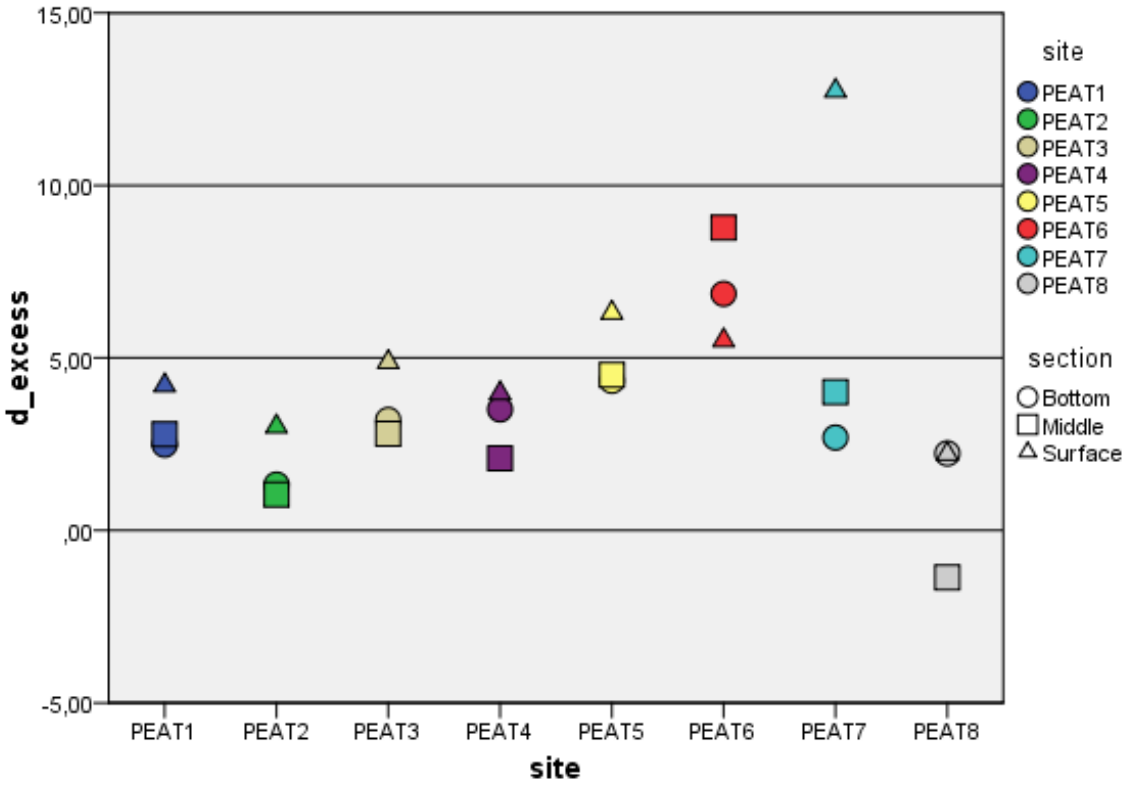

Figure 31: The distribution of the d-excess values in relation to sampling site and section of peat. A weak negative linear correlation exists with d-excess and depth (r = -0.423* pearson correlation).

In six out of the eight locations, the highest d-excess value is seen in the samples taken from the mire surface, the closer this value is to 10, the more it resembles precipitation. At PEAT8 the surface sample has practically the same d-excess as the bottom sample.

5.3 Statistical inspection

The simplest statistical method is bivariate correlation (Table 14), which shows how two different variables correlate with each other. Pearson's correlation coefficient describes the linear relationship between two different variables, while spearman's correlation coefficient imparts the relationship of ranked values. Correlation coefficients adopt values between -1 to 1. with higher absolute value representing better correlation. Pearson correlation coefficient (r) values from .400 to .600 are considered weak correlations, while .600–.800 are moderate and .800–.999 are strong. The significance of a calculated correlation is expressed with Asterix (*) symbol. The used significance tests are double tailed. Double Asterix (**) represents significance at the 0.01 level while single asterix (*) represents significance at the 0.05 level.

There are multiple cases of moderate to strong correlations between variables that have been reported in previous publications concerning natural waters (eg. Lahermo *et al*. 1990) such as the correlation between major cations and electric conductivity. In the study at hand, the relationship between electric conductivity and K, Na and SO4 is not as clear as reported by Lahermo *et al*. (1990). In the case of Na there is also quite a striking difference in the correlation coefficients between the field-measured electric conductivity (EC (field)) and the laboratory measured (EC (lab)). The Pearson correlation coefficients for Na are r = .400 in EC (field) and EC (lab) r = .652**. Insignificant correlation becomes significant.

Table 14: Pearson bivariate correlation matrix. The complete chart, with trace elements shown can be seen in the appendices. Significant correlations are flagged with asterix symbols. Two tailed significance at the 0.05 level is marked with a single asterix, while significance at the 0.01 level has a double asterix symbol.

	pH (field)	pH (lab)	EC (field)	EC (lab)	Na	K	Ca	Mg	Cl	SO4	Alk.	Si	Mn	Fe	d2H	d18O	depth
pH (field)	1	.849**	.563*	.472	.297	-.111	.407	.540*	-.207	.04	.556*	.301	.475	.435	-0.048	0.272	0.446
pH (lab)		1	.709**	.681**	.502*	.023	.606**	.741**	.047	.019	.751**	.453*	.605**	.460*	-0.149	0.13	0.379
EC (field)			1	.777**	.4	-.021	.785**	.819**	-.126	.091	.875**	.459*	.620**	.718**	-0.079	0.078	0.398
EC (lab)				1	.652**	.287	.850**	.925**	.256	.294	.903**	.608**	.672**	.556**	-0.303	-0.165	0.305
Na					1	.616**	.439*	.517**	.574**	.34	.519**	.737**	.338	.264	-.477*	-0.327	0.056
K						1	-.002	.168	.769**	.218	.148	.3	-.064	-.058	-.594**	-.541**	-.414*
Ca							1	.880**	.013	.228	.882**	.411*	.807**	.791**	-0.129	-0.023	,527**
Mg								1	.11	.173	.951**	.481*	.680**	.572**	-0.321	-0.172	0.22
Cl									1	.461*	.021	.301	.091	-.088	-.476*	-.422*	-0.294
SO4										1	-.022	.081	.293	.023	0.182	0.163	0.062
Alk.											1	.567**	.634**	.672**	-0.362	-0.211	0.337
Si												1	.271	.28	-.409*	-0.328	0.163
Mn													1	.786**	0.005	0.124	,554**
Fe														1	-0.089	-0.02	,600**
d2H															1	,928**	0.39
d18O																1	,474*
depth																	1

The correlation between Na and Si was r = .737** in the present study, while Lahermo *et al*. (2002) report a correlation or r = .440** which is somewhat smaller. Dissolved silica is usually interpreted as a reliable chemical tracer for groundwater that originates from long residence time in contact with bedrock (Rautio *et al*. 2015. Rautio & Korkka-Niemi 2015), while Na is usually not strongly related to lithology but rather to seawater influence (Lahermo *et al*. 2002). The influence of local seawater, even relict seawater, can be ruled out in our study area since the area has not been under the influence of seawaters. The sodium that is present in the samples could be dissolved from the bedrock or the sediments in the area. This could explain the rather strong correlation between the bedrock related Si and Na. Another explanation for the sodium comes from the correlation with chloride, which is weaker (r = .574**). Airborne aerosols are capable of transporting Na and Cl from distant seas. Lahermo *et al*. (2002 and 1990) provides figures for inland air-originated sodium and chloride concentrations (<2 mg/L for sodium and 0.5–1.7 mg/L for chloride). There are no values in the water samples that exceed the provided figures. Another complicating factor arises when the snow samples are considered (see Table 6).

If sodium is precipitation related, then it should be present in the snow samples, which was not the case though.

Also interesting is the moderate correlations between the pH measurements and alkalinity (.556* and .751** for pH (field) and pH (lab)). In the one thousand well survey by Lahermo *et al*. (2002), the correlation between pH and alkalinity was .490** in dug wells. In the broader geochemical atlas of Finland, the correlation from a wider dataset resulted in a value of r = .470*. In the study at hand, the very much higher correlation between pH (lab) and alkalinity could result from the generally higher pH values that were measured in the laboratory. As figure 32 shows, pH (lab) moves the pH values closer together by moving most measurements towards higher pH values and thus forming a better correlation. However, the changed pH is probably not strictly representative of the natural state in the mire at this point.

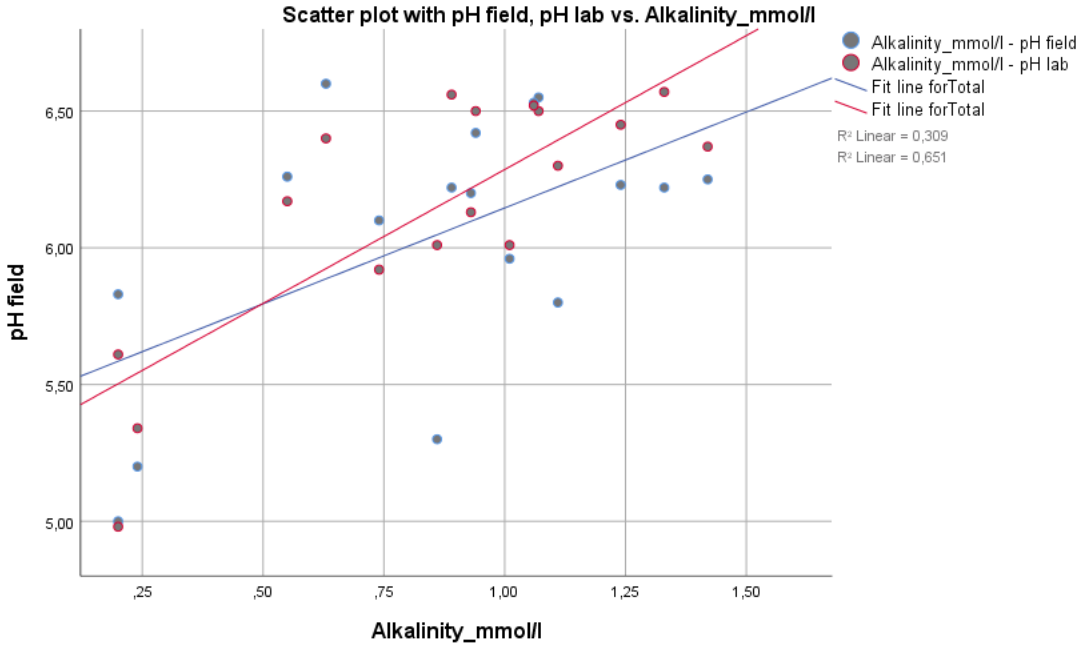

Figure 32: Scatterplot with trendlines for pH (field) and pH (lab) against alkalinity. The red line is the trendline for pH (lab) and has a higher correlation and a steeper slope than the pH (field) trendline.

There were a few interesting trace element correlations as well. Arsenic shows very strong correlations with other trace elements, as well as sulphate. The correlation coefficients for the different element pairs are: As-Mo r = .993**; As-Zn r = .970** and As-Ni r = .924**. On closer inspection, the high correlation coefficients are caused by the extreme

difference in the concentrations of arsenic between p2_404 and all the other samples. The scatterplots show how the outlier affects the best fit line in a radical way (Figure 33).

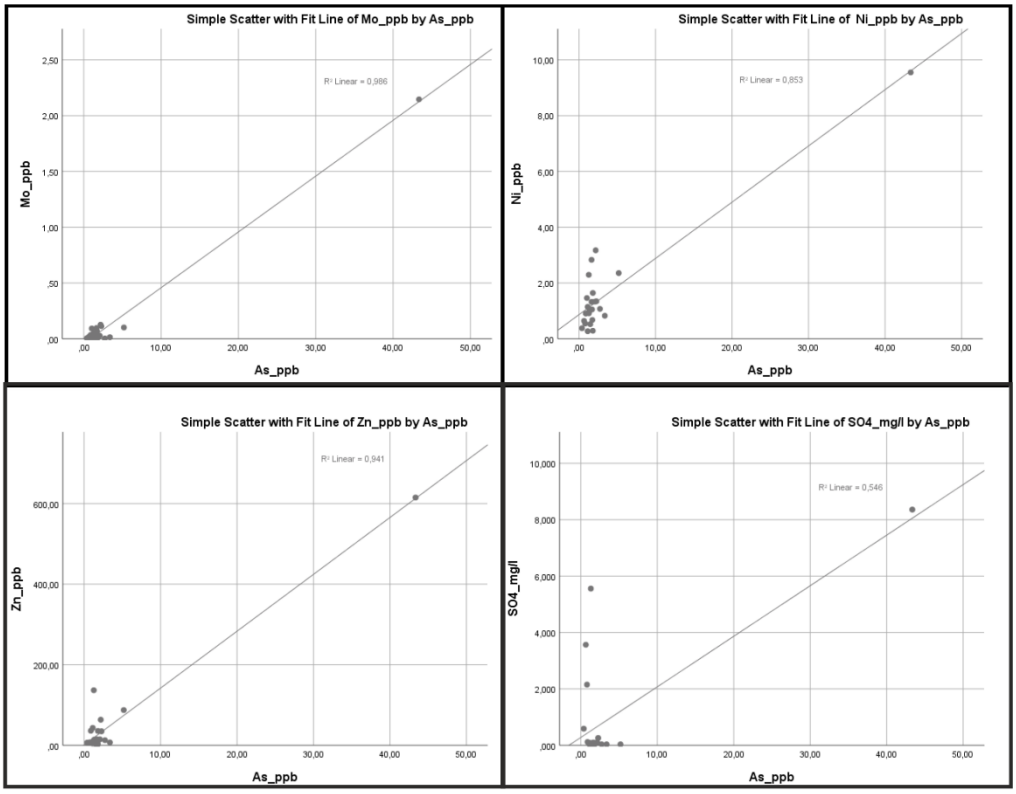

Figure 33: Scatterplots with arsenic and Mo, Ni, Zn and SO4. when the sample p2_404 is included.

Without the outlier data point (p2_404), the correlation between arsenic and the other components becomes statistically insignificant. The same phenomenon may cause exaggerated correlations with other variables as well, since many of the trace elements were not normally distributed and contain outliers.

There were many weak and moderate correlations that involved depth as a variable (Table 15). The strongest correlations with depth were observed in V (r = .680**), Cr (r = .633**) and U (r = .621**).

Table 15: Pearson correlation chart with all the flagged significant correlations that involved depth. Two-tailed significance at the 0.01 level is described with **, while a significance at 0.05 level is *.

Depth	V	Cr	U	Fe	Co	Mn	Ca	Zn	Ni	Al	d18O	As	Mo	K
1	.680**	.633**	.621**	.600**	.589**	.554**	.527**	.508*	.506*	.494*	.474*	.452*	.440*	-.414*

Negative statistically significant correlation of depth and potassium shows that potassium is highly concentrated near the surface, possibly being the result of easy leaching from

decaying plant matter (Verry 1975). The weak correlation between depth and the chemical components suggests another way should be used to compare the concentrations between the samples.

5.3.1 Principal component analysis (PCA) and hierarchical cluster analysis (HCA)

Principal component analysis aims to recognize the parameters that explain the majority of variance between the samples, therefore reducing the number of variables in the data by excluding non-explanatory data. Variables for the analysis were selected initially based on their assumed geochemical significance. After a few sets of variables were chosen, they were compared using the Kaiser Meyer Olkin (KMO) test to find the best set of variables. The KMO test computes the data in order to determine the suitability for use in the PCA. The test yields values in the range of 0–1. and the closer the result is to 1, the better outcome will be with PCA (Kaiser 1974). The variables for the principal component analysis were selected based on their normality and the scoring in the KMO test. The varimax rotated component matrix is seen below (Table 16).

Table 16: The varimax rotated component matrix wtih the explanation values for different components present.

KMO	0.604				
	Component				
	1	2	3	4	5
Percentage of variance explained	37.86	21.64	11.76	9.82	6.35
Na	0.445	**0.642**	-0.368	0.205	0.113
Ca	**0.959**	0.066	0.033	0.099	-0.035
Mg	**0.932**	0.126	-0.158	-0.075	0.003
Cl	-0.022	**0.864**	-0.309	-0.097	0.086
Alk.	**0.936**	-0.032	-0.255	0.059	0.095
Al	0.027	-0.077	0.138	**0.851**	-0.330
Si	0.432	0.289	-0.395	**0.507**	0.413
P	-0.126	0.067	0.017	-0.240	**0.892**
V	0.164	0.008	0.103	**0.953**	-0.024
K	0.053	**0.804**	-0.429	-0.111	0.177
Mn	**0.828**	0.151	0.186	0.078	-0.251
Fe	**0.783**	-0.141	0.005	0.262	-0.133
EC (lab)	**0.890**	0.287	-0.127	0.075	0.113
d2H	-0.156	-0.193	**0.946**	0.104	0.043
d18O	-0.016	-0.152	**0.913**	0.087	-0.045
SO4	0.128	**0.781**	0.412	0.085	-0.174

Extraction Method: Principal Component Analysis.
Rotation Method: Varimax with Kaiser Normalization.

The PCA yielded 5 principal components that explain 87% of the total variance in the data. The number of principal components that were accepted as a result were specified by their eigenvalues, which was set to be > 1.

According to the boxplots, the water chemistry seems to be more section specific than site specific, with exceptions at PEAT2 and PEAT7 where the loadings of components 2, 3 and 5 are clearly above the rest (Figures 34 & 35). Section wise, bottom samples get a heavy loading of component 4, which contains Al, Si and V. This component possibly represents stagnant mire water or groundwater. Silicon is used as a groundwater tracer in many studies (*eg.* Rautio *et al*. 2015) while anthropogenic vanadium is usually linked to metallurgy and the burning of crude oil (Wright & Belitz 2010). Vanadium is unlikely originated from human activities and instead possibly shows mafic bedrock signal. Somewhat weaker, but still relatively strong, is the component 1 loadings in the bottom samples. Component 1 was formed of Ca, Mg, Alkalinity, Mn, Fe and EC (lab). which exist generally as higher concentrations in groundwater. Therefore components 4 and 1 could represent groundwater influenced samples.

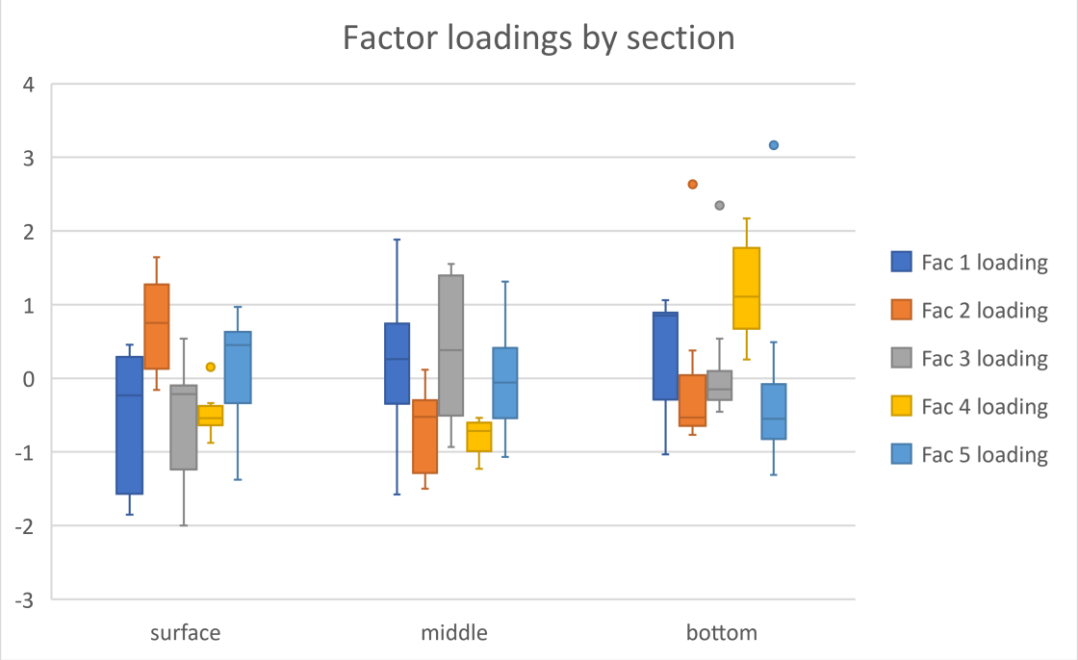

Figure 34: Component/Factor loadings of different samples combined according to the sample section.

Surface samples show a high loading in component 2 and middle samples are generally highest in component 3 loadings. Component 2 contained Na, Cl, K and SO_4. which as discussed previously could be originated from precipitation fallout. It would make sense if surface samples showed most impact of rainfall. Component 3 consists only of the stable isotopes. Variance of component 3 score between the different sections is unspecific beneath the surface. Middle and bottom samples show very similar component loadings altogether, apart from component 4, which is clearly bottom dominated. The possible explanation could be found when the hydraulic conductivity of peat is considered. One of the early observations was that in individual sampling points the K-value decreases with depth. This could hinder the movement of groundwater to the upper parts of the peat.

The PCA inspection is not as fruitful when the component loadings are compared between sampling sites (Figure 35). Component 1 shows systematically consistent results at PEAT1, 2, 3, 4, 5 and 7 while PEAT6 and 8 score considerably lower. The sampling sites contained three samples each and the boxplot is not best suited for such a small dataset. However, two sampling points score anomalous values in component loadings of 2, 3 and 5. PEAT2 shows very high component 2 and 3 loadings, indicating a surface water/rainwater characteristic. PEAT7 on the other hand shows high loadings in components 1 and 5. Component 5 included only phosphorus.

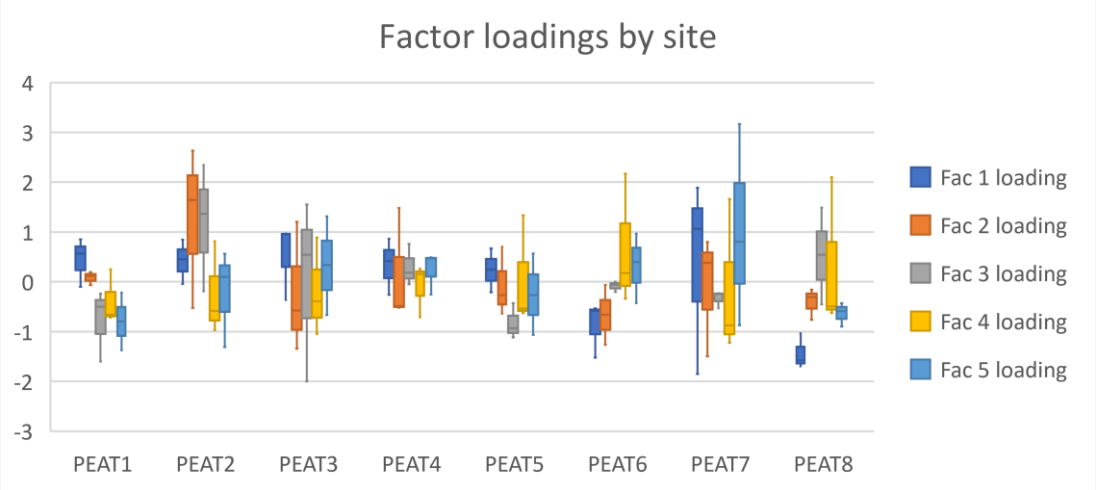

Figure 35: Component loadings of different samples combined according to the the sampling site. The most distinctive sample sites are PEAT2 with high loadings in components 2 and 3. as well as PEAT7 where component 5 reaches high loading values.

Phosphorus is an important nutrient in plants and its behaviour in mire waters seems to be quite complex. Verry (1975) provides a possible explanation to the source of P that is related to the rupture of plant cells during freezing and release of free P during thaw. Shotyk (1988) pointed out that the concentration of P in peats is probably not related to mineral soil. It is the only constituent in the principal component 5, and probably is unrelated to geology. The concentrations of P are generally higher in the surface and middle samples which could be then the result of decaying plant matter instead of mineral soil/bedrock origin. The very high concentrations of phosphorus in PEAT7 remains a mystery until further investigation.

PEAT6 shows a relatively high loading of component 4, also indicating groundwater influence, however a very low loading in component 1 adds to the confusion. PEAT6 had a thin peat cover, following that the bottom and middle samples were taken with only 45 cm of separation. This probably over-emphasizes the effect of V, Al and Si, which are concentrated near the bottom of the peat. The bottom sediment yielded water very poorly with the mini-piezometer. K-values of peat at PEAT6 were also very low. The residence time of water at PEAT6 would therefore be considered high, which would increase the concentrations of dissolved components. The combined loadings for components 1 and 4 could be used to distinguish samples based on their water type (Figure 36).

Component 1 offers more groundwater related variables and combines them to bring another indicator for groundwater influence. In the combined loadings plot of components 1 and 4, the bottom samples, which typically had high EC values and amount of dissolved solids, are located in the upper right sector of the graph (Figure 36). Surface samples on the other hand, are mostly located in the bottom left side of the graph, with PEAT6, PEAT7 and PEAT8 forming a distinct group.

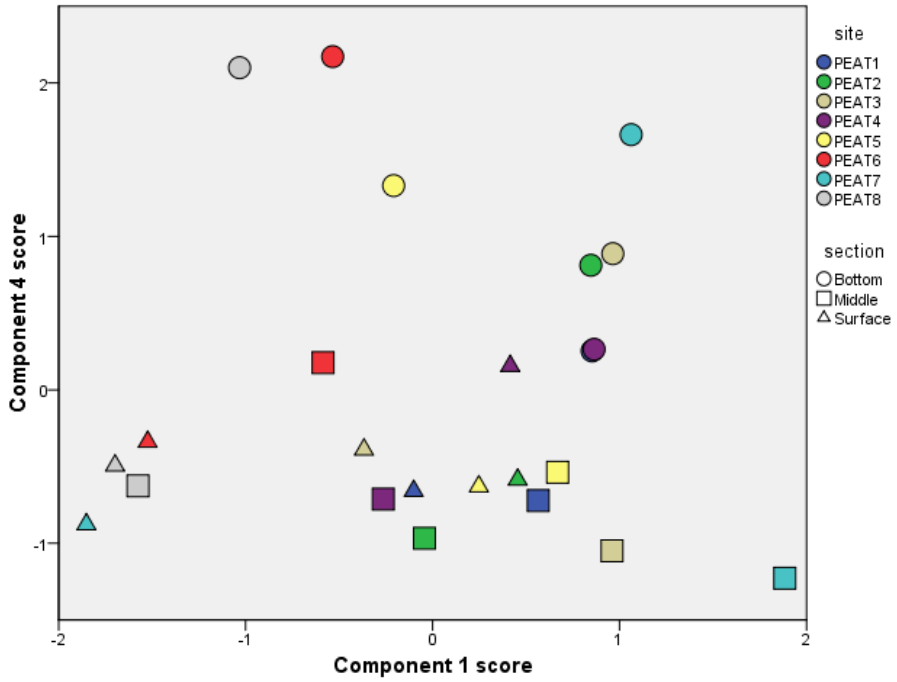

Figure 36: Loadings plot for components 1 and 4. An observation of samples that show the heaviest groundwater/surface water characteristics can be made.

Samples from the bottom section of PEAT6, PEAT8, PEAT7, PEAT5 and PEAT3 show high component 4 loading and no loading in component 2, which could be interpreted as groundwater effect or a long residence time because of poor hydraulic conductivity. The justification for this procedure is challenged with the sample from PEAT4 bottom. The bottom sediment in PEAT4 was a mixture of sand and peat. The bottom contact of the peat in the GPR is discontinuous, suggesting either a disruption caused by groundwater discharge or disturbance of the bottom sediment. Near the sampling point, there were obvious signs of groundwater discharge in the form of molten snow and flowing water at below freezing temperatures. PEAT4 bottom sample could therefore be expected to score high in the loading of component 4, which is not the case. PEAT4 bottom and middle are present in the upper right section of the graph, owing to their loadings in component one.

PEAT2 on the other hand achieves high component 2 scores on the surface and bottom samples. The bottom sample scores high with component 2 because it marks the deepest sample in the dataset p2_404, which showed anomalous concentrations in most elements analysed, including Na, Cl and K. However, the site showed very high EC (lab) values and other groundwater indicators suggested strong groundwater influence at the site. The peat studies showed that PEAT2 had high hydraulic conductivities along the whole peat

profile. It could be possible that groundwater moves with more ease at PEAT2. even seeping all the way to the surface. PEAT2 lies on the slope of a depression which could be a part of a paleo-riverbed consisting of sorted bottom sediments. The *in-situ* water analysis methods were unapplied at the site.

Water chemistry distinguishes the surfaces of PEAT6, PEAT7 and PEAT8 as the least groundwater influenced. Using the well-established chemical tracers (Si, EC, alkalinity), Groundwater seems to influence the composition of water mostly at PEAT1, PEAT2, PEAT3, PEAT4 and PEAT7 under the surface. PEAT6 and PEAT8 show least groundwater influence when all gathered material is considered, which could be partly the result of poor hydraulic conductivity in the peat. The poor hydraulic conductivity at site PEAT6 probably result in increased residence time of water and causes the concentrations of many trace elements to be surprisingly high when the shallow depth is considered.

Based on the chemical and isotopic components that provide the best explanation of the variance in the dataset (i.e. the same data that was used in PCA), HCA was completed to find clusters that have chemical similarities (Figure 37).

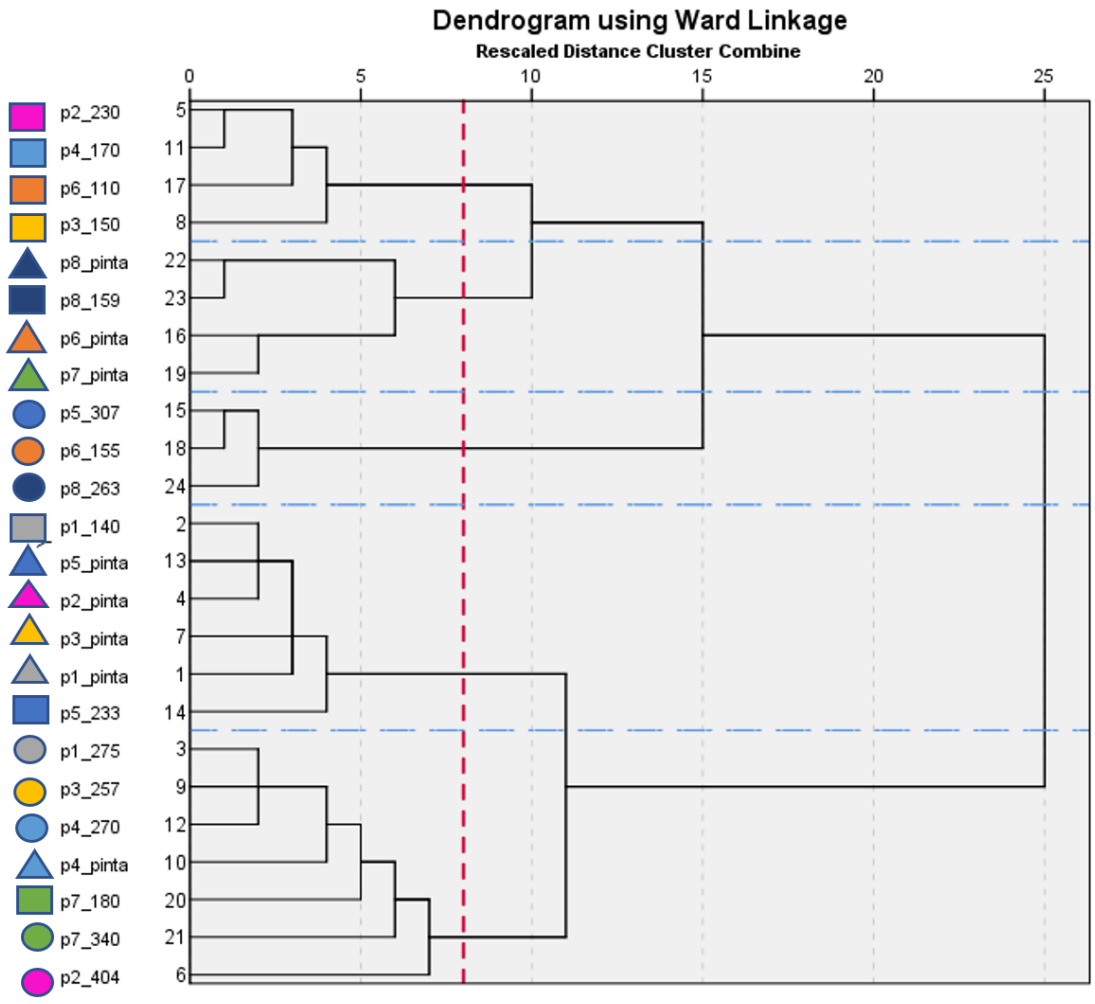

Figure 37: HCA dendrogram using ward's linkage method with Euclidean distance and ranging from 0 to 1.

Five distinct groups can be observed as a result, two in a larger scale. The first group contains five bottom samples, one middle and one surface sample. The second group includes four surface samples and two middle samples. Third group includes three bottom samples from PEAT5, 6 and 8. Fourth group is formed by surface samples of sampling points 6, 7 and 8 with the additional middle sample of PEAT8. The final group contains samples that are taken from the middle sections of the sampling points 2, 3, 4 and 6.

The HCA shows similar results that were discussed previously. Samples that have abundant groundwater characteristics are located in the bottom group. Samples with more surface water characteristics are located in the top 2 groups.

6 CONCLUSIONS

By using hydrogeochemistry and physical properties of peat, it was possible to study the water flow in Viiankiaapa mire. The results showed that the hydraulic conductivity of peat is dependent on the dry density of the peat material. Contrary to other studies of the physical properties of Finnish peats, no correlation with the K-value was found with the sampling depth or humification degree. However, the reason(s) for this were probably related to the used methodology as discussed. The hydraulic conductivity of peat could be a very important factor affecting water flow in the mire. At sampling points PEAT6 and PEAT8 it seemed that very poorly conducting peat acts as an aquiclude, hindering the water flow through the peat. This was observed with the chemical methods as well as in the hydraulic properties of the peat, where groundwater related components were present in high concentrations near the bottom contact of peat and the bottom sediments. On the other hand, sites with the highest K-values (PEAT1, PEAT2 and PEAT7) showed increased groundwater characteristics throughout the sampling depth. The mini-piezometer method gave initial information of the hydraulic properties in the peat by allowing easy extraction of water from highly conductive peat and requiring considerable effort in poorly conductive peat layers. The same reasons prevented the use of *in-situ* water analyses from the most poorly conductive peat layers.

The general water chemistry didn't include many surprises, and most of the samples represented typical Finnish natural waters of Ca–HCO_3 type. Sulphate had affected some samples even quite strongly, but the cause for this was not investigated. Some samples contained very high concentrations of iron, up to 35 ppm. Iron was probably a major component in the water when it was in the anoxic peat. This notion was made only after the samples had their electric conductivities re-analysed in the laboratory, where a dramatic difference in the field EC and laboratory EC was found. The high iron concentration had precipitated as iron(III)hydroxide in the non-preserved samples, causing alkalinity level to decrease as well, ultimately resulting in lowering of the electric conductivity. Although widely used and well-established, the results from stable isotope method did not provide as clear interpretations as the chemistry of the water samples.

Signs of evaporation were present in all samples, and the samples did not form very distinctive groups in respect of the isotopic results. Statistical methods (PCA and HCA) were applied in order to limit the number of studied variables and find groups of samples that are similar to each other. These methods yielded a few distinct groups, most importantly dividing the samples into groups which have high groundwater influence and those with low groundwater influence.

Ground penetrating radar was used in order to obtain information of the sediments beyond the peat layer. Mostly this was successfully achieved, although the interpretations were not very detailed as reference core data was not used. An interpretation of the sediment units was created using mainly the 100 MHz antenna that was used in the survey. A two-layer velocity model was used in the depth conversion, which then was adopted into the sedimentological interpretation. The GPR showed variability in the topography of the bottom contact of the peat, a confirmed bedrock contact was not found in the study. GPR probably revealed discharging groundwater through peat at one sampling point.

The used hydrogeochemical methods proved very reliable and consistent for the purpose of the study, whereas the peat sampling proved somewhat challenging. For future studies, systematic collection of peat samples, including the size as well as even distribution of sampling depths could yield more satisfactory results. It would be advisable to study the humification specifically for the selected samples as well, if possible. Hydraulic conductivity measurements using the standardised laboratory method ISO 17892-11:2019 could provide comparable results and are therefore recommended.

7 ACKNOWLEDGEMENTS

I would like to express immense gratitude towards my supervisor Kirsti Korkka-Niemi for field work instructing, excellent ideas, feedback and the opportunity to work on a subject as interesting as this. Seija Kultti for the same listed reasons and for the excruciating GPR work that she completed. Many thanks to others that were involved throughout the project including but not limited to: Anne Rautio, Jekaterina Pihko and the other helpful hands from AA Sakatti Mining Oy, who assisted during the field work

periods. Olli Nurmilaukas for helping on the first field expedition and Mimmi Takalo for sorting out the field equipment often at awkward times in the day, as well as providing the humification data. University of Helsinki staff members Annika Åberg, for help with preliminary GPR interpretation, and the Environmental laboratory staff with the laboratory equipment instructions. And most importantly my partner Jelina, who showed understanding and didn't abandon hope during the writing period.

8 REFERENCES

Åberg, A. K., Salonen, V.-P., Korkka-Niemi, K., Rautio, A., Koivisto, E. & Åberg, S. C. 2017a. GIS-based 3D sedimentary model for visualizing complex glacial deposition in Kersilö, Finnish Lapland. Boreal Environment Research, 22. 277-298.

Åberg, S. C., Åberg, A. K., Korkka-Niemi, K. I. & Salonen, V.-P. 2017b. Hydrostratigraphy and 3D Modelling of a Bank Storage Affected Aquifer in a Mineral Exploration Area in Sodankylä, Northern Finland. In: Wolkersdorfer, C., Sartz, L., Sillanpää, M. & Häkkinen, A. (eds.). Lappeenranta: Lappeenranta University of Technology. 237–242.

Åberg, S., Korkka-Niemi, K., Rautio, A. B. K., Salonen, V.-P. & Åberg, A. 2019. Groundwater recharge/discharge patterns and groundwater–surface water interactions in a sedimentary aquifer along the River Kitinen in Sodankylä. Boreal Environment Research, 2019. 155-187.

Beckwith, C. W., Baird, A. J. & Heathwaite, A. L. 2003. Anisotropy and depth-related heterogeneity of hydraulic conductivity in a bog peat. I: laboratory measurements. Hydrological Processes, 17. 89-101.

Bigler, P. 2019. Hydrogeology and hydrogeochemistry of the western margin of the Viiankiaapa mire in Sodankylä: Factors affecting the distribution of endangered species. MSc thesis. Helsinki University.

Boelter, D. H. 1965. Hydraulic conductivity of peats. Soil Science, 100. 227-231.

Brownscombe, W., Ihlenfeld, C., Coppard, J., Hartshorne, C., Klatt, S., Siikaluoma, J. K. & Herrington, R. J. 2015. Chapter 3.7 - The Sakatti Cu-Ni-PGE Sulfide Deposit in Northern Finland. In: Maier, W. D., Lahtinen, R. & O'brien, H. (eds.) Mineral Deposits of Finland. Elsevier, 211–252.

Clark, I. & Fritz, P. 1997. Environmental Isotopes in Hydrogeology. Lewis, 290 p.

Clymo, R.S. 2004. Hydraulic conductivity of peat at Ellergower Moss, Scotland. Hydrological Processes, 18. 261-274.

Craig, H. 1961. Isotopic Variations in Meteoric Waters. Science, 133. 1702-1703.

Dai, T. S. & Sparling, J. H. 1973. Measurement of hydraulic conductivity of peats. Canadian Journal of Soil Science, 53. 21-26.

Dalton, M. G. & Upchurch, S. B. 1978. Interpretation of Hydrochemical Facies by Factor Analysis. Groundwater, 16. 228-233.

Dansgaard, W. 1964. Stable isotopes in precipitation. Tellus, 16. 436-468.

Epstein, S. & Mayeda, T. 1953. Variation of O18 content of waters from natural sources. Geochimica et Cosmochimica Acta, 4. 213-224.

Fröhlich, K., Gibson, J. & Aggarwal, P. 2002. Deuterium excess in precipitation and its climatological significance. In: Study of environmental change using isotope techniques. Vienna: International Atomic Energy Agency, C&S Papers Series 13/P, 54–65

Geological Survey of Finland. 2017. Bedrock of Finland 1:200 000. Accessible at: https://hakku.gtk.fi/

Golder associates Oy. 2012. Viiankiaapa – Preliminary hydrological and hydrogeological characterisation.

Hanski, E. & Huhma, H. 2005. Central Lapland greenstone belt. in: Lehtinen, M, Nurmi, P.A. & Rämö, O.T. (ed.) Precambrian geology of Finland: key to the evolution of the Fennoscandian shield. Developments in Precambrian geology 14. Elsevier, Amsterdam. 139–193.

Hill, B. M. & Siegel, D. I. 1991. Groundwater flow and the metal content of peat. Journal of Hydrology, 123. 211-224.

Hirvas, H. 1991. Pleistocene stratigraphy of Finnish Lapland. Geological Survey of Finland. Espoo. 123 p.

Hänninen, P. 1992. Application of ground penetrating radar and radio wave moisture probe techniques to peatland investigations. Geological Survey of Finland. Espoo. 74 p.

Hänninen, P. & Lappalainen, E. 1987. Maatutkan ja suosondin soveltuvuus turvevarojen määrän ja laadun selvittämiseen. Geological Survey of Finland. Report of peat investigation 202. Kuopio. 34 p.

Hänninen, P. & Leino, J. 1998. Selvitys maatutkaluotauksesta turveinventointityössä. Geological Survey of Finland. Report P.31.4.015. 13p

Johansson, P. 1995. The deglaciation in the eastern part of the Weichselian ice divide in Finnish Lapland. Geological Survey of Finland. Rovaniemi. 74 p.

Johansson, P. & Kujansuu, R. (ed.) 2005. Pohjois-Suomen maaperä: maaperäkarttojen 1:400 000 selitys. Summary: Quaternary deposits of Northern Finland - Explanation to the maps of Quaternary deposits 1:400 000. Geological Survey of Finland. Espoo. 236 p.

Jouzel, J., Masson-Delmotte, V., Stiévenard, M., Landais, A., Vimeux, F., Johnsen, S. J., Sveinbjörnsdottir, A. E. & White, J. W. C. 2005. Rapid deuterium-excess changes in Greenland ice cores: a link between the ocean and the atmosphere. Comptes Rendus Geoscience, 337. 957-969.

Kabata-Pendias, A., Pendias, H. 2001 Trace Elements in Soils and Plants. 3rd Edition, CRC Press, Boca Raton, 403 p.

Kaila, A. 1956. Determination of the degree of humification in peat samples. Agricultural and Food Science, 28. 18-35.

Kaiser, H. F. 1974. An index of factorial simplicity. Psychometrika 39. 31–36.

Kendall, C. & Coplen, T. B. 2001. Distribution of oxygen-18 and deuterium in river waters across the United States. Hydrological processes, 15. 1363-1393.

Kesäniemi. O. 2009. Rahkaturvemaiden hydrauliset ominaisuudet. Teknillinen Korkeakoulu. Yhdyskunta- ja ympäristötekniikan laitos, Vesitalouden laboratorio. Licentiate thesis, 144 p.

Korkka-Niemi, K., Kivimäki, A. L. & Nygård, M. 2012. Observations on groundwater-surface water interactions at River Vantaa, Finland. Management of Environmental Quality: An International Journal, 23. 222-231.

Korkka-Niemi, K. I., Rautio, A. B. K., Bigler, P. & Åberg, S. C. 2017. Characterization of Geo-Hydro-Ecological Factors Affecting the Distribution of Endangered Species of Viiankiaapa Mire, in Ore Prospecting Site. In: Wolkersdorfer, C., Sartz, L., Sillanpää, M. & Häkkinen, A. (eds.). Lappeenranta: Lappeenranta University of Technology. 1022–1028.

Kortelainen, N. 2007a. Isotopic Fingerprints in Surficial Waters: Stable Isotope Methods Applied in Hydrogeological Studies. Special publication, 2007. University of Helsinki.

Kortelainen, N. 2007b. Isotopic composition of oxygen and hydrogen in Finnish groundwaters: Tables of groundwater monitoring in 2002–2004. Geological survey of Finland. Report P32.4/2007/49. Espoo. 13 p.

Kortelainen, N. M. & Karhu, J. A. 2004. Regional and seasonal trends in the oxygen and hydrogen isotope ratios of Finnish groundwaters: a key for mean annual precipitation. Journal of Hydrology, 285. 143-157.

Kääriäinen, K. 2016. Reanalysis of the existing regional geochemical data around the Sakatti Ni-Cu-PGE target, Sodankylä, Finland. MSc thesis. Helsinki University.

Laatikainen, M., Leino, J., Lerssi, J., Torppa, J. & Turunen, J. 2011. Turvetutkimusten menetelmäkehitystarkastelu. Abstract: A new approach for peat inventory methods. Geological Survey of Finland. Report of peat investigation 414. Espoo. 136 p.

Lahermo, P. 1970. Chemical geology of ground and surface water in Finnish Lapland. Geological Survey of Finland. Espoo. 111 p.

Lahermo, P., Ilmasti, M., Juntunen, R. & Taka, M. 1990. The Geochemical Atlas of Finland, Part 1: The hydrogeochemical mapping of Finnish groundwater. Geological Survey of Finland. Espoo. 71 p.

Lahermo, P., Tarvainen, T., Hatakka, T., Backman, B., Juntunen, R., Kortelainen, N., Lakomaa, T., Nikkarinen, M., Vesterbacka, P., Väisänen, U. & Suomela, P. 2002. Summary: One thousand wells - the physical-chemical quality of Finnish well waters in 1999. Geological Survey of Finland. Espoo. Report of investigation 155. 92 p.

Lahermo, P., Väänänen, P., Tarvainen, T. & Salminen, R. 1996. Geochemical Atlas of Finland, Part 3: Environmental geochemistry - stream waters and sediments. Geological Survey of Finland. Espoo. 151 p.

Lahtinen, T. 2017. Hydrogeochemical characterization of the Sakatti mine prospecting area, Sodankylä, Finnish Lapland. MSc thesis. Helsinki University.

Lappalainen, E. 1970. Über die spätquartäre Entwicklung der Flussufermoore Mittel-Lapplands, Geological Survey of Finland. Espoo. 91 p.

Lappalainen, E., Hänninen, P., Hänninen, P., Koponen, L., Leino, J., Rainio, H. & Sutinen, R. 1984. Geofysikaalisten mittausmenetelmien soveltuvuus maaperätutkimuksiin. Geological Survey of

Finland. Report P 13.4/84/157. 38 p.
Lappalainen, E. & Pajunen, H. 1980. Lapin turvevarat: yhteenveto vuosina 1962-1975 Lapissa tehdyistä turvetutkimuksista. Geological Survey of Finland. Report P 13.6 / 80 / 20. 220 p.
Lappalainen, E. 2004. Kallio- ja maaperä sekä kasvillisuuden jääkauden jälkeinen kehityshistoria. in: Pääkkö, E. (ed.) Keski-Lapin aapasoiden luonto. Metsähallituksen luonnonsuojelujulkaisuja. Vantaa.18–43.
Lee, R. and Cherry, J. 1976. A field exercise on groundwater flow using seepage meters and mini-piezometers. Journal Geological Education 27; 6–20.
Maunu, M., & Virtanen, K. 2005. Suot ja turvekerrostumat in: Johansson, P. & Kujansuu, R. (ed.) Pohjois-Suomen maaperä: maaperäkarttojen 1:400 000 selitys. Summary: Quaternary deposits of Northern Finland - Explanation to the maps of Quaternary deposits 1:400 000. Geologian tutkimuskeskus. Espoo. 80–86.
Metsähallitus 2006. Viiankiaavan hoito- ja käyttösuunnitelma. Metsähallituksen luonnonsuojelujulkaisuja, Sarja C 11. 51 p.
Mustamo, P., Hyvärinen, M., Ronkanen, A.K. & KlØve, B. 2016. Physical properties of peat soils under different land use options. Soil Use and Management, 32. 400-410.
Neal, A. 2004. Ground-penetrating radar and its use in sedimentology: principles, problems and progress. Earth-Science Reviews, 66. 261-330.
Pääkkö, E. 2004. Keski-Lapin aapasoiden luonto. Metsähallituksen luonnonsuojelujulkaisuja, Sarja A, 145. Vantaa. 153 p.
Päivänen, J. 1968. Tutkimuksia turpeen fysikaalisista ominaisuuksista, erityisesti tilavuuspainosta, vedenläpäisevyydestä ja vedenpidätyskyvystä. Unpublished. Helsinki University, Department of peatland forestry.
Päivänen, J. 1973. Hydraulic conductivity and water retention in peat soils. Acta Forestalia Fennica. 1973. 129:1–70.
Päivänen, J. 1982. Turvemaan fysikaaliset ominaisuudet. Publications from the department of peatland forestry. Helsinki University. 69 p.
Pakarinen, P. 1995. Classification of Boreal Mires in Finland and Scandinavia: A Review. Vegetatio, 118. 29-38.
Pfahl, S. & Sodemann, H. 2014. What controls deuterium excess in global precipitation? Clim. Past, 10. 771-781.
Piper, A. M. 1944. A graphic procedure in the geochemical interpretation of water-analyses. Eos, Transactions American Geophysical Union, 25. 914-928.
Putkinen, N., Eyles, N., Putkinen, S., Ojala, A. E. K., Palmu, J.-P., Sarala, P., Väänänen, T., Räisänen, J., Saarelainen, J., Ahtonen, N., Rönty, H., Kiiskinen, A., Rauhaniemi, T. & Tervo, T. 2017. High-resolution LiDAR mapping of glacial landforms and ice stream lobes in Finland. Bulletin of The Geological Society of Finland, 89. 64-81.
Quinton, W. L., Hayashi, M. & Carey, S. K. 2008. Peat hydraulic conductivity in cold regions and its relation to pore size and geometry. Hydrological Processes, 22. 2829-2837.
Räinä, P. & Hjelt, A. 2004. Linnusto. in: Pääkkö, E. (ed.) Keski-Lapin aapasoiden luonto. Metsähallituksen luonnonsuojelujulkaisuja. Vantaa. 98–124.
Rautio, A., Kivimaki, A. L., Korkka-Niemi, K., Nygard, M., Salonen, V. P., Lahti, K. & Vahtera, H. 2015. Vulnerability of groundwater resources to interaction with river water in a boreal catchment. Hydrology and Earth System Sciences (HESS), 19. 3015-3032.

Rautio, A., Kivimaki, A. L., Korkka-Niemi, K., Nygard, M., Salonen, V. P., Lahti, K. & Vahtera, H. 2015. Vulnerability of groundwater resources to interaction with river water in a boreal catchment. Hydrology and Earth System Sciences (HESS), 19. 3015-3032.

Rautio, A. & Korkka-Niemi, K. 2011. Characterization of groundwater-lake water interactions at Pyhajarvi, a lake in SW Finland. Boreal Environment Research, 16. 363-380.
Rautio, A. & Korkka-Niemi, K. 2015. Chemical and isotopic tracers indicating groundwater/surface-water interaction within a boreal lake catchment in Finland. Hydrogeology Journal, 23. 687-705.
Reeve, A. S., Siegel, D. I. & Glaser, P. H. 2000. Simulating vertical flow in large peatlands. Journal of Hydrology, 227. 207-217.
Reimann, C. & Filzmoser, P. 2000. Normal and lognormal data distribution in geochemistry: death of a myth. Consequences for the statistical treatment of geochemical and environmental data. Environmental Geology, 39. 1001-1014.
Reynolds, J. M. 2011. An Introduction to Applied and Environmental Geophysics, Chichester, UK, Wiley.
Ronkanen, A.-K. & Klöve, B. 2005. Hydraulic soil properties of peatlands treating municipal wastewater and peat harvesting runoff. Suo, 56.

Sarala, P., Räisänen, J., Johansson, P. & Eskola, K. O. 2015. Aerial LiDAR analysis in geomorphological mapping and geochronological determination of surficial deposits in the Sodankylä region, northern Finland. GFF, 137. 293-303.

Sarasto, J. 1963. Tutkimuksia rahka- ja saraturpeiden vedenläpäisevyydestä. Suo- Mires and peat 14. 32–35.

Shapiro, S. S. & Wilk, M. B. 1965. An Analysis of Variance Test for Normality (Complete Samples). Biometrika, 52. 591-611.

Shotyk, W. 1988. Review of the inorganic geochemistry of peats and peatland waters. Earth-Science Reviews, 25. 95-176.

Silvennoinen, A. 1998. Pohjois-Suomen liuskealueet, kerrosintruusiot ja granuliittialue. in: Lehtinen, M., Nurmi, P. & Rämö, T. (ed.) Suomen kallioperä: 3000 vuosimiljoonaa. Suomen Geologinen Seura ry. Helsinki. 375 p.

Soveri, J., Mäkinen, R. & Peltonen, K. 2001. Pohjaveden korkeuden ja laadun vaihteluista Suomessa 1975-1999. Suomen ympäristö 420. Suomen ympäristökeskus. 307 p.

Suomi, T. & Mäkilä, M. 2000. Maatutkaluotausten soveltuvuus keidassoiden tutkimuseen. Geological Survey of Finland. Report P 31.4.023, 26 p.

Suonperä, E. 2016. Holocene paleohydrology of Viiankiaapa mire, Sodankylä, Finnish Lapland. MSc thesis. University of Helsinki, Department of geosciences and geography.

Verry, E. S. 1975. Streamflow chemistry and nutrient yields from upland-peatland watersheds in Minnesota. Ecology, 56(5), 1149-1157.

Virkanen, J., Reijola, H. and Vaahtojärvi, T. 2017. Geotieteiden ja maantieteen laitoksen ympäristölaboratorioiden toimintakäsikirja. Unpublished work manual [in Finnish].

Vuorenmaa, J., Juntto, S., & Leinonen, L. 2001. Sadeveden laatu ja laskeuma Suomessa 1998. Suomen ympäristökeskus & Ilmatieteen laitos. Helsinki 115 p.

Winston, R. B. 2020. GW_Chart version 1.30 : U.S. Geological Survey Software Release, 26 June 2020. https://doi.org/10.5066/P9Y29U1H

Wong, L. S., Hashim, R. & Ali, F. 2009. A Review on Hydraulic Conductivity and Compressibility of Peat. Journal of Applied Sciences, 9. 3207–3218.

Wright, M. & Belitz, K. 2010. Factors Controlling the Regional Distribution of Vanadium in Groundwater. Ground water, 48. 515-25.

9 APPENDICES

Appendix 1: Unrounded results of the trace element analyses of water and snow samples.

	Al ppb	Si ppm	P ppb	V ppb	Cr ppb	Mn ppb	Fe ppb	Co ppb	Ni ppb	Cu ppb	Zn ppb	As ppb	Se ppb	Mo ppb	Cd ppb	Pb ppb	U ppb
p1_pinta	16.80	6.42	28.01	0.086	0.69	198.87	11277.45	1.03	0.27	0.079	4.81	1.13	0.017	<0.005	0.060	0.062	<0.001
p1_140	2.43	7.53	91.39	0.086	1.16	298.92	25714.88	2.49	0.68	0.17	6.09	1.74	0.026	0.032	0.0050	0.013	<0.001
p1_275	49.06	7.07	66.49	2.13	2.57	383.57	25700.67	3.10	1.64	0.53	35.662	1.80	0.027	0.023	<0.002	0.041	0.0081
p2_pinta	<1.5	8.71	141.15	0.17	1.29	270.99	17676.31	1.71	0.64	0.20	6.88	0.66	0.022	0.018	0.010	0.026	0.0013
p2_230	3.48	4.01	125.20	0.13	0.60	270.49	20150.30	2.55	1.32	0.35	9.30	1.64	0.018	0.057	0.012	0.012	0.0015
p2_404	57.12	5.90	55.96	4.53	8.85	423.93	30734.26	5.35	9.55	1.12	615.09	43.35	0.030	2.15	0.018	0.16	0.030
p3_pinta	19.08	6.69	161.06	0.20	0.76	120.78	20625.83	1.45	1.05	0.45	12.47	1.70	0.037	0.070	0.025	0.14	0.0011
p3_150	20.25	3.84	232.55	0.19	0.50	268.54	28764.90	2.66	0.83	0.076	7.13	3.37	0.033	0.014	0.062	0.0055	<0.001
p3_257	68.47	6.38	51.90	3.63	4.12	308.86	29748.41	3.09	2.29	0.22	136.72	1.27	0.033	0.049	0.037	0.019	0.016
p4_pinta	46.83	7.75	105.67	1.53	2.94	206.19	17078.30	1.42	0.98	0.072	13.83	1.31	0.017	0.035	0.0057	0.011	0.0062
p4_170	9.11	4.72	153.48	0.20	0.61	207.03	20273.38	1.78	0.29	0.10	2.56	1.80	0.020	0.0080	<0.002	0.0047	0.0012
p4_270	46.78	7.97	106.87	1.52	2.91	205.06	17257.28	1.43	0.91	0.063	11.57	1.29	0.017	0.031	0.011	0.0093	<0.001
p5_pinta	<1.5	7.69	165.86	0.12	1.07	262.95	25336.33	2.01	1.07	0.53	12.72	2.73	0.024	<0.005	0.0095	0.013	0.0091
p5_233	11.67	5.32	74.76	1.48	1.81	298.64	34963.92	2.82	2.36	0.31	87.53	5.19	0.040	0.10	0.17	0.042	0.019
p5_307	60.23	5.83	109.62	5.21	4.14	227.29	25298.49	1.98	1.33	<0.06	14.78	2.06	0.035	0.027	0.0026	0.0070	0.0085
p6_pinta	16.24	6.03	192.95	0.047	0.31	100.64	5494.35	1.00	1.46	0.57	5.06	1.03	0.035	0.092	0.027	0.037	<0.001
p6 _110	27.70	6.16	144.91	1.33	3.34	165.14	21105.40	1.30	2.83	3.13	15.08	1.64	0.032	0.10	0.017	0.10	0.0072
p6_155	81.05	7.00	66.73	5.67	6.86	197.16	26549.20	1.53	3.17	1.62	63.45	2.18	0.036	0.13	0.044	0.11	0.017
p7_pinta	3.86	3.39	224.27	0.056	0.57	43.46	7132.08	0.54	0.55	0.44	7.50	0.81	0.033	<0.005	0.018	0.071	<0.001
p7_180	<1.5	5.01	59.05	0.12	0.83	279.45	32451.11	1.33	0.52	0.10	3.75	1.47	0.013	0.011	<0.002	0.0066	0.0013
p7_340	17.21	12.99	221.72	5.55	10.36	211.11	26219.06	0.73	1.34	0.23	34.84	2.27	0.033	0.11	0.012	0.026	0.012
p8_pinta	7.41	4.27	61.54	0.14	0.74	44.32	8129.30	1.16	0.38	0.25	6.55	0.39	0.027	0.0051	0.021	0.043	0.0021
p8_159	19.87	1.86	84.66	0.19	0.80	62.98	6624.33	1.75	0.91	0.66	36.11	0.88	0.024	0.034	0.0093	0.11	0.0047
p8_263	86.30	7.18	43.77	4.90	2.57	147.83	22113.28	5.20	1.15	0.27	43.32	1.13	0.040	0.037	0.0036	0.022	0.0098
pintalumi	<1.5	<0.003	19.82	0.047	<0.02	0.25	1.92	0.0056	0.041	0.11	1.29	0.011	<0.01	<0.005	<0.002	0.0044	<0.001
lumi10	<1.5	<0.003	15.20	0.030	0.090	0.31	1.49	0.010	0.080	0.13	4.20	0.010	0.020	<0.005	0.0030	0.046	<0.001
lumi2030	<1.5	<0.003	14.80	0.030	<0.02	0.22	0.67	0.010	0.070	0.16	0.80	<0.01	<0.01	<0.005	<0.002	0.0080	<0.001
lumi4050	<1.5	<0.003	14.30	0.060	<0.02	0.41	1.51	0.030	0.18	0.24	2.13	<0.01	0.010	<0.005	0.043	0.024	<0.001
detection limit	1.5	0.003	1	0.002	0.02	0.06	0.3	0.002	0.03	0.06	0.05	0.01	0.01	0.005	0.002	0.003	0.001

Appendix 2: Complete water chemistry results of the snow samples.

pH lab	Na ppm	K ppm	Ca ppm	Mg ppm	F ppm	Cl ppm	NO_3 ppm	SO_4 ppm	Alkalinity [mmol/l]	Al ppb	Si ppm	P ppb	V ppb	Cr ppb	Mn ppb	Fe ppb	Co ppb	Ni ppb	Cu ppb	Zn ppb	As ppb	Se ppb	Mo ppb	Cd ppb	Pb ppb	U ppb
5.01	< 0.2	< 0.26	< 0.2	< 0.07	< 0.11	1.041	0.144	0.271	< 0.2	<1.500	0.006954	19.81816	0.04701	<0.020	0.253491	1.920791	0.005606	0.04077	0.109886	1.292979	0.010901	<0.010	<0.005	<0.002	0.004406	<0.001
4.82	< 0.2	< 0.26	< 0.2	< 0.07	< 0.11	0.891	0.365	0.294	< 0.2	<1.500	0	15.2	0.03	0.09	0.31	1.49	0.01	0.08	0.13	4.2	0.01	0.02	< 0.005	0.003	0.046	< 0.001
4.87	< 0.2	< 0.26	< 0.2	< 0.07	< 0.11	1.001	0.2	0.263	< 0.2	<1.500	0	14.8	0.03	< 0.020	0.22	0.67	0.01	0.07	0.16	0.8	< 0.01	< 0.01	< 0.005	< 0.002	0.008	< 0.001
4.81	< 0.2	< 0.26	< 0.2	< 0.07	< 0.11	0.957	0.246	0.303	< 0.2	<1.500	0	14.3	0.06	< 0.020	0.41	1.51	0.03	0.18	0.24	2.13	< 0.01	0.01	< 0.005	0.043	0.024	< 0.001
	0.2	0.26	0.2	0.07	0.11	0.001	0.04	0.07	0.2	1.5	0.003	1	0.002	0.02	0.06	0.3	0.002	0.03	0.06	0.05	0.01	0.01	0.005	0.002	0.003	0.001

Appendix 3: Pearson bivariate correlation matrix. The flagged significant correlations represent 2-tailed significance at 0.01 level (**) and at 0.05 level (*). The meaning of the rows: r=pearson correlation coefficient, Sig.= 2-tailed significance and N = number of measurements.

		pH field	pH lab	EC_field	Na	K	Ca	Mg	Cl	SO4	Alkalinity	Al	Si	P	V	Cr	Mn	Fe	Co	Ni	Cu	Zn	As	Se	Mo	Cd	Pb	U	d2H	d18O	depth	EC_2020
pH field	r	1																														
	Sig.																															
	N	17																														
pH lab	r	,849**	1																													
	Sig.	0																														
	N	17	24																													
EC_field	r	,563*	,709**	1																												
	Sig.	0,019	0																													
	N	17	23	23																												
Na	r	0,297	,502*	0,4	1																											
	Sig.	0,246	0,013	0,059																												
	N	17	24	23	24																											
K	r	-0,111	0,023	-0,021	,616**	1																										
	Sig.	0,671	0,916	0,925	0,001																											
	N	17	24	23	24	24																										
Ca	r	0,407	,606**	,785**	,439*	-0,002	1																									
	Sig.	0,105	0,002	0	0,032	0,993																										
	N	17	24	23	24	24	24																									
Mg	r	,540*	,741**	,819**	,517**	0,168	,880**	1																								
	Sig.	0,025	0	0	0,01	0,434	0																									
	N	17	24	23	24	24	24	24																								
Cl	r	-0,207	0,047	-0,126	,574**	,769**	0,013	0,11	1																							
	Sig.	0,426	0,829	0,567	0,003	0	0,953	0,609																								
	N	17	24	23	24	24	24	24	24																							
SO4	r	0,04	0,019	0,091	0,34	0,218	0,228	0,173	,461*	1																						
	Sig.	0,88	0,928	0,68	0,104	0,305	0,285	0,418	0,023																							
	N	17	24	23	24	24	24	24	24	24																						
Alkalinity	r	,566*	,796**	,822**	,543**	0,172	,863**	,943**	0,087	-0,005	1																					
	Sig.	0,018	0	0	0,006	0,421	0	0	0,685	0,982																						
	N	17	24	23	24	24	24	24	24	24	24																					
Al	r	0,284	0,095	0,219	-0,063	-0,273	0,122	-0,011	-0,181	0,151	0,057	1																				
	Sig.	0,27	0,66	0,316	0,77	0,196	0,57	0,958	0,397	0,482	0,791																					
	N	17	24	23	24	24	24	24	24	24	24	24																				
Si	r	0,301	,453*	,459*	,737**	0,3	,411*	,481*	0,301	0,081	,536**	0,174	1																			
	Sig.	0,241	0,026	0,028	0	0,154	0,046	0,017	0,153	0,708	0,007	0,416																				
	N	17	24	23	24	24	24	24	24	24	24	24	24																			
P	r	-0,453	-0,366	-0,153	-0,085	0,291	-0,142	-0,116	0,213	-0,083	-0,109	-,439*	0,105	1																		
	Sig.	0,068	0,079	0,485	0,692	0,167	0,509	0,589	0,319	0,7	0,611	0,032	0,622																			
	N	17	24	23	24	24	24	24	24	24	24	24	24	24																		
V	r	0,236	0,143	0,283	0,226	-0,213	0,288	0,035	-0,112	0,158	0,171	,802**	,454*	-0,239	1																	
	Sig.	0,361	0,505	0,191	0,289	0,318	0,172	0,872	0,603	0,461	0,425	0	0,026	0,26																		
	N	17	24	23	24	24	24	24	24	24	24	24	24	24	24																	
Cr	r	0,233	0,195	0,348	,465*	-0,093	,437*	0,19	0,046	0,369	0,242	,533**	,580**	-0,076	,859**	1																
	Sig.	0,369	0,361	0,104	0,022	0,664	0,033	0,374	0,832	0,076	0,254	0,007	0,003	0,725	0																	
	N	17	24	23	24	24	24	24	24	24	24	24	24	24	24	24																
Mn	r	0,475	,605**	,620**	0,338	-0,064	,807**	,680**	0,091	0,293	,637**	0,168	0,271	-0,276	0,253	0,338	1															
	Sig.	0,054	0,002	0,002	0,106	0,767	0	0	0,672	0,164	0,001	0,432	0,201	0,191	0,233	0,106																
	N	17	24	23	24	24	24	24	24	24	24	24	24	24	24	24	24															
Fe	r	0,435	,460*	,718**	0,264	-0,058	,791**	,572**	-0,088	0,023	,639**	0,255	0,28	-0,184	,439*	,422*	,786**	1															
	Sig.	0,081	0,024	0	0,213	0,787	0	0,004	0,682	0,914	0,001	0,229	0,185	0,389	0,032	0,04	0																
	N	17	24	23	24	24	24	24	24	24	24	24	24	24	24	24	24	24														
Co	r	0,288	0,252	0,205	-0,044	-0,181	0,265	0,043	0,096	0,321	0,101	,513*	-0,059	-,433*	0,402	0,238	,567**	,496*	1													
	Sig.	0,262	0,236	0,349	0,84	0,399	0,211	0,843	0,657	0,127	0,638	0,01	0,784	0,035	0,052	0,263	0,004	0,014														
	N	17	24	23	24	24	24	24	24	24	24	24	24	24	24	24	24	24	24													
Ni	r	-0,115	-0,05	0,071	0,201	-0,066	0,337	0,007	0,194	,642**	-0,059	,419*	0,034	-0,241	,489*	,641**	,489*	0,387	,588**	1												
	Sig.	0,66	0,816	0,747	0,347	0,759	0,108	0,974	0,363	0,001	0,785	0,042	0,876	0,256	0,015	0,001	0,015	0,062	0,003													
	N	17	24	23	24	24	24	24	24	24	24	24	24	24	24	24	24	24	24	24												
Cu	r	-,551*	-,422*	-0,09	-0,124	-0,135	-0,205	-0,369	-0,196	0,061	-,480*	0,188	-0,044	0,009	0,168	0,281	-0,068	0,031	-0,003	,456*	1											
	Sig.	0,022	0,04	0,684	0,565	0,529	0,336	0,076	0,358	0,778	0,017	0,38	0,84	0,968	0,432	0,184	0,751	0,884	0,99	0,025												
	N	17	24	23	24	24	24	24	24	24	24	24	24	24	24	24	24	24	24	24	24											
Zn	r	-0,019	0,04	0,062	0,24	-0,031	0,37	0,073	0,288	,712**	0,016	0,354	-0,011	-0,296	,418*	,574**	,499*	0,344	,647**	,949**	0,213	1										
	Sig.	0,941	0,852	0,78	0,258	0,885	0,075	0,735	0,173	0	0,942	0,09	0,959	0,161	0,042	0,003	0,013	0,1	0,001	0	0,317											
	N	17	24	23	24	24	24	24	24	24	24	24	24	24	24	24	24	24	24	24	24	24										
As	r	0,123	0,032	0,036	0,245	-0,001	0,365	0,085	0,343	,739**	0,01	0,224	-0,025	-0,19	0,314	,511*	,496*	0,32	,595**	,924**	0,201	,970**	1									
	Sig.	0,638	0,881	0,871	0,249	0,997	0,08	0,693	0,101	0	0,963	0,293	0,907	0,373	0,134	0,011	0,014	0,127	0,002	0	0,347	0										
	N	17	24	23	24	24	24	24	24	24	24	24	24	24	24	24	24	24	24	24	24	24	24									
Se	r	-0,344	-,463*	-0,266	-0,166	0,128	-0,181	-,429*	0,123	-0,132	-0,289	0,388	0,05	0,183	,474*	0,279	-0,147	0,189	0,285	0,267	0,278	0,163	0,09	1								
	Sig.	0,176	0,023	0,22	0,439	0,553	0,398	0,037	0,567	0,539	0,171	0,061	0,817	0,393	0,019	0,186	0,493	0,376	0,177	0,208	0,188	0,446	0,676									
	N	17	24	23	24	24	24	24	24	24	24	24	24	24	24	24	24	24	24	24	24	24	24	24								
Mo	r	0,001	0,007	0,008	0,257	0,002	0,314	0,044	0,331	,752**	-0,034	0,253	-0,003	-0,199	0,339	,542**	,446*	0,262	,569**	,936**	0,245	,973**	,993**	0,095	1							
	Sig.	0,998	0,973	0,971	0,226	0,992	0,135	0,838	0,114	0	0,875	0,233	0,99	0,352	0,105	0,006	0,029	0,216	0,004	0	0,249	0	0	0,66								
	N	17	24	23	24	24	24	24	24	24	24	24	24	24	24	24	24	24	24	24	24	24	24	24	24							
Cd	r	-0,274	-0,061	-0,094	-0,097	0,03	0,231	0,047	0,008	-0,136	0,083	-0,072	-0,146	-0,094	-0,033	-0,057	0,116	0,276	0,06	0,109	-0,006	0,077	0,044	0,383	-0,009	1						
	Sig.	0,288	0,778	0,669	0,651	0,889	0,278	0,827	0,971	0,527	0,7	0,736	0,495	0,661	0,877	0,791	0,588	0,191	0,782	0,611	0,976	0,72	0,839	0,065	0,967							
	N	17	24	23	24	24	24	24	24	24	24	24	24	24	24	24	24	24	24	24	24	24	24	24	24	24						
Pb	r	-0,18	-0,327	-0,259	0,178	0,294	-0,213	-0,345	0,315	0,349	-0,386	0,19	-0,17	-0,136	0,157	0,304	-0,135	-0,112	0,117	,613**	,586**	,545**	,526**	0,331	,569**	0,099	1					
	Sig.	0,49	0,118	0,232	0,407	0,164	0,317	0,098	0,134	0,095	0,063	0,375	0,426	0,526	0,464	0,148	0,529	0,603	0,587	0,001	0,003	0,006	0,008	0,114	0,004	0,646						
	N	17	24	23	24	24	24	24	24	24	24	24	24	24	24	24	24	24	24	24	24	24	24	24	24	24	24					
U	r	0,064	0,088	0,251	0,291	-0,113	,454*	0,094	0,095	,430*	0,13	,576**	0,214	-0,362	,720**	,753**	,498*	,563**	,588**	,835**	0,305	,791**	,693**	0,399	,686**	0,312	0,402	1				
	Sig.	0,808	0,684	0,249	0,167	0,599	0,026	0,663	0,657	0,036	0,546	0,003	0,316	0,082	0	0	0,013	0,004	0,003	0	0,148	0	0	0,053	0	0,137	0,051					
	N	17	24	23	24	24	24	24	24	24	24	24	24	24	24	24	24	24	24	24	24	24	24	24	24	24	24	24				
d2H	r	-0,048	-0,149	-0,079	-,477*	-,594**	-0,129	-0,321	-,476*	0,182	-0,352	0,205	-,409*	0	0,158	0,215	0,005	-0,089	0,258	0,335	0,207	0,339	0,291	-0,039	0,314	-0,181	0,088	0,212	1			
	Sig.	0,854	0,486	0,72	0,018	0,002	0,547	0,127	0,019	0,394	0,091	0,338	0,047	1	0,461	0,312	0,982	0,679	0,223	0,109	0,333	0,105	0,168	0,856	0,135	0,396	0,684	0,319				
	N	17	24	23	24	24	24	24	24	24	24	24	24	24	24	24	24	24	24	24	24	24	24	24	24	24	24	24	24			
d18O	r	0,272	0,13	0,078	-0,327	-,541**	-0,023	-0,172	-,422*	0,163	-0,162	0,19	-0,328	-0,152	0,148	0,193	0,124	-0,02	0,374	0,291	0,007	0,348	0,303	-0,138	0,319	-0,189	0,015	0,201	,928**	1		
	Sig.	0,291	0,545	0,725	0,119	0,006	0,914	0,422	0,04	0,446	0,448	0,373	0,118	0,477	0,489	0,366	0,562	0,926	0,072	0,168	0,973	0,095	0,15	0,52	0,129	0,377	0,946	0,346	0			
	N	17	24	23	24	24	24	24	24	24	24	24	24	24	24	24	24	24	24	24	24	24	24	24	24	24	24	24	24	24		
depth	r	0,446	0,379	0,398	0,056	-,414*	,527**	0,22	-0,294	0,062	0,347	,494*	0,163	-0,259	,680**	,633**	,554**	,600**	,589**	,506*	-0,002	,508*	,452*	0,172	,440*	0	-0,014	,621**	0,39	,474*	1	
	Sig.	0,072	0,068	0,06	0,794	0,044	0,008	0,301	0,163	0,773	0,097	0,014	0,448	0,221	0	0,001	0,005	0,002	0,002	0,012	0,994	0,011	0,026	0,422	0,032	0,998	0,95	0,001	0,059	0,019		
	N	17	24	23	24	24	24	24	24	24	24	24	24	24	24	24	24	24	24	24	24	24	24	24	24	24	24	24	24	24	24	
EC_2020	r	0,472	,681**	,777**	,652**	0,287	,850**	,925**	0,256	0,294	,894**	0,059	,608**	-0,032	0,175	0,363	,672**	,556**	0,147	0,171	-0,284	0,243	0,256	-0,325	0,234	-0,125	-0,18	0,185	-0,303	-0,165	0,305	1
	Sig.	0,056	0	0	0,001	0,175	0	0	0,228	0,163	0	0,785	0,002	0,88	0,413	0,081	0	0,005	0,493	0,426	0,179	0,253	0,228	0,121	0,271	0,561	0,4	0,388	0,151	0,442	0,147	
	N	17	24	23	24	24	24	24	24	24	24	24	24	24	24	24	24	24	24	24	24	24	24	24	24	24	24	24	24	24	24	24

Appendix 4: Sliced interpretations from the 100 MHz GPR profile, with the processed but unmodified data on the lower side.

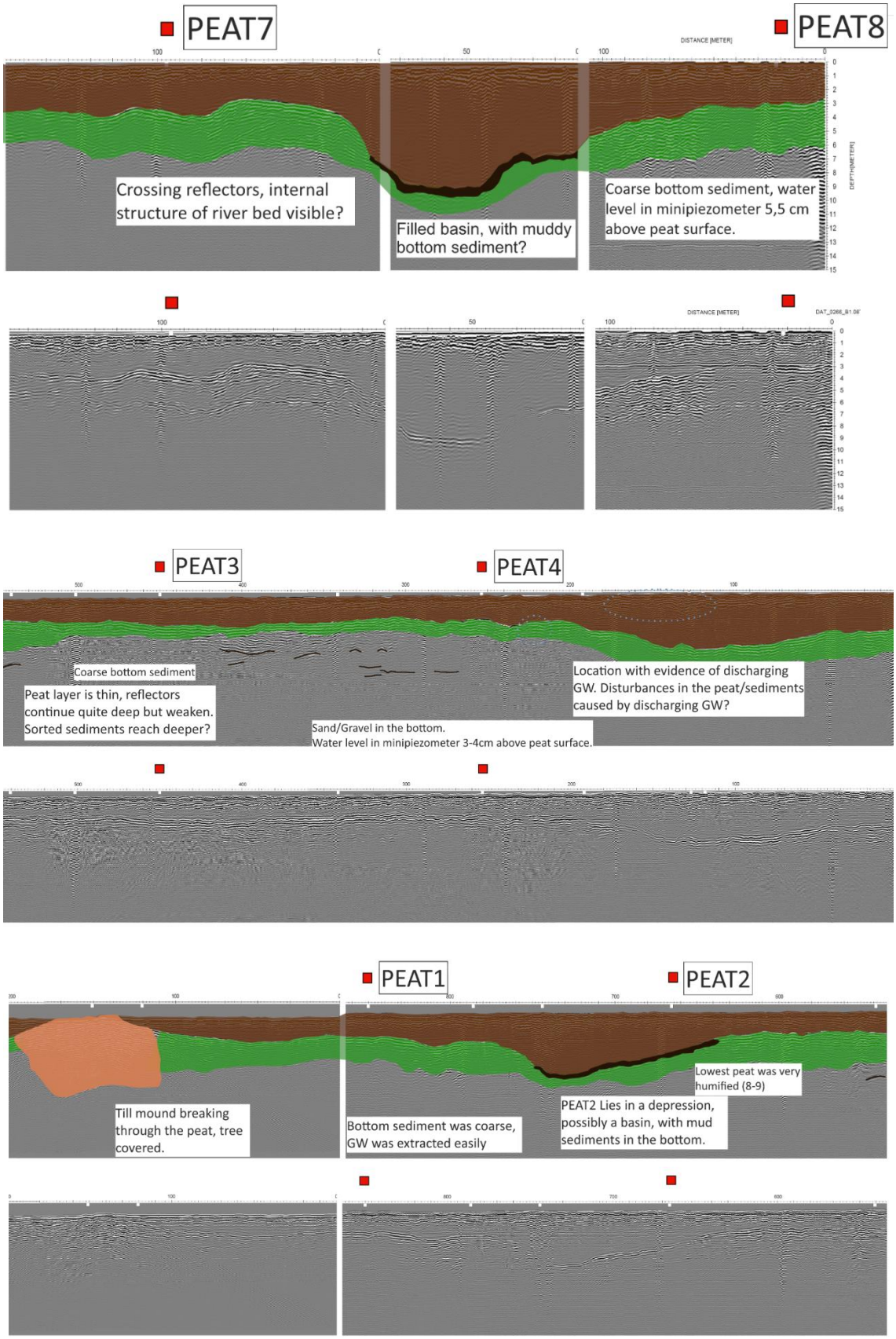

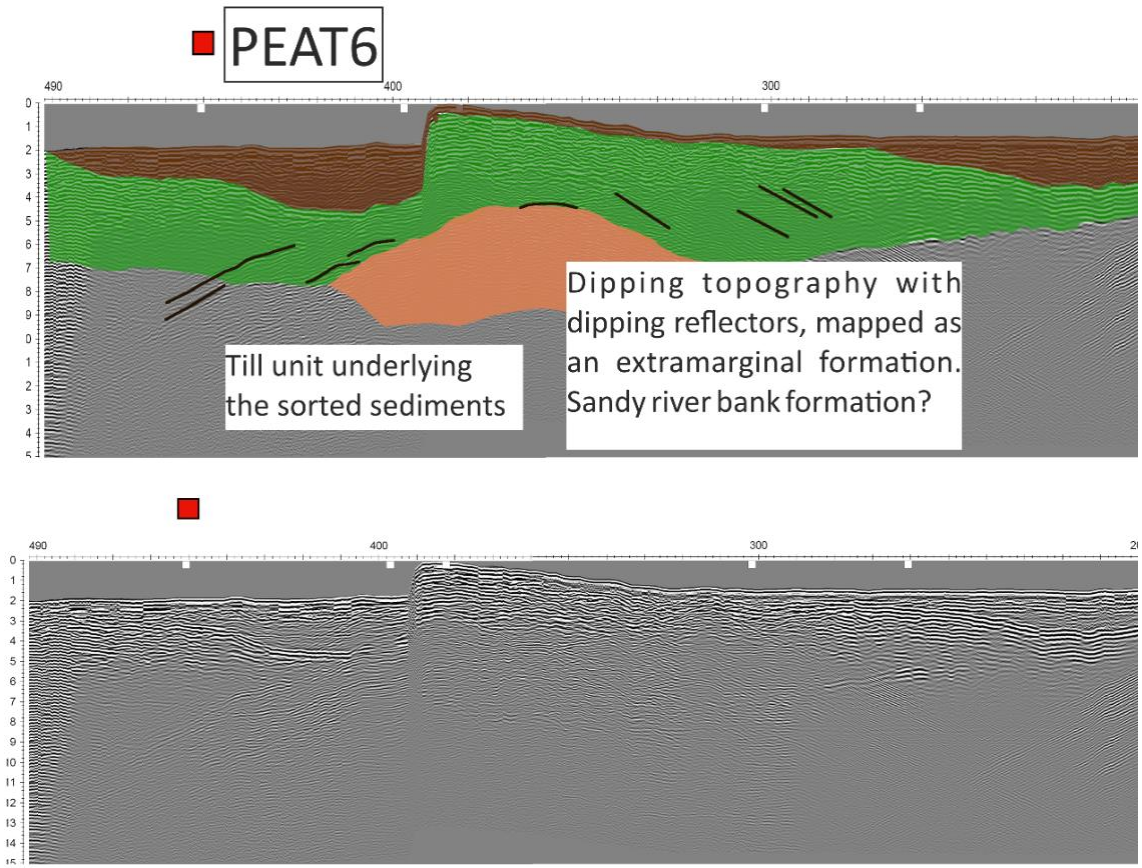
PEAT6
490
400
300
Till unit underlying the sorted sediments
Dipping topography with dipping reflectors, mapped as an extramarginal formation. Sandy river bank formation?
490
400
300

Appendix 5: The complete 100 MHz GPR profile for comparison.

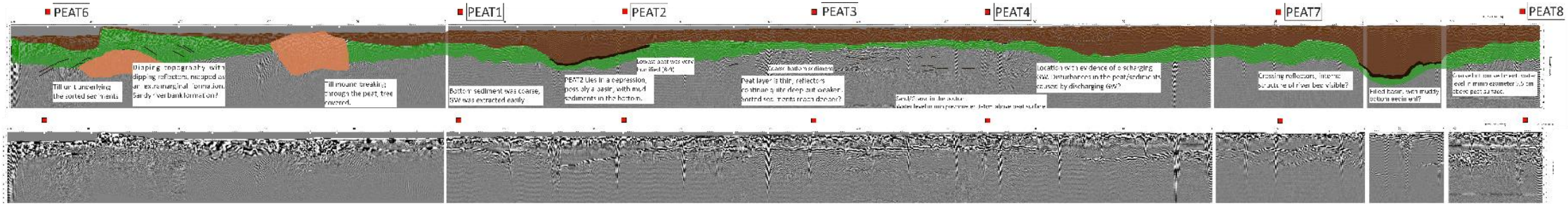

Appendix 6: The complete 30 MHz GPR profile with no interpretations shown, because the interpretations were made using the data from the 100 MHz antenna.